Dynamic Properties of Neural Networks

Thesis by Dawei Dong

In Partial Fulfillment of the Requirements
for the Degree of
Doctor of Philosophy

California Institute of Technology
Pasadena, California
1991
(Defended April 15, 1991)

Special thanks to my advisor Professor Hopfield: he guided me into the research field of neural networks and helped me all the way through.

Parts of the thesis are published papers. Thanks to all the coauthors: John Hopfield, Christof Koch, Zhengwei Peng, David Van Essen, and Udo Wehmeier.

Thanks to the people in our group who helped me in various way: Brooke Anderson, Eric Baum, Ron Benson, Joe Bryngelson, Andreas Herz, Douglas Kerns, Zhaoping Li, Hans Liljenstrom, David MacKay, Ronny Meir, and Ken Miller.

Thanks to my parents, Rujie Sun and Hongxun Dong, they made this possible.

Abstract

Two kinds of dynamic processes take place in neural networks. One involves the change with time of the activity of each neuron. The other involves the change in strength of the connections (synapses) between neurons. When a neural network is learning or developing, both processes simultaneously take place, and their dynamics interact. This interaction is particularly important in feedback networks. A Lyapunov function is developed to help understand the combined activity and synapse dynamics for a class of such adaptive networks. The methods and viewpoint are illustrated by using them to describe the development of orientation selective cells in cat primary visual cortex. Within this model, orientation selectivity originates from feedback pathways within an area of cortex, rather than feedforward pathways between areas.

1.1

Dynamic Properties of Neural Network Introduction

Neuron network

In our journey to understand the mysteries of nature, perhaps one of the most mysterious and least understood part is the ability itself to undertake such a journey — the ability our minds possess. This journey has been slow. For a long period of time, people did not even know where the mind was. People used to think that the mind was in the heart instead of the brain. In our daily language, whether Chinese or English, our hearts still feel and think.

Nature has created wonderful organisms which perform well in a complex environment, both physically and mentally. Take a look at a pigeon: one is in awe of how well it performs a takeoff, a diving and a landing. Humans do not have that ability themselves, but we have learned from birds the mechanics of flying and built airplanes to do the task. A pigeon also performs well in mental tasks like recognizing food and natural predators. Do we understand the underlying pattern recognition mechanics? Not quite. Can we build a machine to perform a similar task? Not yet. We do not quite understand and cannot yet build a brain — not even a pigeon's brain.

Today's knowledge of biology tells us that the mind is in brain, which can be viewed as a network of neurons. The state of the mind, in a large extent, can be viewed as the state of the neuron network, which is described both by the activities of neurons and the structure of the network. Most of features of thinking, learning and other mental activities must be represented by the state changes of neuron network.

What the neuron network is doing is a kind of computation. A human mind can do addition, subtraction, multiplication and division. But here we are talking about computation in a more general sense: on the left hand of an "equals" sign could be a huge amount of visual information, like that which our retina receives, and on the

right hand side of the "equals" sign would be the recognition of certain pattern. This kind of computation is complicated information processing.

There is often an analogy between brain and computer, neuron and transistor, since the brain is a network of neurons and the computer is a network of transistors. This might help to understand the neuron network a little, since both of them are complex networks built with simple units and both of them, in principle, can do the same computational task. But the efficiencies of a biological brain and a digital computer are really different and very dependent on tasks.

The human brain is not even good at the four fundamental arithmetic operations. A calculator will outperform us easily. A digital computer is not good at doing pattern recognition, one of the most common tasks for a biological being to survive. The human brain consists of about 10^{11} neurons. A typical personal computer nowadays has about 10^7 transistors. But to do multiplication, it takes a human $1sec$; it only takes $10^{-7}sec$ for a personal computer. For a task like pattern recognition in a natural scene, a personal computer is no match to a pigeon with only about 10^9 neurons. Even after discounting the device speed, one can still draw the same conclusion. (Hopfield, 1990.)

The abilities of flying and pattern recognition were developed over million of years by the selection of nature, yet we can understand the structure of the wing and the dynamics of flying, and as a result we can build airplanes. It is still a challenge for human beings to further understand the structures and dynamics of the neuron network and to build more intelligent machines which can perform well on tasks such as pattern recognition.

Adaptive neuron network dynamics

A brain and a digital computer have very different structures and follow very different dynamics. For instance, in a personal computer, each transistor connects

to three or four other transistor and the connections are most feedforward. In the human, there are many more connections, both feedforward and feedback. For another example, the connections between neurons change during the development of the brain and during learning or adapting to the environment. One of the most important features of a neuron network is adaptation.

If we describe the state of a neuron network by two sets of variables, namely neuron activity and the connections between neurons, adaptation is reflected in the change of connections, i.e., change of network structure. Generally, this kind of change is responsible to development and maturation, memorizing, learning and acquiring motor skills. It is a vital part of the neuron network dynamics. Biology tells that the connections are learned or developed while the network is functioning, i.e., when the neurons are active, and furthermore that the synaptic development and modification depends on neuronal activity. The activities of the two neurons which are connected by a particular synapse are particularly important for changes in that synapse.

Genetics determine the form and structure of a brain to a considerable extent, but a lot of neuron connections are formed and/or modified by adapting to the environment. For example, a newborn baby can't even focus. Most of its visual nervous system, including the visual "front end", the retina and several stages following that are developed in the first few weeks. The development is strongly influenced by the environment. Experiments on monkeys reveal that a monkey raised in an environment with a bias of more vertical bars than horizontal bars will have more neurons reponding to vertical stimuli due to the projection pattern of the inter-layer connections tending to be vertical selective (Hubel, 1988). In some sense, the "operating system" itself is a result of adaptation or self-organization.

Learning is another feature consequence of adaptation. Researchers have trained pigeons to do certain pattern recognition tasks which would not occur in a natural

scene — to pick out photos in which a certain person appears. The pigeons did a strikingly good job (Herrnstein, Loveland, Cable, 1976). No digital computer with known algorithm can perform as well. An animal with a brain which does not learn will have a difficult time to surviving in a changing environment. The fact is that the brains which are most capable of learning are dominating this world.

The synaptic connection change interacts with neuron activity change, and contributes to the performance of general computation tasks. In case of short term memory and facilitation, the two dynamics of synapse change and activity change are in a similar time scale, and it becomes important to consider the two dynamics at the same time in order to understand how the computation is done.

The main purpose of the research described in this thesis is to study the neuron network as a dynamic system with both neuron activity change and connection change while the system is under the influences of environment inputs to the system, i.e., to study the neuron network with adapting synapses in a changing world.

Outline

Two kinds of dynamic processes take place in neural networks. One is the change of activity of each neuron. The other is the change of connection between neurons. When neural network is learning or developing, both of these two processes take place and interact with each other, which, we believe, is the basic scenario of neural network dynamics (Dong, 1991).

It is believed in physics that certain general behavior can even emerge from relatively simple model. One of the simple models of neuron networks is Hopfield model (Hopfield, 1982, 1984). It states that the input to a neuron is linear summation of activities of other neurons and environmental input, the input changes with a relaxation time and the activity of the neuron sigmoid input-output relation to the input. One of the simplest yet most important adaptation rules is Hebbian rule (Hebb, 1948).

It states that the connection between two neurons is positive correlated to the correlation of their activities. In Chapter 2, we laid out the theoretical bases of neuron network dynamics incorporating simultaneously both dynamics as a mechanism both for developing and learning in a neuron network.

By using the abstracted properties of neuron activation and connection modification, some interesting developing or learning features appear. Under certain conditions the network develops connections according to the correlation pattern of the environment inputs. Under other conditions the network develops connections corresponding to single environment input.

A specific correlation pattern — center-surround environmental correlated inputs — is used Chapter 3. The network can learn either the center-surround correlation as the interconnections between neurons, or oriented stripes, depending on the different parameters in the dynamic equations.

It is useful to study in some detail the structure of a neural network. A real biological neuronal network has layered structures. One layer of neurons supplies the primary inputs of another layer; this is so called feedforward connections which contribute to transfer information from one stage to the next. Within each layer (stage), neurons have massive interconnections which also contribute to the information processing. In fact, in any area of the cortex, the majority of synapses come from axons originating within the same layer. This kind of connection is both feedforward and feedback.

Given the widespread interest in the mammalian visual system from both the neuroscience and the computer vision community, we felt that it would be useful to apply our dynamic model to this particular system. A great amount of biological data is available, but meanwhile there is great controversy as to the wiring underlying orientation selectivity in mammalian visual cortex.

The structures of cat visual system are studied in Chapter 4, 5 and 6, extending from the retina to the lateral geniculate nucleus and then to the area 17 of the cortex. These are the early stages of visual information processing. We emphasize the crucial nature of inhibition from interconnected neurons in shaping orientation selectivity.

In Chapter 7 we discuss the developmental issue of the interconnection in the mammalian visual system. The questions left in Chapter 3 about the application of the theory to a biological system will be addressed here. The main developmental character will remain for a less idealized system with not-quite symmetric connections, a system driven by action potential signals and a system with separated inhibitory and excitatory connections. Further, we study the emerging global structure of orientation columns. Again, we emphasize the crucial role played by the interconnections.

A program is listed in Appendix A to illustrate how the simulation of the network was done. This program is the one used to simulate the results in Chapter 2. A simpler model of orientation selectivity is presented in Appendix B which emphasize the important role of the interconnections to the emerging property of a layered network. Dynamics of feedforward connections is discussed briefly in Appendix C to tell the whole story about orientation selectivity.

Overall, the thesis can be divided into two major parts : 1) Chapter 2, 3 and 7 are about the development of orientation selective structures, which can be understood fairly well without going into details of biology; 2) Chapter 4, 5 and 6 are about the function of the orientation selective structures, where physics approach is used to model biology more closely. What appears to us is a clearer picture about one neural network, a small piece of brain. What excites us is a bit more understanding about the mystery of mind.

2.1

Dynamic Properties of Neural Networks with Adapting Synapses

Introduction

Model neural networks, abstractions from neurobiology, are conceived in terms of two different kinds of variables. One class of variables represents the activity of the nerve cells, or "units". The other class of variables describes the synapses, or connections, between the nerve cells. A complete model of an adaptive neural system requires two sets of dynamical equations, one for each class of variables, to specify the evolution and behavior of the neural system.

Most prior research has focussed separately on one or the other of these sets of equations. For example, work on associative memory and optimization involving feedback networks has chiefly asked questions about the dynamics of the activity of neurons with a fixed set of connections (Hopfield, 1982, 1984; Wehmeier, Dong, Koch, and Van Essen, 1989). Studies of adaptive feedforward networks designed to imitate the development of connectivity patterns in the visual cortex have ignored all real dynamics of neural activity, and involve only the dynamics of synapse changes (Bienenstock, Cooper and Munro, 1982; Linsker, 1986; Miller, 1989).

This research develops aspects of the theory of feedback networks in which both kinds of dynamics are simultaneously important. It shows that there is a class of systems which have a Lyapunov or "energy" functions behind the joint dynamics, which lead to stability of the combination of synapses and activities. These ideas are then applied, both in mathematics and in simulations, to the problem of the development of synaptic connections in the visual cortex, which have previously been studied only with feedforward networks (essentially static) and synapse dynamics.

The dynamical model

The equations describing the dynamics of the activity of the neurons will be

described as follows, in the notation of Hopfield (1984). A neuron i is described as an input-output device, with the output V_i a function of the input u_i. Thus

$$V_i = g_i(u_i) \qquad [2.1]$$

The typical input-output relation is monotonic and sigmoid, with asymptotes V^+ and V^-. The strength of the synaptic connection from neuron j to neuron i is T_{ij}. The set of equations describing the evolution of the state of activity of the neurons is

$$a_i \frac{du_i}{dt} = -u_i + \sum_j T_{ij} V_j + I_i \qquad [2.2]$$

in which a_i is a time constant and I_i represents any additional inputs to the ith neuron besides those described by connection matrix T_{ij}. For a typical layered neuron network, the input or external driving force I_i represents the influence from neurons of other layers and/or from the outside world.

If the connections are fixed, the T_{ij} do not depend on time, and this is the only set of dynamical equations. However, if the synapses adapt, a second set of equations describes the way the synapses change with time due to neuronal activity. Many synaptic change rules have been used by others (Minsky, 1969; Kohonen, 1984; Rumelhart, 1986). Ours is closely linked to the Hebb (1948) idea, but is in detail a novel variant, and will next be described.

The basic idea described by Hebb was that the change of a connection strength should be due to correlated activity of the pre- and post-synaptic cells. The two components of this idea are that learning should be local (the description of synapse change should involve only the activity of the two neurons adjacent to the synapse), and that the strength of what we would now term an excitatory synapse should tend to increase when there is a positive correlation between the activity of its two particular cells. Thus the strength T_{ij} of a synapse which is capable of change (not all synapses

need to be adaptable, nor need an adaptable synapse be changeable throughout the life of an animal) will depend on time through a set of equations which involve the neuronal activity.

The complete set of variables which describes the state of the network then becomes $\{V_i(t), T_{ij}(t)\}$. Let the connection variable T_{ij} be a bounded, continuous and monotonic increasing function of the "recent" correlation s_{ij} of the neuron activities V_i and V_j:

$$T_{ij} = H_{ij}(s_{ij}) \qquad [2.3]$$

The following quantity is used as the measure of the recent correlation between $V_i(t)$ and $V_j(t)$:

$$s_{ij}(t) = \frac{1}{B_{ij}} \int_{-\infty}^{t} e^{\frac{x-t}{B_{ij}}} V_i(x) V_j(x) dx \qquad [2.4]$$

in which B_{ij} is a time constant and $e^{\frac{x-t}{B_{ij}}}$ is a weight factor. Because an exponential kernel is used in Equation 2.4, the integral equation is equivalent to the differential equation

$$B_{ij} \frac{ds_{ij}}{dt} = -s_{ij} + V_i V_j \qquad [2.5]$$

This equation represents Hebbian learning with a decay term. If the time constants $B_{ij} = B_{ji}$, then s_{ij} and s_{ji} are the same for all sufficiently long times; any initial bias must die out in a time of the order of B. Then $s_{ij}(t) = s_{ji}(t)$. If also $H_{ij}(x) = H_{ji}(x)$ (for example, if all input functions $H_{ij}(s)$ have the same form), then $T_{ij}(t) = T_{ji}(t)$ for all t. This learning rule implies that T_{ij} will always be symmetric, an essential point in the following energy analysis.

Lyapunov function analysis

The convergent flow to stable states is a fundamental feature of this system of joint evolution of the activity and the connections. We will show this by constructing

a bounded "energy function" which always decreases in time under the equations of motion of the system.

In a system with a constant symmetric T (i.e., $T_{ij} = T_{ji}$), one can construct an energy function which is always decreasing in time:

$$E = -\frac{1}{2}\sum_{ij} T_{ij} V_i V_j + \sum_i \int u_i dV_i + \sum_i \int I_i dV_i \qquad [2.6]$$

Its time derivative is

$$\begin{aligned} \frac{dE}{dt} &= \sum_i \frac{\partial E}{\partial V_i}\frac{dV_i}{dt} = -\sum_i (-u_i + \sum_j T_{ij} V_j + I_i)\frac{dV_i}{dt} \\ &= -\sum_i a_i \frac{du_i}{dt}\frac{dV_i}{dt} = -\sum_i a_i g_i^{-1\prime}(\frac{dV_i}{dt})^2 \end{aligned} \qquad [2.7]$$

Since the inversed gain function $g_i^{-1}(V_i)$ is a monotonic increasing function and the time constant a_i is a positive number, therefore

$$\frac{dE}{dt} \leq 0 \qquad \text{and} \qquad \frac{dE}{dt} = 0 \quad \rightarrow \quad \frac{dV_i}{dt} = 0 \quad \text{for all } i, j \qquad [2.8]$$

This equation and the boundedness of E guarantee that the state flow in the continuous state space of $\{V_i\}$ terminates in a nearby stable state, i.e., a nearby local minimum of the energy function.

One useful T_{ij} matrix is constructed as

$$T_{ij} = \sum_m^M V_i^m V_j^m \qquad [2.9]$$

in which $V_i^m = \pm 1$, and $\mathbf{V^m}$ is the mth pattern vector stored by the network. Such a T matrix is useful for associative memory, and can be generated by a Hebbian mechanism. But in most of the literature of feedback associative memories, the "writing" of T_{ij} and the recall of memories are separate events, and their dynamics is not combined.

In the model including synapse dynamics, the set of variables $\{V_i(t),\ T_{ij}(t)\}$ are used to describe the state of the network which is undergoing both kinds of dynamic processes at the same time. The complete set of the dynamic equations is

$$\begin{aligned} a_i\frac{du_i}{dt} &= -u_i + \sum_j T_{ij}V_j + I_i \\ V_i &= g_i(u_i) \\ B_{ij}\frac{ds_{ij}}{dt} &= -s_{ij} + V_iV_j \\ T_{ij} &= H_{ij}(s_{ij}) \end{aligned} \qquad [2.10]$$

Define

$$L = -\frac{1}{2}\sum_{ij} T_{ij}V_iV_j + \sum_i \int u_i dV_i + \sum_i I_iV_i + \frac{1}{2}\sum_{ij}\int s_{ij}dT_{ij} \qquad [2.11]$$

Elementary differentiations and substitutions yield

$$\begin{aligned} a_i\frac{du_i}{dt} &= -\frac{\partial L}{\partial V_i} \\ B_{ij}\frac{ds_{ij}}{dt} &= -\frac{\partial L}{\partial T_{ij}} \end{aligned} \qquad [2.12]$$

Therefore,

$$\begin{aligned} \frac{dL}{dt} &= \sum_i \frac{\partial L}{\partial V_i}\frac{dV_i}{dt} + \sum_{ij}\frac{\partial L}{\partial T_{ij}}\frac{dT_{ij}}{dt} + \sum_i \frac{\partial L}{\partial I_i}\frac{dI_i}{dt} \\ &= -\sum_i a_i\frac{du_i}{dt}\frac{dV_i}{dt} - \sum_{ij} B_{ij}\frac{ds_{ij}}{dt}\frac{dT_{ij}}{dt} + \sum_i V_i\frac{dI_i}{dt} \\ &= -\sum_i a_i g_i^{-1\prime}(\frac{dV_i}{dt})^2 - \sum_{ij} B_{ij}H_{ij}^{-1\prime}(\frac{dT_{ij}}{dt})^2 + \sum_i V_i\frac{dI_i}{dt} \end{aligned} \qquad [2.13]$$

When the inputs I_i are constant,

$$\frac{dL}{dt} = -\sum_i a_i g_i^{-1\prime}(\frac{dV_i}{dt})^2 - \sum_{ij} B_{ij}H_{ij}^{-1\prime}(\frac{dT_{ij}}{dt})^2 \qquad [2.14]$$

The inversed gain functions $g_i^{-1}(V_i)$ and $H_{ij}^{-1}(T_{ij})$ are monotonic increasing functions, and the time constant a_i and B_{ij} are positive numbers. Therefore

$$\frac{dL}{dt} \le 0 \qquad \text{and} \qquad \frac{dL}{dt} = 0 \quad \rightarrow \quad \frac{dV_i}{dt} = 0 \quad \text{and} \quad \frac{dT_{ij}}{dt} = 0 \quad \text{for all } i,j \qquad [2.15]$$

These equations and the boundedness of L show that L is a Lyapunov function of the system (Wiggins, 1988). The time evolution of the state in the space of $\{V_i(t), T_{ij}(t)\}$ leads to attractors which are at local minima of L.

Stable points

Let $\{V_i, T_{ij}\}$ and correspondingly $\{u_i, s_{ij}\}$, be a time-independent (steady state) solution of Equation 2.10 (i.e. a fixed point). Consider the motion of a small perturbation $\{\delta u_i, \delta s_{ij}\}$ around that solution.

$$\begin{aligned} a_i \frac{d\delta u_i}{dt} &= -\delta u_i + \sum_j (T_{ij} g'_j \delta u_j + H'_{ij} V_j \delta s_{ij}) \\ B_{ij} \frac{d\delta s_{ij}}{dt} &= -\delta s_{ij} + V_i g'_j \delta u_j + g'_i V_j \delta u_i \end{aligned} \qquad [2.16]$$

in which $\{V_i, T_{ij}\}$ and $\{g'_i, H'_{ij}\}$ take the values of the fixed point. If $\{\delta u_i, \delta s_{ij}\}$ approach zero asymptotically, this fixed point is stable.

In the space of $\{V_i, T_{ij}\}$, suppose the origin, i.e., $\{V_i = 0, T_{ij} = 0\}$, is a fixed point (which it is in the special case $g(0) = 0$ and $H(0) = 0$). Equation 2.16 then becomes

$$\begin{aligned} a_i \frac{d\delta u_i}{dt} &= -\delta u_i \\ B_{ij} \frac{d\delta s_{ij}}{dt} &= -\delta s_{ij} \end{aligned} \qquad [2.17]$$

showing that the origin is stable.

Similarly, suppose a corner in $\{V_i, T_{ij}\}$ space is a steady state solution. (In the high gain limit, all steady state solutions which are not at the origin are at corners of the hypercube $\{V_i \to g^{\pm}, T_{ij} \to H^{\pm}\}$, where $g^{\pm}$ and $H^{\pm}$ are the upper (+) and lower (−) bound of the monotonic increasing function $g(u)$ and $H(s)$.) Again

$$\begin{aligned} a_i \frac{d\delta u_i}{dt} &\to -\delta u_i \\ B_{ij} \frac{d\delta s_{ij}}{dt} &\to -\delta s_{ij} \end{aligned} \qquad [2.18]$$

so those corners are also stable.

For an illustrative special case, consider two neurons (V_1 and V_2) and one symmetric connection T.

$$\begin{aligned} a\frac{du_1}{dt} &= -u_1 + TV_1 \\ a\frac{du_2}{dt} &= -u_2 + TV_2 \\ V &= F(gu) \\ B\frac{ds}{dt} &= -s + V_1V_2 \\ T &= F(Hs) \end{aligned} \qquad [2.19]$$

in which g and H are constants, and piecewise linear functions are used for the nonlinear functions, defined by

$$F(x) = \begin{cases} +1, & \text{if } x > +1; \\ x, & \text{if } -1 < x < +1; \\ -1, & \text{if } -1 > x. \end{cases} \qquad [2.20]$$

Therefore

$$L(V_1, V_2, T) = -TV_1V_2 + \frac{1}{2g}V_1^2 + \frac{1}{2g}V_2^2 + \frac{1}{2H}T^2 \qquad [2.21]$$

In the space of $\{V_1, V_2, T\}$, the origin $(0,0,0)$ is a fixed point and if $g > 1$ and $H > 1$ the corners $(1,1,1)$, $(-1,-1,1)$, $(1,-1,-1)$ and $(-1,1,-1)$ are also time-independent solutions of Equation 2.19. (Note that out of eight corners only four of them are fixed points.) All those fixed points are stable points, point attractors for the motion of the dynamic system. (It can be generally proved only those fixed points satisfying $T_{ij} = sign(V_iV_j)$ and the origin are stable points.) Figure 2.1 shows the function $L(V_1, V_2, T)$ exhibiting a central minimum and corner minima in a reduced space ($T = F(HV_1V_2)$).

The stability of these points should be considered in a context of learning. First, the origin is the state of unlearned connections with no neuronal activities. It is stable, ensuring that a small perturbation from a weak signal will not result in learning

anything. Second, after the network learns a pattern, forming connections which are the outer product of a memory vector with itself, that corner is stable. The stability of that corner makes the network disregard other incoming patterns unless they are very strong, which will be discussed further in the next section.

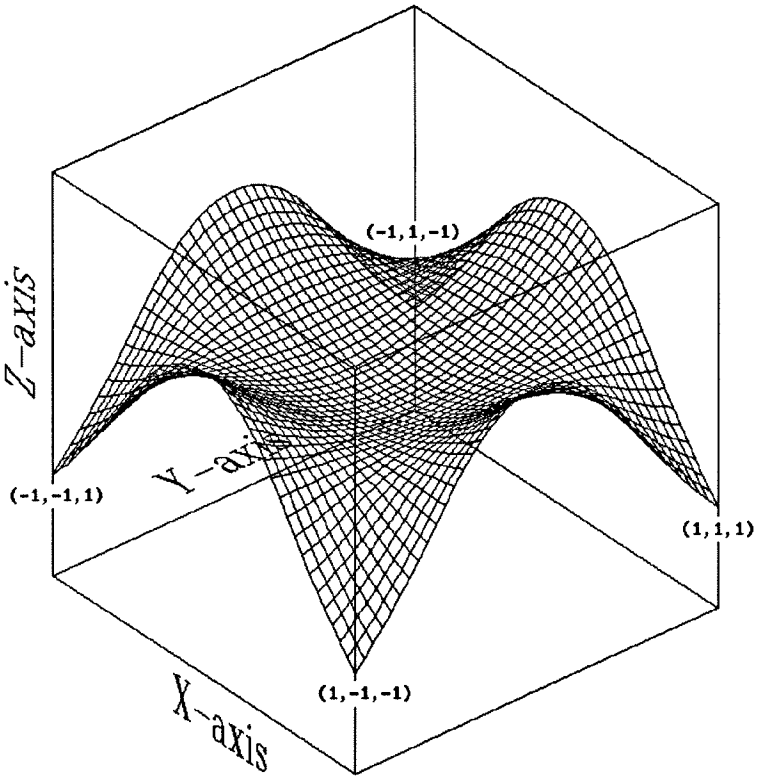

Figure 2.1 The Lyapunov function is drawn in $\{V_1, V_2\}$ space (along the surface $s = V_1 V_2$ in $\{V_1, V_2, T\}$ space). The constants are chosen $g = 2.0$, $H = 2.0$ (what is not shown here is when $g < 1$ and $H < 1$ only the origin is stable point). The X-axis is V_1, the Y-axis V_2 and Z-axis the Lyapunov function. The origin and the four corner points are local minima.

Behavior during learning

I^k defines a set of K input patterns (k=1,2, ... , K). During learning, the time-dependent input $I_i(t)$ is generated by switching sequentially from one input vector to another. To make the system have a plausible correspondence with developmental neurobiology, the time duration of each exposure t_h is longer than the neural activity time constant a_i, but shorter than the time necessary to change the connections

appreciably, i.e., $t_h << B_{ij}$.

During learning, the neural activity arising from the state of activity of the system produces the synaptic changes. The state of the neuron activity is driven by the input signals $I_i(t)$, but not only by it. After learning has proceeded for a while, the synaptic connections become appreciable, and the activity becomes influenced both by the sequence of patterns and by the partially learned connections. The state of the network changes according to the set of Equation 2.10.

In the following study, the gain functions are

$$g_i(x) = F(gx) \qquad [2.22]$$

$$H_{ij}(x) = F(Hx) \qquad [2.23]$$

in which g and H are constants (gain) and $F(x)$ is defined in Equation 2.20. By a simple variable transformation, $u_i \rightarrow gu_i$ and $s_{ij} \rightarrow Hs_{ij}$,

$$\begin{aligned} a_i \frac{du_i}{dt} &= -u_i + g \sum_j T_{ij} V_j + AI_i \\ V_i &= F(u_i) \\ B_{ij} \frac{ds_{ij}}{dt} &= -s_{ij} + HV_i V_j \\ T_{ij} &= F(s_{ij}) \end{aligned} \qquad [2.24]$$

in which a scale constant A is introduced to the input current I_i.

When the input is strong compared to the signals coming by way of the interconnections, the neuron activities V_i will be largely determined by current I_i. For the period of time t_0 to $t_0 + t_h$ when pattern I_i^k presents, $V_i(t)$ is approximately equal to $F(AI_i^k)$. Since $t_h << B_{ij}$, the first order approximation will give

$$s_{ij} = \frac{H}{K} \sum_{k=1}^{K} F(AI_i^k) F(AI_j^k) \qquad [2.25]$$

in which K is the number of input patterns. When $A > 1$ and $H = 1$, this will result in an T_{ij} which is the average over K patterns of the outer product of vectors I^k as shown in Figure 2.2.

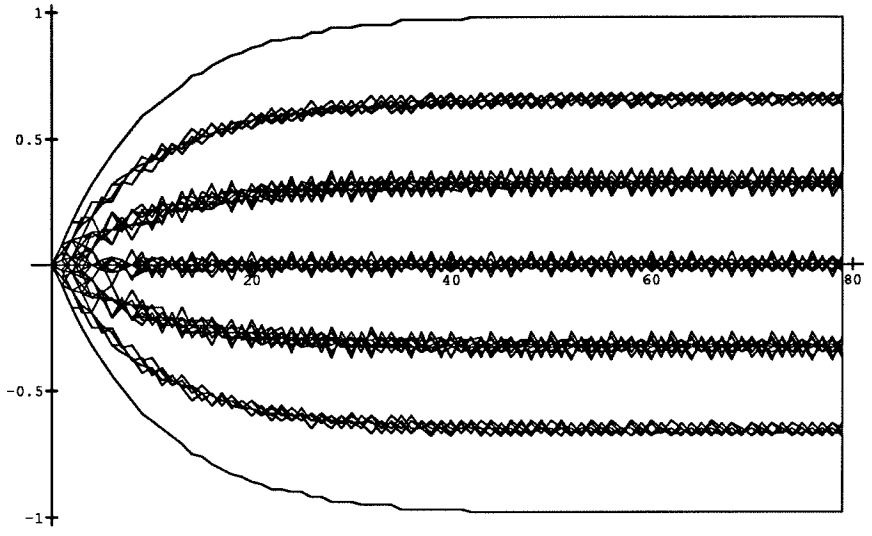

Figure 2.2 The strengths of the developing connections as a function of time for an 81 neurons network when input signals dominate. (Only the connections to/from neuron 1 are plotted in the graph.) Six random input $(-1, 1)$ vectors which have correlation (inner product) between them no larger than 3 were presented to the network. The learning parameters were $a_i = 1.0$, $B_{ij} = 300.0$ (the unit along time axis is in $0.1B_{ij}$), $g = 0.3$, and $H = 1.0$. The input pattern changes every $t_h = 12.0$ and loops through all the six memory vectors which have a large amplitude ($A = 30.0$). The connections strengths converge to seven values, 6/6, 4/6, 2/6, 0, $-2/6$, $-4/6$ and $-6/6$, which correspond to the values of average over the outer product of the input pattern set ($T_{ij} = \frac{1}{6}\sum_{k=1}^{6} I_i^k I_j^k$). The network memorizes all 6 of the input vectors. The simulation program is listed in Appendix A.

Figure 2.3 shows the development of connection strengths for parameters such that the connections can become large. Even when the connections ultimately become very strong, they are weak at the beginning of learning or development. Thus at the beginning of learning, the $T_{ij}(t)V_j$ term contributes much less than the input I_i in the neuronal dynamics equation. The neuronal activities will take on a pattern similar to the input $\{I_i\}$, and the learning will be very much like the sum of outer product

method. This case is illustrated in Figure 2.3, where before time step 30 the learning curves are very similar to those of Figure 2.2.

When the contribution from the interconnections becomes comparable to that from the input (which happens when the network has partially learned connections as the summation over outer products), the bias of input I_i can no longer dictate the neuron state. When the connections become much larger, the small input I_i can even be ignored. As pointed out earlier, for this case the origin and some of the corners are the local minima in the landscape of L, so the flow will be attracted to those points. The initial learning with the relatively strong input influence will bias the L landscape, and this bias will determine the choice of broken symmetry solution. All connections ultimately go to a single magnitude and reflect the choice of a single corner in the L landscape. Figure 2.3 illustrates this occurrence.

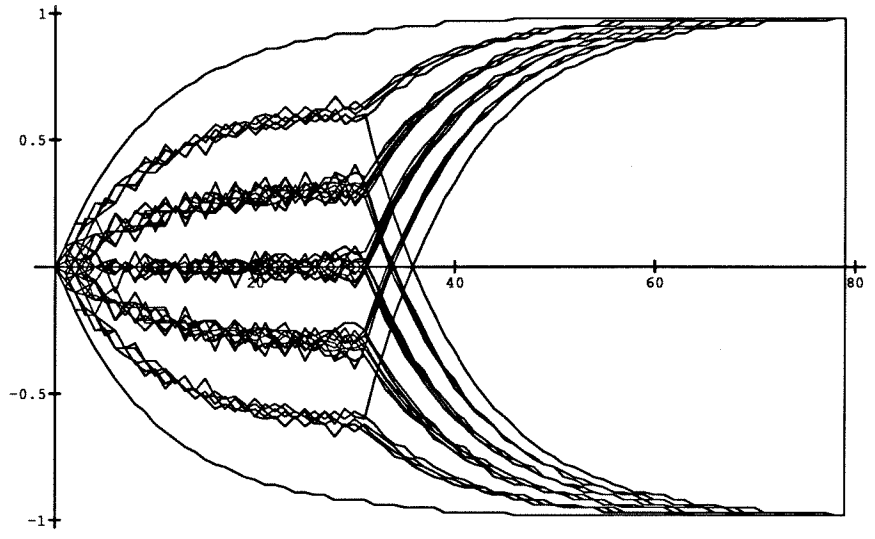

Figure 2.3 The strengths of the developing connections as a function of time in an 81 neuron network when the connections can become dominating. Compare this figure with Figure 2.2. (The connections to/from the same neuron as in Figure 2.2 are plotted.) The parameters are the same as in Figure 2.2 except that the input pattern strengths have been decreased by a factor of 10 ($A = 3.0$). The network here selects one input memory to memorize while the network of Figure 2.2. memorizes all six input vectors. Since at the very beginning the connections are small, in the energy E landscape the attractors of the six input

pattern are not deep and the influence of the interconnections does not contribute much. The early learned connections are similar to those which are learned with a high amplitude of input. The symmetry breaking happens at about $t = 3B_{ij}$.

After the network has selected a pattern, it becomes hard to switch between the learning patterns. This feature has two effects: the learning process is stable, and also, the network will be unable to learn any other pattern or to notice the inputs. The only way to get away from this state is to input a stronger pattern to drive the network out of the corner. These effects are not necessarily beneficial in a context of memory, but may be useful in the biological development of connectivity patterns.

3.1

Dynamic Properties of Neural Networks Dynamics of Connections

Application to a problem of development in the visual system

The ideas and equations presented in last chapter will now be applied to the development of orientation selectivity by a network of neurons representing the first stage of cortical visual processing in mammals. This case has been previously investigated chiefly with feed-forward networks (Linsker, 1986; Miller, 1989), while the actual neurobiology of visual cortex involves extensive feed-back circuitry (Gilbert and Wiesel, 1989; see Appendix B also).

The network is a two-dimensional spatial array of processing neurons, chosen to represent the earliest processing area in mammalian visual cortex. This cortical area receives primary input from the LGN (lateral geniculate nucleus). The LGN can for present purposes be also regarded as a two-dimensional array. The "center-surround" organization of the early visual system results in a pattern of connections such that in the absence of a visual stimulus, the noise output of an LGN cell is positively correlated with its nearby neighbors, and negatively correlated with its more distant neighbors (Hubel and Wiesel, 1961; Cleland, Dubin, and Levick, 1971; Shapley and Lennie, 1985). An important feature of the developing visual cortex is thus the fact that it receives a noise input which has a characteristic spatial correlation function like that of the LGN. The correlation function, in which the inputs to nearby neurons are correlated and the inputs to further away neurons are anti-correlated, is shown in Table 3.1. We will examine the effects of this noise on the development of interconnections between the array of processing neurons, and the effect of the developed connections on the processing done by this first layer of visual cortex.

Table 3.1 The correlation matrix of the inputs I_i. On the center pixel, the correlation of the same input to itself is scaled to 1.00. The general pattern is a center-surround structure with a positive correlation center and a negative

correlation surround. The mean is 0.10 (omiting the central point).

$$\begin{pmatrix} -0.19 & -0.17 & -0.11 & -0.10 & 0.01 & -0.10 & -0.11 & -0.17 & -0.19 \\ -0.17 & -0.15 & -0.07 & -0.05 & 0.02 & -0.05 & -0.07 & -0.15 & -0.17 \\ -0.11 & -0.07 & 0.01 & 0.10 & 0.23 & 0.10 & 0.01 & -0.07 & -0.11 \\ -0.10 & -0.05 & 0.10 & 0.35 & 0.54 & 0.35 & 0.10 & -0.05 & -0.10 \\ 0.01 & 0.02 & 0.23 & 0.54 & 1.00 & 0.54 & 0.23 & 0.02 & 0.01 \\ -0.10 & -0.05 & 0.10 & 0.35 & 0.54 & 0.35 & 0.10 & -0.05 & -0.10 \\ -0.11 & -0.07 & 0.01 & 0.10 & 0.23 & 0.10 & 0.01 & -0.07 & -0.11 \\ -0.17 & -0.15 & -0.07 & -0.05 & 0.02 & -0.05 & -0.07 & -0.15 & -0.17 \\ -0.19 & -0.17 & -0.11 & -0.10 & 0.01 & -0.10 & -0.11 & -0.17 & -0.19 \end{pmatrix}$$

The connections of one neuron to/from the others are only allowed within a small rectangular region centered on the neuron. All the connections start with strength equal to zero. Periodic boundary conditions are used on the horizontal and vertical boundaries of the $9x9$ array.

The set of variables $\{V_i(t),\ T_{ij}(t)\}$ are used to describe the state of the network which is undergoing the two kinds of dynamic processes at the same time. The set of the dynamic equations is the same as Equation 2.24.

$$\begin{aligned} a_i \frac{du_i}{dt} &= -u_i + g \sum_j T_{ij} V_j + A I_i \\ V_i &= F(u_i) \\ B_{ij} \frac{ds_{ij}}{dt} &= -s_{ij} + H V_i V_j \\ T_{ij} &= F(s_{ij}) \end{aligned} \qquad [3.1]$$

The input current I_i here is generated by weighted summation over an input layer of random noise ($+1$ and -1) signal. The weights are shown in the Table 3.2.

Table 3.2 The summation weight matrix. It is center excitatory and surround inhibitory. The correlation matrix calculated from this is shown in Table 3.1.

$$\begin{pmatrix} -1 & -1 & -1 & -1 & -1 & -1 & -1 & -1 & -1 \\ -1 & -1 & -1 & 1 & 1 & 1 & -1 & -1 & -1 \\ -1 & -1 & 1 & 1 & 1 & 1 & 1 & -1 & -1 \\ -1 & 1 & 1 & 1 & 1 & 1 & 1 & 1 & -1 \\ -1 & 1 & 1 & 1 & 1 & 1 & 1 & 1 & -1 \\ -1 & 1 & 1 & 1 & 1 & 1 & 1 & 1 & -1 \\ -1 & -1 & 1 & 1 & 1 & 1 & 1 & -1 & -1 \\ -1 & -1 & -1 & 1 & 1 & 1 & -1 & -1 & -1 \\ -1 & -1 & -1 & -1 & -1 & -1 & -1 & -1 & -1 \end{pmatrix}$$

Development of a center-surround structure

A center-surround symmetric structure is formed when the input is strong compared to the interconnections. This kind of structure has positive interconnections with square symmetry to nearby neurons, and negative connections with square symmetry to neurons which are further away. The connection pattern is "circularly symmetric", i.e, exhibits the highest symmetry possible given the square array arrangement. In this case the neuron activities V_i are largely determined by inputs I_i. Thus the correlation function s_{ij} of neuron i and neuron j will resembles the correlation of the inputs to these two neurons. Figure 3.1 and Table 3.3 show the learning results.

The learning captured the correlation pattern of the input into the connections, and is organized into a center-surround structure. The connection strength of the learned center-surround structure and the calculated autocorrelation function of the input current have in most places the same signs but differ in magnitude, a not surprising consequence of the nonlinearity of the dynamical equations. The comparison is shown in Table 3.1 and the following Table 3.3.

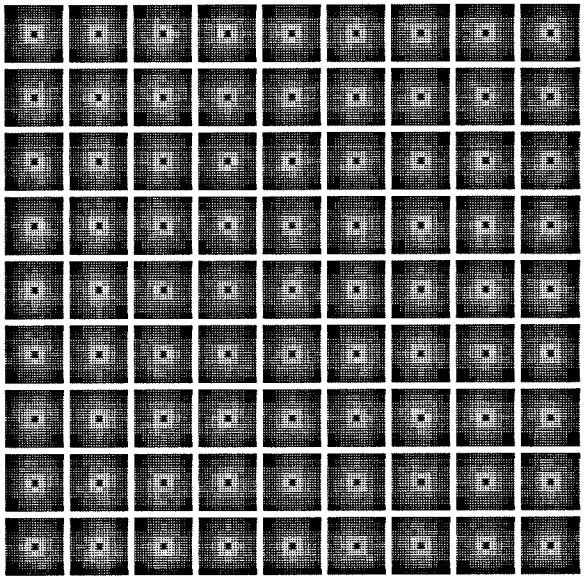

Figure 3.1 Each large square, composed of $9x9$ pixels, describes the connections of one of the 81 neurons to the others. Each pixel has a blackness which describes the strength and sign of the connection of this particular cell to another cell in the array. White represents positive connections, black represents negative connections. In this case, of a relatively large input strength compared to the interconnections, a square-symmetric center-surround structure of connections is developed. The parameters used in this simulation are $a_i = 1.0$, $B_{ij} = 300.0$, $g = 0.3$, $H = 2.0$, and amplitude of the input currents $A = 10.0$. The values of the connections (averaged over all neurons) are shown in Table 3.3.

Table 3.3 The learned receptive field when the input is strong $A = 10.0$. It is a center-surround structure with excitatory connections in the center and inhibitory connections in the surround. There is no connection to the neuron itself (on the center, it is shown as 0.00). The mean is -0.66 The regions of '+' and '-' are almost the same as of the input correlation shown in Table 3.1. The patterns have been averaged over all the 81 neurons.

−0.95	−0.60	−0.26	−0.06	0.01	−0.07	−0.27	−0.60	−0.95
−0.57	−0.43	−0.12	0.06	0.12	0.06	−0.13	−0.45	−0.57
−0.22	−0.10	0.14	0.32	0.39	0.33	0.14	−0.10	−0.23
−0.03	0.10	0.35	0.76	0.91	0.76	0.35	0.10	−0.03
0.03	0.17	0.43	0.92	0.00	0.92	0.43	0.17	0.03
−0.03	0.10	0.35	0.76	0.91	0.76	0.35	0.10	−0.03
−0.23	−0.10	0.14	0.33	0.39	0.32	0.14	−0.10	−0.22
−0.57	−0.45	−0.13	0.06	0.12	0.06	−0.12	−0.43	−0.57
−0.95	−0.60	−0.27	−0.07	0.01	−0.06	−0.26	−0.60	−0.95

The influence of the center-surround structure on processing

After the formation of the center-surround structure, we tested the *neuronal activity* dynamics starting from a small random activity. The stable states are patterns of horizontal or vertical bars, at any translational position. The dynamics starting from random states exhibited equal probabilities of ending up in a pattern of horizontal or vertical bars, and at all positions.

The following mathematical analysis indicates why these are the stable patterns. With the periodic boundary conditions, a two-dimensional Fourier analysis on the neuronal dynamic equation can be done, with an assumed center-surround connection G(x,y) as the (initially learned) connection strength for all of the neurons. The equation for neuronal activities V_i is

$$\frac{du_i}{dt} = -u_i + g\sum_{ij} V_j T_{ij} \qquad [3.2]$$

In the linear range $u_i = V_i$ so

$$\frac{dV_i}{dt} = -V_i + g\sum_{ij} V_j T_{ij} \qquad [3.3]$$

and in a continuous limit in two-dimensional space becomes

$$\frac{dV(x,y)}{dt} = -V(x,y) + \int\int G(x-x', y-y')V(x',y')dx'dy' \qquad [3.4]$$

After the Fourier transformation,

$$\frac{dF(V)}{dt} = -F(V) + F(G)F(V) \qquad [3.5]$$

Those modes with $F(G) > 1$ will exponentially grow; those with $F(G) < 1$ will exponentially decay with time. The biggest $F(G)$ mode will dominate at long time. If there are several modes which have the similar large $F(G)$, they compete with each other when nonlinearities become important.

The form of $F(G)$ are easily illustrated by using a DOG (difference of Gaussian) as the $G(x, y)$ function. The transformation into the frequency space yields another DOG but upside down, as shown in Figure 3.2. The peak value is the same along all possible wave vector directions.

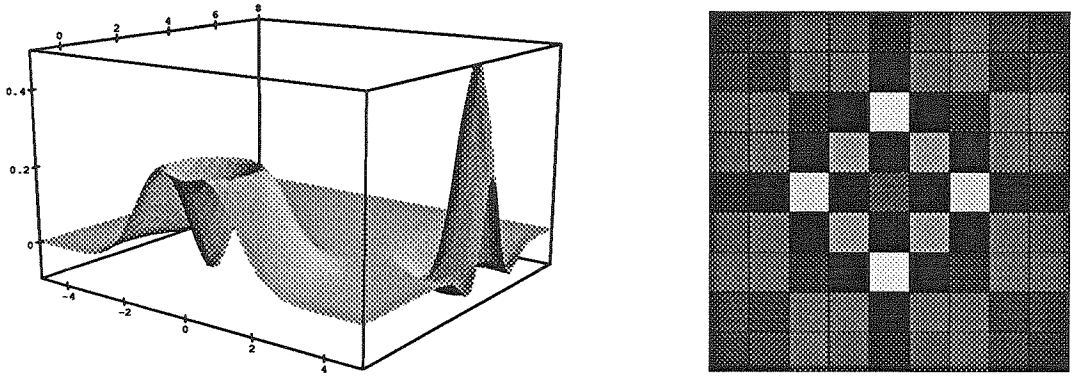

Figure 3.2 On the left is the Fourier transform of ideal DOG (difference of Gaussian) receptive field: $exp(-(x^2+y^2)/2)-exp(-(x^2+y^2))$. The DOG receptive field in x, y space is also shown at the left, with an origin at $(4.5, 4.5)$: $exp(-((x-4.5)^2+(y-4.5)^2)*2)-exp(-((x-4.5)^2+(y-4.5)^2))/2$. It is symmetric for all orientations. On the right is the Fourier transform of the learned center-surround connections (Table 3.3). The horizontal and vertical oriented modes have the biggest values. The wavelength is 9.

For the discrete center-surround structure, the Fourier transformation of the learned kernel has its biggest $F(G)$ in the vertical and horizontal directions (Figure 3.2, right). The next biggest ones at 45 degrees are much smaller (5.4/2.7) and all the others are smaller than 1. $F(G)$ is not isotropic since the chosen geometry of our system is a cubic structure, but it is identical for the vertical and horizontal directions. For orientation selectivity (which is characteristic of cells in primary visual cortex) this symmetry must be broken.

Breaking the symmetry

When the amplitude of the input is low, the network develops further. In the early stage of the learning process, it exhibits features similar to the center-surround case just described; the neuronal states resemble the input patterns changing with time,

and the connections from one neuron to the others becomes excitatory for nearby cells and inhibitory for further away ones. But when the connections grow stronger, the neuronal state begins to spend more and more time in those patterns resembling horizontal and vertical bars at various possible positions, with the interconnections preserving the center-surround structure. Ultimately, when this tendency has grown strong, because a little more time is spent by chance in a particular one of these patterns, the connections become slightly biased to that activity state. This state, as a result of learning, becomes an even deeper attractor and the fluctuation grows. Finally the neuronal excitation pattern stays in only one of these states, and the interconnections grow to reflect that single pattern. Figure 3.3 shows two typical symmetry-breaking results.

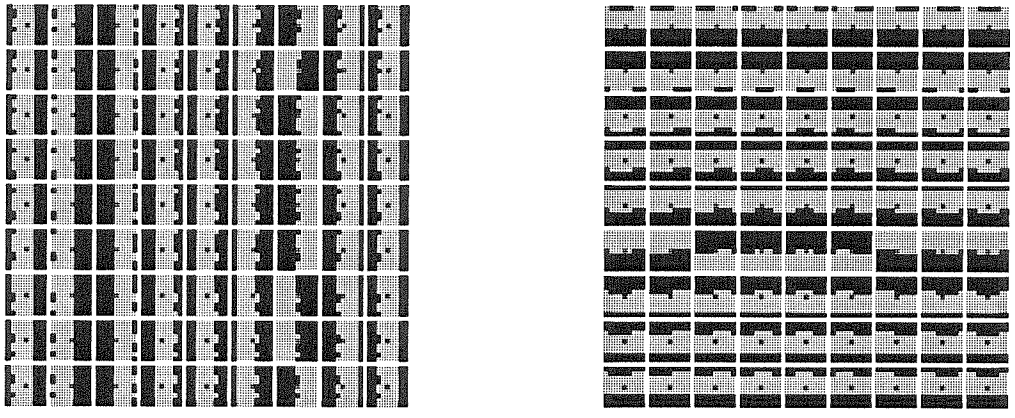

Figure 3.3 The network no longer preserves the center-surround structure. The symmetry about the orientation is broken. The figure on the left shows a structure of vertical preference in which each neuron connects to other neurons with vertical excitatory and inhibitory bands. The figure on the right shows a structure of horizontal preference with horizontal excitatory and inhibitory bands. All the parameters are the same as in Figure 3.1 except that the magnitude of input currents is smaller $A = 1.2$ compared to $A = 10.0$ in Figure 3.1. Both structures have a period of 9 as expected from Figure 3.2.

The corresponding time courses for the symmetry breaking results of Figure 3.3 are shown in Figure 3.4. The qualitative explanation for the broken symmetry result developed to explain Figure 2.3 applies to the more complicated case presented here.

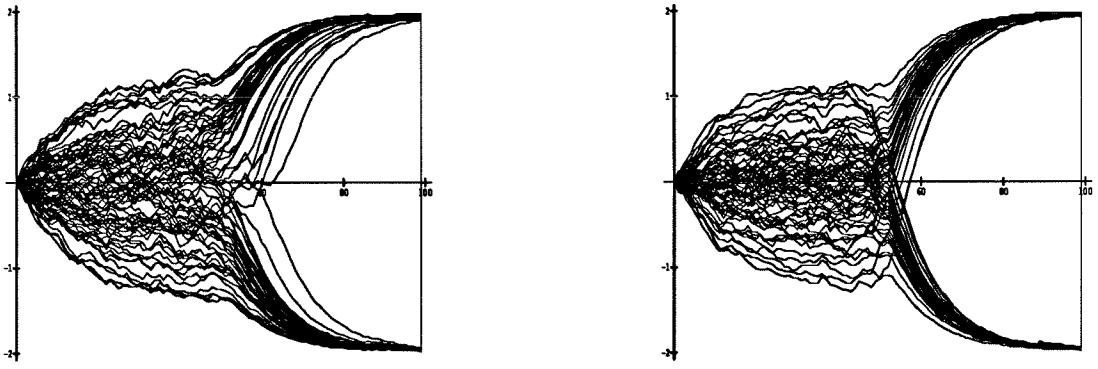

Figure 3.4 The time courses of connection development with a smaller amplitude of input $A = 1.2$ (the corresponding symmetry breaking results are shown in Figure 3.3). All the other parameters except A are the same as in Figure 3.1. The vertical axle indicates the strength of the connections from one neuron to the others, s_{ij}, note that $T_{ij} = F(s_{ij})$. (Only the connections of neuron 1 — the one at the up-left corner — are plotted.) At the beginning, the connections are developed very similar to the center-surround structure as shown in Figure 3.1. At later stage, about $t = 6Bij$, the symmetry about vertical and horizontal orientations is broken. The network flows to one of the structures with orientation preference.

Discussion

This kind of dynamical system has the unique feature of learning the correlation of input vectors under certain conditions and selecting a unique final learning result under other conditions. It is an example of "symmetry breaking" since there are several equivalent patterns possible from which it chooses one. When these dynamics was used to simulate the development of visual cortex connections, it first developed a center-surround form of connections, which is rotationally symmetric and has no chosen orientation. At a later stage, the orientation symmetry is broken, and an interconnection structure of oriented stripes develops.

In a typical neurobiological systems, the axons from one particular neuron usually form either excitatory or inhibitory connections to other neurons, but usually do not produce both kinds from a single neuron. Our model has used a single class of neuron which can form both excitatory and inhibitory connections. However, within the same

layer of cortex, there are often many interneurons connecting between other neurons. Our simplified model neuron could be viewed as representing a group of neurons; the input as the total input to that group and the output as the total output from that group. Similarly, the model connections can represent the total effect of one group of neurons on the others, including effects of interneurons. In such a sense, the model described can have a mathematics in plausible correspondence to neurobiology. This simplification of a single cell type and synapses of both signs has been much used in the modeling literature (Cohen and Grossberg, 1983; Hopfield, 1984; Kohonen, 1984; Rumelhart, 1986).

Studies of the development of early vision pathways with a more biological plausible model will be presented in the following chapters. But the basic feature of the dynamic as shown in this chapter. are preserved in spite of the addition of a wealth of observed electrophysiological and biophysical detail. Such a model with realistic dynamics of neuronal activity and synaptic connections learns the center-surround input correlation at the beginning of the development; keeps the correlation as the final learning result as long as the influence of the interconnections between neurons is not as strong as the inputs; and leads to the selection of an oriented pattern when the connections become strong enough at some learning stage. Thus by constructing an energy function based on symmetric connections, tractable mathematics has been constructed to understand a far more complex situation involving the development in a feedback network.

4.1

Modeling the Mammalian Visual System Review

Introduction

Given the widespread interest in the mammalian visual system from both the neuroscience and the computer vision community, we felt that it would be useful to apply our dynamic model to this particular system. Accordingly, we will describe detailed computer simulations of the early visual system in the cat, extending from the retina to the cortex. We will mainly discuss those biological aspects of the model that differ from previous chapters.

The principal aim of the work discussed here is to understand the neuronal circuitry underlying one of the most elementary properties of cells in the visual cortex of mammals, namely their preference to maximally respond to elongated bars of a certain orientation (for a review see Ferster and Koch, 1987). Cells can be so selective to this particular feature that a mere 10° angle displacement off the optimal orientation can reduce the maximal neuronal response by a factor of 2. The major question that any model of this phenomenon must address is how the response of cortical neurons is so critically dependent on the orientation, even though their input fibers, arising from cells in the lateral geniculate nucleus (LGN), are largely insensitive to orientation. The first—and most influential—model for orientation selectivity was proposed over twenty-eight years ago (Hubel and Wiesel 1962). It postulated that orientation selectivity arises from an appropriate alignment of synaptic input, such that cells whose receptive fields fall along a row excite the cortical cell (see Figure 4.1a).

Alternative models have invoked the use of inhibition to shape orientation tuning (Benevento, Creutzfeldt, and Kuhnt, 1972; Bishop, Coombs, and Henry, 1971; Braitenberg and Braitenberg, 1979; Morrone, Burr, and Maffei, 1982; Sillito, 1975; Sillito, Kemp, Milson, and Berardi, 1980; Heggelund, 1981, 1986; Orban, 1984): the cell is

prevented from firing at nonoptimal orientations by the action of inhibitory cortical interneurons. Current electrophysiological evidence is ambiguous, since support can be found for both classes of models.

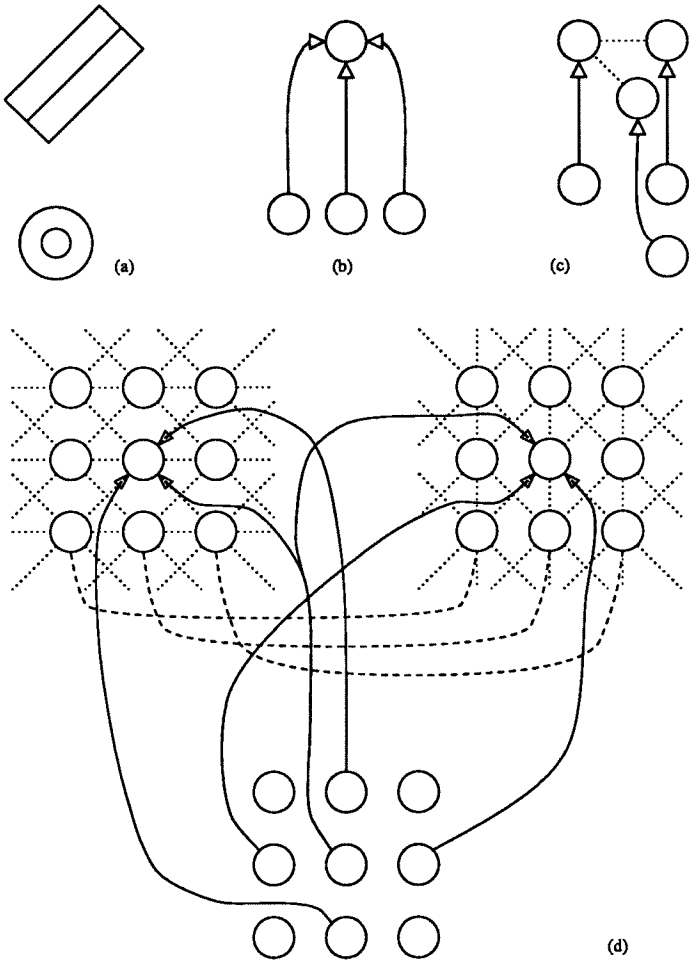

Figure 4.1 Wiring underlying orientation selectivity. (a) The concentric center-surround receptive field of geniculate cells contrasts with the elongated receptive fields of their cortical target cells. (b) The excitatory-only model put forth by Hubel and Wiesel (1962). A number of geniculate cells whose receptive fields are located along a given axis monosynaptically excite the cortical cell (open arrows). Here and in the following, only the excitatory centers of the geniculate cells are drawn. (c) One instance of an inhibitory-only model. Nonoriented cortical inhibitory (dotted lines) interneurons shape the orientation tuning of their target cell by suppressing its response at nonoptimal orientations. In the example shown, a horizontal bar will lead to activation of the interneuron, which will inhibit the vertically oriented cortical cell. (d) Eclectic model combining features of all models (Koch, 1987; Ferster and Koch, 1987). An excitatory Hubel and Wiesel type

of presynaptic arrangement is superimposed upon two inhibitory ones: reciprocal inhibition among similarly oriented cortical cells with spatially nonoverlapping receptive fields (dotted lines) and cross-orientation inhibition among orthogonal oriented cells (dashed lines). Due to the massive feedback among the participating cortical neurons, each cell acquires orientation selectivity via a collective computation.

These models are all instances of what Sejnowski, Koch, and Churchland (1988) term simplifying brain model, in that they show how orientation can be computed by invoking some of the principal structural features of the visual system, for instance center-surround receptive fields or the columnar organization of cortex. In other words, these models demonstrate that—given some general anatomical and physiological constraints—orientation can be computed in the manner postulated. However, in order to answer the question of which of these models is compatible with all of the relevant anatomical and physiological data, for instance with the large amount of divergence between the lateral geniculate nucleus and visual cortex or with the massive feedback within cortex, much more detailed simulations have to be attempted.

Since our detailed model of orientation selectivity incorporates a novel idea—that massive inhibitory cortical feedback can establish orientation selectivity without the need for nonoriented interneurons—we first evaluated its ability to correctly compute orientation using a very simplified model of neurons, based on Hopfield's elegant (1984) formalism (Appendix B). Given the great simplicity of this model—compared to our detailed simulations—it allows us to understand quickly some of the key aspects of the model without a heavy programming burden. For instance, massive inhibition among cortical cells (Figure 4.1d) establishes orientation selectivity for all cortical cells and enables the system to work over a large range of stimuli contrast values (Ferster and Koch, 1987). Questions such as the dynamic behavior of the system (for instance, the convergence time) cannot be tested on the other hand, since the Hopfield model does not account for dendritic and axonal propagation times. Moreover, detailed biophysical modeling directly mimics electrophysiological

results and can thus lead to new and very specific predictions, a crucial requirement of any successful theory. The price one pays for the added realism is a substantial increase in effort on the part of the programmer and the requirement of more powerful computers. The distinction between these two types of models is strongly reminiscent of Chomsky's (1965) distinction between competence and performance models in language understanding. A competence model mimics the behavior of the system, i.e., in producing oriented cells. The performance model does the same but in a manner commensurate with the internal properties of the system, i.e., in agreement with the anatomy and physiology.

Thus, to reiterate, the aim of the kind of very detailed model discussed in this chapter and Chapters 5 and 6 is not to demonstrate that any particular circuitry could lead to cortical orientation selectivity, but to study and gain an intuitive understanding—based on numerical simulations—of how the existent circuitry is responsible for establishing orientation tuning.

The Structure of the Model

Instead of modeling the visual system in a generic mammal, we chose to simulate the early visual pathway of the adult cat in view of the considerable amount of anatomical and physiological cat data available in the literature. Thus, unless otherwise mentioned, all experimental data will refer to the cat. Although the organization of the visual system of most mammals is similar, compared to say the visual system of birds, there do exist sufficient differences within mammals (for instance, all cells in area 17 in cat are orientation-selective while cells in layer IVc in monkey visual cortex are still of the center-surround type) to make it difficult to generate specific electrophysiological predictions for a given animal in such a generic model. In keeping with this approach, we chose to model only a small monocular patch of the visual system of the cat, instead of attempting to simulate the entire system. Given the limi-

tation on computing time, we feel that for our type of model a detailed, finely-grained model of part of the system is superior to a coarser description of the entire system. Accordingly, we simulate a small monocular patch of the X pathway comprising 2° by 2° of visual angle at approximately 4° eccentricity. This permits modeling a field of view adequate for the presentation of an effective visual stimulus without representing the high cone density within the *area centralis*. Rather than sparsely modeling the complete field of view, we are thus able to represent the neural circuitry with realistic cell densities, and at the appropriate scale, to specify individual connections. This 2° by 2° patch of the visual scene is subsequently traced through each of the anatomical structures of the early visual system, from retina to the lateral geniculate nucleus, and subsequently to layer IV of area 17 in visual cortex.

Neurons in the early visual system of mammals have been classified according to a host of different electrophysiological properties (for a thorough review see Rodieck, 1979; Sherman, 1985; Stone, 1983). The principal classification is in terms of X and Y cells and is based on the capacity of cells to integrate input linearly throughout their receptive field (Enroth-Cugell and Robson, 1966). Retinal ganglion cells of the X type respond in a linear fashion to a sine-grating, have a sustained response when stimulated in the center of the receptive field, and respond to higher spatial and lower temporal frequencies as compared to Y cells, which are not capable of linear summation. The response of Y cells is also much more transient than the response of X cells, and their receptive field is significantly larger than that of X cells at the same eccentricity. Finally, the conduction velocity of X cell axons is roughly half that of Y cells. A popular but overly simplistic view associates the X system with high-acuity form vision while the Y system is generally linked with the system relaying temporal information, such as motion, to the cortex. A third, very inhomogeneous class of cells, called W or non-X, non-Y, contains cells with large

receptive fields, sluggish responses, and a number of nonlinear properties, such as direction selectivity (Cleland and Levick, 1974). In the retina, X, Y, and W cells correspond to very distinct anatomical classes (Boycott and Wässle, 1974). Using the physiological classification combined with intracellular dye injection, X cells have been identified with β cells, Y with α cells, and W cells with γ and δ cells (Peichl and Wässle, 1979; Wässle, Boycott, and Illing, 1981; Wässle, Peichl, and Boycott, 1983). In the present model, we constrain our model in that we only implement the X pathway. Furthermore, for reasons of computational efficiency, we have limited the retinal population under consideration to only those β cells belonging to the physiological on-center classification, which corresponds to half of the β ganglion cells in the retinal patch. In other words, all retinal neurons described here are excited if a stimulus falls within their center and are inhibited if the stimulus falls on the surround. This system then provides input to the lateral geniculate nucleus, acting as simple relay in our present model, and subsequently to the input layer IV in striate cortex.

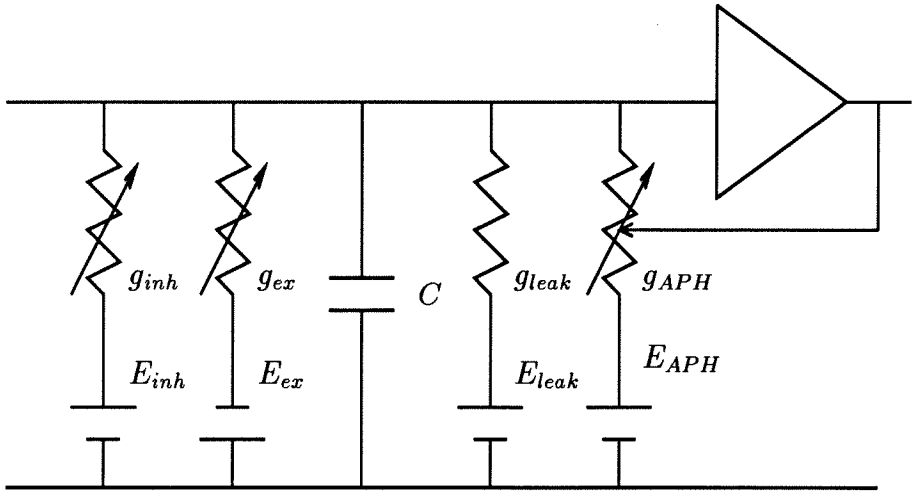

Figure 4.2 Electrical equivalent circuit of a single geniculate or cortical neuron (see Equation 4.1). Each neuron consists of a single lumped soma with a

number of excitatory and inhibitory synapses in series with a capacity (C) and a leakage pathway (g_{leak} in series with the battery E_{leak}). In the absence of any synaptic input, the intracellular potential will be stabilized at $E_{leak} = -71\ mV$. Each synapse is modeled by a time varying conductance g_{ex} or g_{inh} in series with the synaptic reversal potential E_{ex} or E_{inh}. For silent or shunting inhibition, $E_{inh} = E_{leak}$, while for hyperpolarizing synaptic inputs, $E_{inh} < E_{leak}$. An action potential is assumed to be initiated if the potential exceeds the threshold V_{thresh}. Subsequent to this event, a time-varying inhibitory synaptic input g_{AHP}, corresponding to the potassium conductance seen during the afterhyperpolarization, is activated (with $E_{AHP} < E_{leak}$). This will lead to a period during which initiation of action potentials is more difficult (refractory period).

Single-cell Model

As the purpose of this simulation is to model the time-varying behavior of real cells, our simulated neurons exhibit realistic responses. Each cell has a set of features that includes its membrane potential, spiking threshold, level of spontaneous activity, and its set of synaptic connections. The dynamic behavior of each neuron is described by the simple electrical circuit in Figure 4.2, and is determined by a first-order, nonlinear differential equation.

Each cell is modeled by a single compartment with a passive, leak conductance (g_{leak}) in parallel with a membrane capacity C. The passive time constant of the cell is $\tau = C/g_{leak}$. The contribution of an activated synapse is given by the time-varying conductance change $g(t)$, in series with the synaptic battery E. In contrast with the computation of continuous valued membrane potentials and conductances, action potentials are modeled as discrete, binary events. If $V(t)$ exceeds a fixed threshold, V_{thresh}, at any time, an action potential is generated (that is, a binary variable is set) and relayed, with the appropriate delay times, to all postsynaptic target cells. Following each action potential, the neuron experiences an afterhyperpolarization and is inhibited from spiking for a specified interval by increasing a membrane conductance (g_{AHP}) with a reversal potential negative to the cell's resting potential ($E_{AHP} = -90\ mV$). Functionally, this mimics the activation of the fast potassium currents (I_C and/or I_K) seen following action potential generation (Wilson, Bower, 1989).

The action potential has no other direct effect on the cell's voltage trajectory. The equation of motion for the subthreshold voltage response is thus given by:

$$\begin{aligned} C\frac{dV_m(t)}{dt} &= \sum_{j=1}^{k} g_{ex}(t-t_j)(V_m(t)-E_{ex}) \\ &+ \sum_{j=1}^{l} g_{inh}(t-t_j)(V_m(t)-E_{inh}) \\ &+ g_{AHP}(t-t_{spike})(V_m(t)-E_{AHP}) \\ &+ g_{leak}(V_m(t)-E_{leak}) \end{aligned} \qquad [4.1]$$

where k and l are the total number of excitatory and inhibitory synapses for this particular cell, t_j, the arrival time of its presynaptic action potential to the associated synapse, $g_{ex}(t)$ and $g_{inh}(t)$, the induced conductance changes which are given by the function:

$$g(t) = \begin{cases} g_{peak}\frac{t}{t_{peak}}e^{1-\frac{t}{t_{peak}}}, & \text{if } t > 0; \\ 0, & \text{if } t < 0. \end{cases} \qquad [4.2]$$

E_e and E_i are the associated synaptic batteries, and t_{spike}, the time at which the neuron generated an action potential, that is $V_{thresh} < V_m(t)$, $g_{AHP}(t)$ is also given by the function 4.2. Shunting or silent inhibition is modeled by setting E_{inh} to the resting potential of the cell, given by E_{leak} in our model (see Table 5.1 in Chapter 5), while for hyperpolarizing inhibition the battery is set to the reversal potential of potassium, $-90\ mV$.

All cellular parameters are constant within any given neuronal population with the exception of the voltage threshold V_{thresh}, which was randomly chosen from a uniform distribution of values falling between -45 and $-35\ mV$. This introduced sufficient stochastic elements into our simulation to prevent phase-locking among neurons. With the exception of a low spontaneous activity introduced in the retinal β ganglion cells, additional noise is not incorporated into our cells, although this may be easily accomplished. It can be seen that our model represents an elaboration of the

simpler integrate-and-fire model, but stops short of a full Hodgkin and Huxley-type description as in Wilson and Bower (1989). This results in a physiological realistic behavior of individual neurons without requiring a computationally expensive implementation of specific channels and dendritic geometries. Once again, the selection of appropriate scale at which to implement our model determines the computational feasibility of the simulation.

5.1

Modeling the Mammalian Visual System Retina and Lateral Geniculate Nucleus

Retina

As previously described, our simulated retina comprises a two-dimensional distribution of on-center β ganglion cells with circular receptive fields. Wässle et al. (1981) showed that upon injecting HRP into the lateral geniculate nucleus, all retinal β cells were labeled. In this way they could show that all β on-center and off-center cells are located on two independent lattices. The amount of spatial jitter in the exact positions of the ganglion cells did not allow Wässle and colleagues to distinguish between a rectangular and a hexagonal lattice. In the absence of more precise information, we located all of our retinal ganglion cells on a noisy hexagonal grid. Instead of modeling a patch of retinal cells around the *area centralis* with its β on-center cell density of 3250 $cells/mm^2$, we located our patch at 1 mm away from the *area centralis*, where the on-center β density drops to 900 $cells/mm^2$ (Peichl and Wässle, 1979). Since 1° is equivalent to 0.226 mm in the cat retina (Bishop, Kozak, and Vakkur, 1962), 1 mm eccentricity corresponds to about 4.5°. The associated intercellular distance of a hexagonal array is $(2/(\sqrt{3}\rho))^{1/2} = 36\ \mu m \approx 9.5'$, where ρ is the cell density and $\sqrt{3} \cdot 9.5' = 16.5'$ is the distance between the cells on the hexagonal grid (Peichl and Wässle, 1979). Using this spacing, we are modeling a 1 mm by 1 mm patch of cells, corresponding to about 900 cells. Thus, our model retina subtends about 4.5° by 4.5° of visual angle (see Figure 5.1 for the retinal layout).

The response of individual ganglion cells is based on extensive physiological evidence that their receptive fields can be readily described by Gaussian sensitivity profiles for both center and surround (Rodieck, 1965; Enroth-Cugell and Robson, 1966; Linsenmeier, Frishman, Jakiela, and Enroth-Cugell, 1982). The spatial receptive field is then obtained by subtracting the surround response from the center.

Thus the name of this filter is "difference of a gaussian" or DOG for short. The center response is described by

$$G_c(x,y) = K_c\, e^{-\frac{x^2+y^2}{2\sigma_c^2}} \qquad [5.1]$$

and the surround response by

$$G_s(x,y) = K_s\, e^{-\frac{x^2+y^2}{2\sigma_s^2}} \qquad [5.2]$$

Using measurements of contrast sensitivity of ganglion cells in response to drifting gratings, Linsenmeier et al. (1982) obtained four parameters that characterize the sizes (σ_c, σ_s) and peak sensitivities (K_s, K_c) of the center and surround fields. A typical X cell receptive field profile is described using $\sigma_s/\sigma_c = 3$ and $K_c/K_s = 17$ (Figure 5.2). Peichl and Wässle (1979), measuring the receptive field center size of X cells using three different methods, found sizes between 20′ and 40′. We choose a value of $30' = 0.5°$, which corresponds to a σ_c of 10.6′. Since we only assigned a value to the ratio of the sensitivities, we have one free parameter in our model, which allows us to scale the total response of our simulated ganglion cells. We can now compute the physiological coverage factor, which is given by the area of the excitatory receptive field (diameter of 30′) divided by the area per cell. For the above values, we find a coverage factor of 9, in good agreement with data (Peichl and Wässle, 1979).

The ratio of the center to the surround signal in response to full-field light stimulation is given by $K_c\sigma_c^2/(K_s\sigma_s^2) = 0.53$. In a perfectly balanced cell, this ratio will be 1 and no response will be elicited for a full-field stimulus. However, while most retinal neurons still respond weakly to a full-field stimulus, this number is most likely an underestimate. $\sigma_s/\sigma_c = 4$ should yield a more physiological result (Linsenmeier et al., 1982). A perfectly balanced receptive field, such as the Laplacian of a Gaussian filter proposed by Marr and Hildreth (1980), would give a zero response to such a diffuse light stimulus. However, in order to approximate the Laplacian of a Gaussian

filter by a DOG, the ratio of σ_s/σ_c should be equal to 1.6 (Marr and Hildreth, 1980), which is clearly not the case.

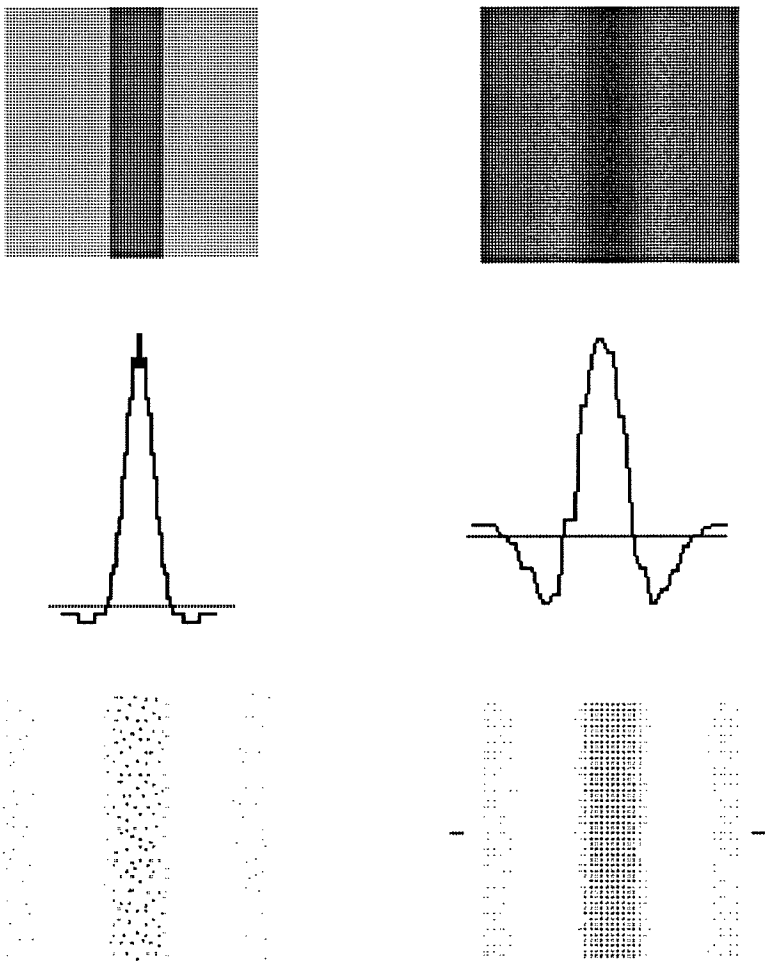

Figure 5.1 The retinal layout. The upper left panel shows our standard stimulus, a bar of variable contrast, orientation and width. This pattern is now convolved with the spatio-temporal kernel of the X ganglion cells (Equations 5.5 and 5.6). The result is displayed in the upper right corner. The spatial part of the receptive field is shown on the same spatial scale in the left middle panel. The middle right plot shows a horizontal cross section of the convolved image. This convolved image is then subsampled on a noisy hexagonal grid, corresponding to the location of the 900 simulated on-center β ganglion cells (lower left-hand corner) and thresholded. The only difference between the retina and the LGN (lower right-hand corner) is the four times increased geniculate cell density.

The temporal response of both the center and the surround response are modeled by low-pass filters

$$L_c = \frac{1}{\tau_c} e^{\frac{-t}{\tau_c}} \qquad [5.3]$$

and

$$L_s = \frac{1}{\tau_s} e^{\frac{-t}{\tau_s}} \qquad [5.4]$$

with $\tau_c = 10\ msec$ and $\tau_s = 20\ msec$. Richter and Ullman (1982) compared the temporal response of sustained X-like ganglion cells in the primate retina against this model and found good qualitative agreement. Equations 5.3 and 5.4 are simplifications, however. Victor (1987) studied the dynamics of the center of X type cat retinal ganglion cells and derived a complete—but substantially more complex—description of their temporal behavior. We introduced a delay $\delta t = 3\ msec$ between the center and surround response, in agreement with the theoretical prediction of Richter and Ullman (1982) as well as with the experimental evidence of Enroth-Cugell, Robson, Schweizer-Tong, and Watson (1983).

Under the assumption that the spatio-temporal receptive field is separable into a purely spatial and a purely temporal component. (Note: Dawis, Shapley, Kaplan, and Tranchina (1984) examined this assumption in cat retinal X cells and found that separability holds for the center response but that the spatial extent of the surround depends on the temporal frequency of the stimulus and thus separability does not hold for the surround. However, for our purposes the assumption seems sufficient to account for cortical properties like orientation selectivity.) We can now compute the response of the center and surround to a light stimulus $I(x, y, t)$ by the following convolution integrals

$$C(x,y,t) = \int_0^t \int_{-\infty}^{+\infty} \int_{-\infty}^{+\infty} G_c(x',y') L_c(t') I(x-x', y-y', t-t') dx' dy' dt' \qquad [5.5]$$

and

$$S(x,y,t) = \int_0^t \int_{-\infty}^{+\infty} \int_{-\infty}^{+\infty} G_s(x',y') L_s(t') I(x-x', y-y', t-t') dx' dy' dt' \qquad [5.6]$$

with the total response of the ganglion cells given by

$$F(x,y,t) = C(x,y,t) - S(x,y,t-\delta t) \qquad [5.7]$$

For reasons of computational economy, the Gaussian kernel $G(x,y)$ is only being integrated within $2\sigma_s$. For any particular ganglion cell located at x,y, we can then compute its response $F(x,y,t) = F_{x,y}(t)$. Since the output of the retinal ganglion cells $F_{x,y}(t)$ represents a sort of neuronal excitability, it can never be negative. Thus, if $F_{x,y}(t) < 0$, $F_{x,y}(t)$ is set to zero. If we were to model off-center ganglion cells, their response would be given by $S(x,y,t) - C(x,y,t-\delta t)$.

This continuous neuronal excitability function $F_{x,y}(t)$ needs to be converted into discrete, stochastic, all-or-none events corresponding to action potentials. Assuming that the action potentials have a Poisson distribution, the probability that the ganglion cell fires an action potential in the small interval between t and $t + \Delta t$ (with $\Delta t << 1$) is given by

$$p_{x,y}(t) = p_0 \cdot \Delta t \cdot F_{x,y}(t) \qquad [5.8]$$

where p_0 is an appropriate normalization constant. This neglects the small probability of two or more action potentials occurring within t and $t + \Delta t$ (an event with a probability of the order of $(p_0 \cdot \Delta t)^2$). We are superimposing onto the neuronal spiking rate in response to the visual stimulus $I(x,y,t)$ a low, spontaneous spiking activity of 10 *Hz* (Bullier and Norton, 1979). Figure 5.2 illustrates the firing rate of one retinal ganglion cell in response to a vertical bar. We simulate the effect of varying the contrast of the stimulus $I(x,y,t)$ by modulating the probability of action potential generation via variation of p_0. Equivalently, we could pass the light intensity

distribution falling onto the retina through a compressive nonlinearity, such as $log(I)$ or $I/(I + I_c)$, to mimic the gain control properties of the rod and cone pathways in the retina (for a review see Shapley and Enroth-Cugell 1984), prior to evaluating the convolution integrals in Equation 5.5 and 5.6. However, we can essentially achieve the same result using the simple trick of varying p_0 in Equation 5.8. This technique has the added advantage that the convolution integrals need only be evaluated once.

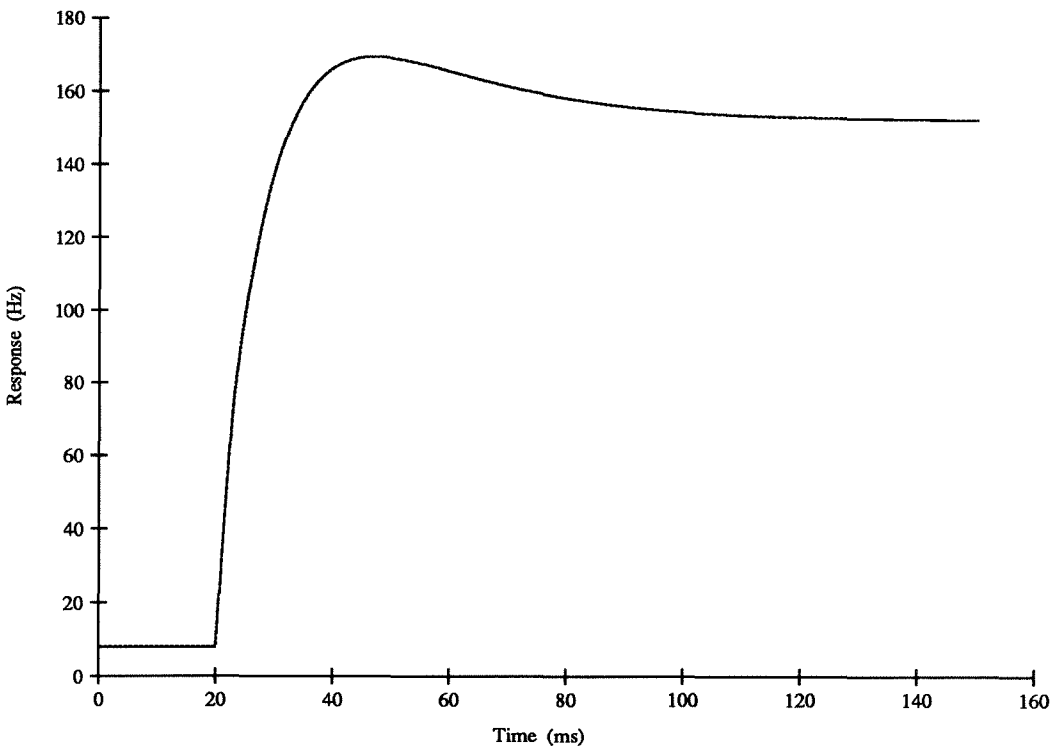

Figure 5.2 Poststimulus time histogram of a single β ganglion cell in response to a vertical, high-contrast bar as computed via Equation 5.7. At 20 *msec* the bar (of 0.5° width) is superimposed onto the middle of the receptive field. Following the initial burst of activity, the response decays to a sustained level as a result of the delayed activation of the inhibitory surround. This continuous function is then converted into discrete action potentials used as geniculate inputs via Equation 5.8. The spontaneous firing frequency of the retinal cell is 10 *Hz*.

It should be noted that a realistic approximation of retinal activity is all that is needed to investigate the geniculate and cortical activity patterns, and selecting the correct precision and scale with which to simulate the retina results in considerable

computational savings. Thus, for our purposes, it appears to be sufficient to model the retina as a linear system without explicitly modeling photoreceptors, horizontal, bipolar, and amacrine cells (for an example of this type of approach, see Gremillion, Mandell, and Travis 1987).

Lateral geniculate nucleus

All retinal ganglion cells project heavily to the lateral geniculate nucleus, or LGN. With few exceptions, each geniculate cell seems to receive its innervation from a single or a few retinal ganglion cells of the same class, and the response properties of these geniculate neurons are essentially the same as those of their retinal counterparts with closely overlapping receptive fields (Hubel and Wiesel ,1961; Singer and Creutzfeldt, 1970; Cleland, Dubin, and Levick, 1971). Thus, there is no significant receptive field transformation in the relay of retinal information on its way to cortex, although the massive corticofugal pathway from layer VI is most likely involved in controlling the transmission of visual information via its action on geniculate cells (Crick, 1984; Sherman and Koch, 1986). Retinal X ganglion cells project mainly into the A layers of the LGN, lamina A receiving input from the contralateral and lamina A1 from the ipsilateral eye. Of the approximately 450,000 cells in the LGN (Sanderson, 1971), two-thirds are located in the A and A1 laminae and about two-thirds of these are of the X type. Thus, on the average each retinal X on-center ganglion cell from one eye innervates three to four geniculate relay cells. In our current model, we neglect the small degree of convergence seen among LGN cells and assume that each retinal cell projects onto four neighboring geniculate cells. Thus, the coverage factor increases to 36.

This projection from 900 retinal ganglion cells to 2,304 geniculate relay cells (Note: Not every retinal cell from our retina projects to exactly four geniculate cells.) is strictly topographic and thus preserves the spatial ordering of the original input

image. The axonal propagation delay between retinal X ganglion cells and their geniculate target cells varies between 3 and 4 *msec* (Cleland et al., 1971). The passive time constant τ for the geniculate X cells is 10 *msec* (based on intracellular current injections; Bloomfield, Hamos, and Sherman, 1987); hence the LGN introduces an integrating component into the early visual stream. For the other cellular parameters see Table 5.1.

Since our model geniculate cells derive their input from a single retinal ganglion cell, they basically share its nonoriented, circular symmetric receptive field. The stronger inhibitory surround effects reported for geniculate cells (Hubel and Wiesel, 1961; Cleland et al., 1971; Shapley and Lennie, 1985), as well as the orientation bias seen by Vidyasagar and Heide (1984) in response to moving sine wave grating of high spatial frequency, could easily be incorporated into our model by explicitly including inhibitory geniculate interneurons. These interneurons, staining positive for γ-aminobutyric acid (GABA), the principal inhibitory neurotransmitter used in subcortical and cortical structures, comprise perhaps 20–30% of the neurons in the A and A1 laminae (Fitzpatrick, Penny, and Schmechel, 1984).

Since this interconnection generally will not change the neuronal activity pattern very much and the function of this surrounding inhibition is mostly to enhance the surround effects, we could simply include this in our simulation of next step by neglecting them but letting the center-surround signal stronger.

Table 5.1 : Parameters for geniculate and cortical cells

Symbol	Parameter	LGN	Cortex
C	membrane capacitance	$1nF$	$2nF$
g^*_{leak}	leakage conductance	$0.1\mu S$	$0.1\mu S$
E_{leak}	leakage reversal potential	$-71mV$	$-71.0mV$
g^*_{ex}	peak excitatory conductance	$0.15\mu S$	$0.011\mu S$
E_{ex}	excitatory synaptic reversal potential	$20mV$	$20.0mV$
g^*_{inh}	peak inhibitory conductance	-	$0.055\mu S$
E_{inh}	inhibitory synaptic reversal potential	-	$-71.0mV$
g^*_{AHP}	peak afterhyperpolarization conductance	$0.59\mu S$	$0.59\mu S$
t_{peak}	time to peak for all conductance changes	$1.0ms$	$1.0ms$
V_{thresh}	spiking threshold	$-40 \pm 5mV$	$-40 \pm 5mV$

* corresponding to $g_{peak} = g(t = t_{peak})$ in Equation 4.2.

6.1

Modeling the Mammalian Visual System Visual Cortex

Visual cortex

The primary target for geniculate relay cells is the primary visual cortex (also called area 17 or V1). While X cells from the geniculate A layers appear to project only to area 17, geniculate Y cells project to a number of areas in extrastriate cortex (reviewed in Sherman, 1985). Both X and Y cells project mainly into layer IV and to a less extent into the upper part of layer VI. The question of whether the projection from these two cell populations (X and Y) is segregated into a lower and an upper part of layer IV (confusingly termed layers IVa and IVb by one school and layers IVab and IVc by another) is still controversial. In the current model, we are assuming that the X on-center cells in the LGN project to the lower part of layer IV. This layer, which is devoid of the large neurons seen in the upper part of layer IV, is approximately 250 μm thick (as compared to the total cortical thickness of $\approx 1,600$ μm; Beaulieu and Colonnier 1983) and contains on the order of $14,000$ neurons per mm^2 (as compared to $80,000$ neurons per mm^2 for all layers combined; Beaulieu and Colonnier 1983).

The projection of the visual image onto the surface of cortex is topographic, such that adjacent points in the visual field map onto adjacent points in the visual cortex. However, there is a certain degree of scatter superimposed onto this orderly representation such that nearby cells (during tangential, i.e., within the cortical plane, electrode penetrations) have receptive fields whose centers are not adjacent in visual space. For cells separated by less than 200 μm cortical distance, the fluctuation in receptive field center appears to be random (Albus, 1975). In other words, the projection is topographic on a macroscopic, but random on a microscopic scale (for a fact-filled treatise on the physiology of cat visual cortex, see Orban, 1984). Finally, the visual field is distorted in a systematic manner when projected onto the cortex,

such that much more area is devoted to representing the *area centralis* than the visual periphery. In fact, this projection can be roughly approximated by a logarithmic mapping (Fischer, 1973; Tusa, Palmer, and Rosenquist, 1978; Schwartz, 1980). The cortical magnification factor M specifies how many mm of cortical distance correspond to one degree of visual angle (Albus, 1975; Orban, 1984). For our chosen eccentricity of 4.5°, M is approximately 0.6 mm per 1° (Albus, 1975). Thus, our 2° by 2° visual field projects onto a 1.2 by 1.2 mm^2 area of visual cortex, comprising roughly 20,000 cells, of which half are primarily driven by input from one eye.

We will not attempt to model all of these cells but, in accordance with the model of orientation selectivity postulated by Koch (1987), only the subclass of inhibitory interneurons. The presence in the mammalian cerebral cortex of the classical inhibitory neurotransmitter GABA and its synthesizing enzyme, glutamic acid decarboxylase (GAD), has been known for a long time (for more information on the form, function, and distribution of inhibitory interneurons, see the "Cerebral Cortex" series by Peters and Jones, 1984). Quantitative assessments in monkey cortex indicate that approximately 25% of the neuronal population in any cortical area is GABA- or GAD-immunoreactive (Hendry, Schwark, Jones, and Yan, 1987). Morphologically, these neurons are nonpyramidal, their dendrites lack significant populations of dendritic spines, and their axons seem to be intrinsic to the cortex. In the visual cortex of the cat, these cell types included basket cells, clutch cells, and chandelier cells or axo-axonic cells (Martin, Somogyi, and Whitteridge, 1983; Kisvarday, Martin, Whitteridge, and Somogyi, 1985; Jones, Hendry, and DeFelipe, 1987). Electron microscopic studies of the visual cortex of the cat (Tömböl, 1974; Winfield, Gatter, and Powell, 1980) indicate that about 30% of all cells are small stellate cells, presumably using GABA as neurotransmitter. All of these inhibitory cells receive direct excitatory synapses from the cells in the lateral geniculate nucleus (Freund, Martin,

Somogyi, and Whitteridge, 1985a,b; LeVay, 1987) and make extensive contacts among each other as well as onto excitatory pyramidal cells. Based on these numbers, we assumed that 25% of cortical cells are inhibitory, which brings our total cell count down to 2,300 cells in a 1.44 mm^2 patch of layer IV in area 17 (see Figure 6.1). We do not identify these cells with any particular subpopulation of inhibitory interneurons.

What is the divergence and the convergence associated with the geniculo-cortical pathway? When HRP was injected intracellularly into physiologically identified geniculate X cells, their axons terminate within a single continuous clump of surface area between 0.6 and 0.9 mm^2, with an average of 0.72 mm^2 (Humphrey, Sur, Uhlrich, and Sherman, 1985), with anywhere between 300 and 3,000 synaptic contacts. In other words, since the cell population in a 0.72 mm^2 patch of layer IVb is about 10,000, the potential coverage factor is very large. Using a sophisticated double staining method, Freund et al. (1985a, b) revealed that the maximum number of synapses made between one geniculate axon and a single postsynaptic cell in cortex was 8, although in many cases it was only 1. Thus, with an average of 4 synaptic contacts per cell, an X cell afferent could in principle contact anywhere between 70 and 700 cells. Since we are only concerned with the 25% inhibitory interneurons, the divergence in our model, that is the number of cortical cells postsynaptic for a single geniculate cell, is roughly 220. This can be easily seen in Figure 6.1a. (Note: Given this large divergence over a relatively large area (relative to the size of our cortex), only the central 2° by 2° patch of geniculate cells projects completely to the cortex. This subfield is outlined in Figure 6.1 by a small white rectangle superimposed onto the LGN.) The axonal propagation delay of the geniculate-cortex pathway is set to 2 $msec$ with some small random variations from cell to cell (Lee, Cleland, and Creutzfeldt, 1977; Hoffman, Stone, and Sherman, 1972).

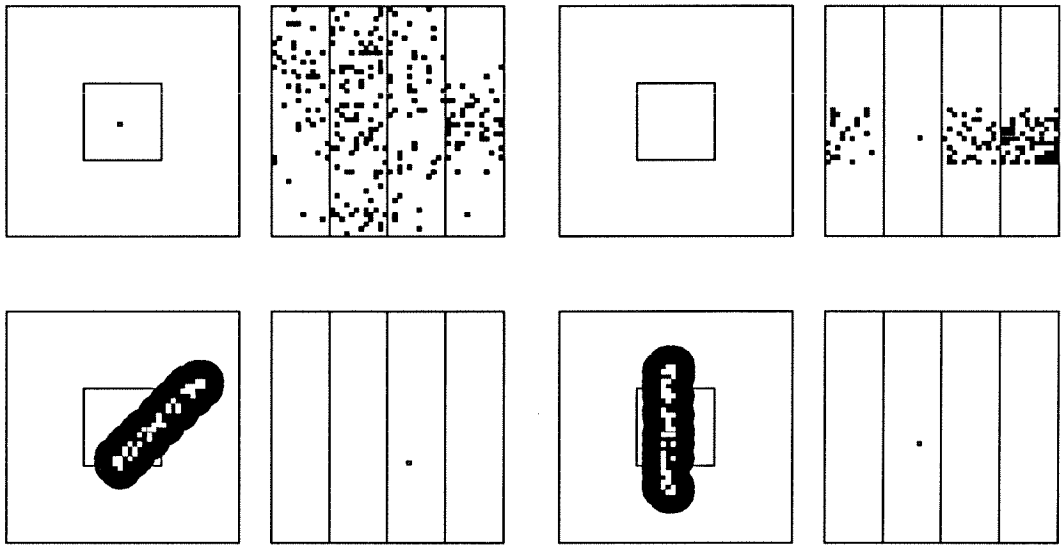

Figure 6.1 Structural features of the simulated cat visual cortex. The 48 by 48 array of cells in the lateral geniculate nucleus is illustrated in the left part of each of the four panels and the 48 by 48 array of cells in layer IVc of striate cortex on the right side. (a) Each geniculate cell projects to a large number (about 220) of cortical cells. (b) A typical cortical interneuron inhibits a large number of other cortical neurons. The cortex module measures $1.2mm$ on each side, about the dimension of a hypercolumn in the cat. Cells are grouped into four orientation columns. The receptive field of two such cells is plotted in (c) and (d). They correspond to simple cells with a $1:3$ to $1:4$ aspect ratio and a width of about $0.5°$.

The most dramatic difference between geniculate and cortical receptive fields is their organization and shape. One population of cortical cells, the simple cells, is distinguished by the discrete subregions that can be found in their receptive fields (see Figure 4.1a in Chapter 4 and also Figure 6.1). These cells, which are found throughout layer IV and the upper part of layer VI, have regions that resemble the centers of the receptive fields of on-center and off-center neurons in the LGN in that light increment in an ON region or light decrement in an OFF region excites the cell. In contrast to geniculate cells, however, cortical cells have elongated receptive fields, their width being similar to the diameter of the receptive field centers of neurons in the LGN (Stone and Dreher, 1973; Shermann, 1985). Simple receptive fields vary in the number of subregions observed, in the elongation of each subunit, and in the

overall elongation of the field. The aspect ratio of these subfields, i.e., the ratio of width to length, varies with the type and the layer of the neuron. Observed values for simple cells range from 0.2 (1:5 elongation) to 0.92 (nearly round), although cells in layer IV tend to have aspect ratios between 0.5 and 0.66 (Watkins and Berkley, 1974; Gilbert, 1977; Jones, Stepnoski, and Palmer, 1987). Note that the aspect ratio directly determines the amount of orientation tuning in the feedforward Hubel and Wiesel type model (a smaller aspect ratio increases the tuning), while it is one among many factors shaping orientation tuning in the mixed models.

For our current simulations, we wired simple cells with an aspect ratio varying between 1:2.5 and 1:4. The appropriate receptive fields can be visualized by retracing all the geniculate afferents to any particular cortical cells. The result is illustrated in Figure 6.1c and 6.1d. Note that these cells currently do not contain any OFF subunits. The convergence of the geniculo-cortical pathway can be visualized by retracing all geniculate afferents to these cells (marked in red in Figure 6.1c and 6.1d). On the average, simple cells receive input from 20 to 30 cells whose centers are aligned along a row in visual space, as postulated by Hubel and Wiesel's original model (1962). These numbers are in rough agreement with the convergence ratio obtained from cross-correlation studies (Tanaka 1983).

We construct the receptive fields of our simple cells as follows. For a cell within a given orientation column, we first decide where the receptive field should be located. To do this, we backproject the cell into the LGN (e.g., a cell in the upper left corner is projected back into the upper left corner of the LGN). Take a vertical orientation cell as an example. A rectangle of a given size is centered (for instance, 3° by 4°) around this geniculate cell and divided into a number of vertical strips (eight 3° by 0.5° strips). The size of this rectangle depends on the extent of the geniculo-cortical arborization (in our case 0.72 mm^2). Each of the geniculate cells within this rectangle

could then, in principle, make a synapse with the simple cell under consideration. We then randomly choose one of these strips. In a final step, we again choose randomly from all cells within this strip (assuming a uniform probability distribution) those cells that actually project to the simple cell. This procedure (1) leads to jitter in the exact receptive field position but preserves the overall topography, and (2) generates oriented simple cells using the scheme proposed by Hubel and Wiesel (1962). Note that this scheme explicitly computes the afferent projection into cortex (Figure 6.1c and 6.1d) but only implicitly the efferent projection from the LGN (Figure 6.1a).

In our current version of the model, two separate inhibitory, intracortical pathways are implemented. One system corresponds to long-range inhibition among cells with approximately overlapping receptive fields but different preferred orientations. This pathway represents an anatomical substrate of cross-orientation inhibition, for which both physiological and pharmacological evidence exists (Bishop et al., 1971; Sillito, 1975; Morrone et al., 1982; Ramoa, Shadlen, Skottun, and Freeman, 1986; however, see also Ferster, 1986, 1988). In our model, each cell projects into the three neighboring orientation columns and has a given and fixed probability of forming inhibitory synapses onto these cells. Both pre- and postsynaptic cells have spatially overlapping receptive fields but different preferred orientations (Figure 6.1). We usually assume that each cortical neuron inhibits 40 cells out of a 12 by 12 patch of cells in the orientation column orthogonal to its own orientation and a somewhat smaller number of neurons in the two directly adjacent orientation columns (see Figure 6.1b). A second inhibitory projection is assumed to exist between neurons with similar preferred orientations but spatially offset receptive fields. Intracellular recordings support the existence of such a system (Ferster 1986). The pattern of this local inhibition varies and depends on the preferred orientation of the column. Given the spatial jitter in the receptive field locations of neighboring cells, this inhibition can, in

principle, suppress firing activity among cells with identical receptive fields (in terms of their orientation and location) and could therefore act to dampen the response of the entire population. In the next chapter, we will show how such inhibitory synapses could be selectively removed and pruned away during development.

Both inhibitory pathways take account of the propagation times of action potentials, which are computed on the basis of the distance between the pre- and post-synaptic cell and the conduction velocity of the particular axonal process (usually assumed to vary between 1–2 m/sec). The high degree of divergence witnessed in the inhibitory projections leads to a very large number of intracortical synapses (2,300 cells each of which makes about 100 synapses or a total of 250,000 synapses).

Simulation results

The model was implemented on SUN workstations in C using the techniques described by Wilson (1989). Some results are illustrated in color in Figure 6.3, for the case of a cortex where all inhibitory cortical interactions have been blocked and only a Hubel and Wiesel (1962) type of geniculo-cortical arrangement is assumed (see Figure 4.1b in Chapter 4). The selectivity of the system can be monitored by the action potential count displayed above each orientation column. This is simply the total number of spikes occurring in any cell within that particular orientation column.

Stimulus conditions were as follows. Initially, the "cat" sees a blank screen. Under these conditions, the spontaneous spiking activity (10 Hz) in the optic nerve can be seen to activate geniculate cells and depolarize cortical cells. At 20 $msec$ a vertical, 0.5° wide and elongated light bar is projected onto the retina (Figures 5.1 and 5.2 in Chapter 5). The response in the LGN reflects this stimulus (Figure 6.3a). The nonexcited regions in the LGN correspond to the perceptual phenomena of Mach bands, caused by inhibitory interactions mediated by the inhibitory surround mechanism of retinal ganglion cells. Spontaneous activity is actually suppressed, as can

be seen by comparison with the outside regions next to the geniculate boundary. In cortex, neurons in the vertical orientation column respond vigorously to the vertical bar, while simple cells in the neighboring orientation columns fail to generate action potentials; they are, however, nonetheless depolarized to some degree (between 5 and 20 mV from rest as can be seen in the intracellular potential plots of two cortical cells; Figure 6.3). This is a natural consequence of the finite aspect ratio of the receptive fields. If we had used aspect ratios of 1:1.5 to 1:2.5, which is more in tune with experimentally observed values (Watkins and Berkley, 1974; Gilbert, 1977; Jones et al., 1987; Jones and Palmer, 1987), the selectivity of the model would degrade. Since such excitatory postsynaptic potentials at nonoptimal orientations are not observed during intracellular recordings (Ferster, 1986, 1988), inhibitory mechanisms must be introduced in order to block or shunt these EPSPs. At 150 $msec$ the bar is rotated into the horizontal position and cells in the geniculate start responding to this new stimulus. Note that, different from most conventional neural networks where a new stimulus requires the reinitialization of the network (usually resetting the activity state of all neurons to zero or some other median value), traces of the old stimulus are still visible, in form of the intracellular potential, at the cellular level in both the LGN and in cortex. Cells in the horizontal orientation column now respond to the horizontal bar (Figure 6.3b).

Now, unlike before, intracortical inhibition among cells with different orientations is now included in the simulation, as specified in Figure 6.1b. While the cell is as responsive to a properly aligned stimulus as before, its response to nonoptimal stimuli is significantly reduced. Individual EPSPs, caused by the geniculate afferents, are still visible, as well as fast steep reductions in the intracellular potential caused by the action of intracortical inhibition, which is assumed to reverse around the resting potential of the cell (silent or shunting inhibition). Under these conditions, IPSPs

should never be visible, except when the cell is depolarized by current injections (e.g., Ferster, 1986, 1988). The intracellular potential will have a smoother time course if a larger divergence is used for the intracortical inhibition.

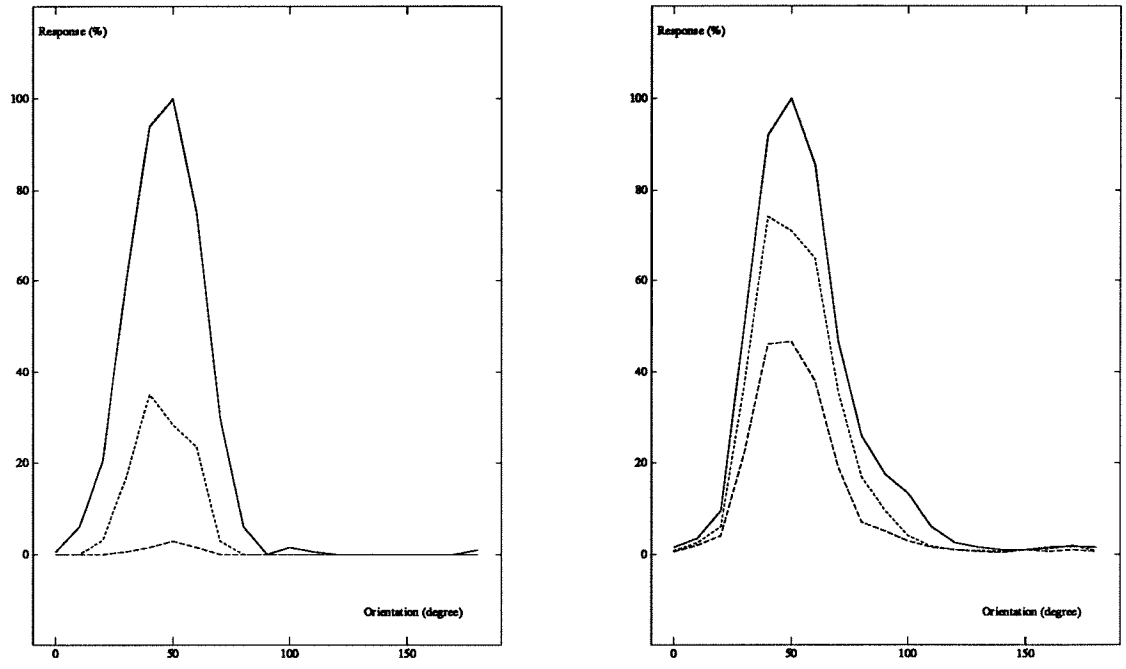

Figure 6.2 On the left is shown the sensitivity of the Hubel and Wiesel model to visual contrast. The total number of action potentials within one orientation column during a 500 *msec* presentation of a bar of varying orientation (at 10° increments) is shown (normalized to peak response) at three different contrast values. The retinal activity in the three curves is multiplied by 1.0, 0.75, and 0.5, via variation of p_0 in Equation 5.8 in the last chapter. At the lowest contrast value, cortical cells are barely excited, reflecting the lack of gain control of the straightforward Hubel and Wiesel wiring scheme. On the right is shown the sensitivity of a mixed excitation and inhibition model to visual contrast. The presence of cross-orientation inhibition superimposed onto a Hubel and Wiesel synaptic arrangement leads to a much improved gain control. While the response of the cortex decreases with decreasing stimulus contrast, the bandwidth remains virtually unchanged, in agreement with experimental data (Skottun et al. 1987).

While the color graphic display (Figure 6.3a and 6.3b) of the intracellular potential of all cortical neurons greatly facilitates understanding the working of the model, detailed quantitative measures must be used to assess the validity of the different models of orientation selectivity. Here, the modeler is in a somewhat similar situation

to the experimentalist using multielectrode recordings, facing an embarrassing wealth of data. The main quantitative measure we use is spike counts for individual cells or for large cell populations.

If the contrast of the visual stimulus is decreased, retinal and geniculate cells will be less excited. Ultimately, in the straightforward excitation-only Hubel and Wiesel model, cortical cells will stop responding to the bar, since not enough geniculate-induced EPSPs will be present to carry the somatic voltage in the cortical cell above threshold (left in Figure 6.2). In other words, this model lacks gain control properties. If, however, cortical inhibition is superimposed onto a Hubel and Wiesel type of synaptic arrangement, a smaller contrast stimulus results in less geniculo-cortical excitation, but consequently also in less intracortical inhibition. Thus, the range of contrast values for which the eclectic model still responds is significantly higher, as borne out on the right in Figure 6.2. Experimentally, the orientation tuning of area 17 simple cells changes little when varying the contrast between 2% and 80% (Skottun, Bradley, Sclar, Ohzawa, and Freeman, 1987).

Discussion

We have shown the role of the intracortical connections in shaping the orientation selectivity. In next chapter, the formation of the orientation columns will be discussed. Again the intracortical connections play a very important role.

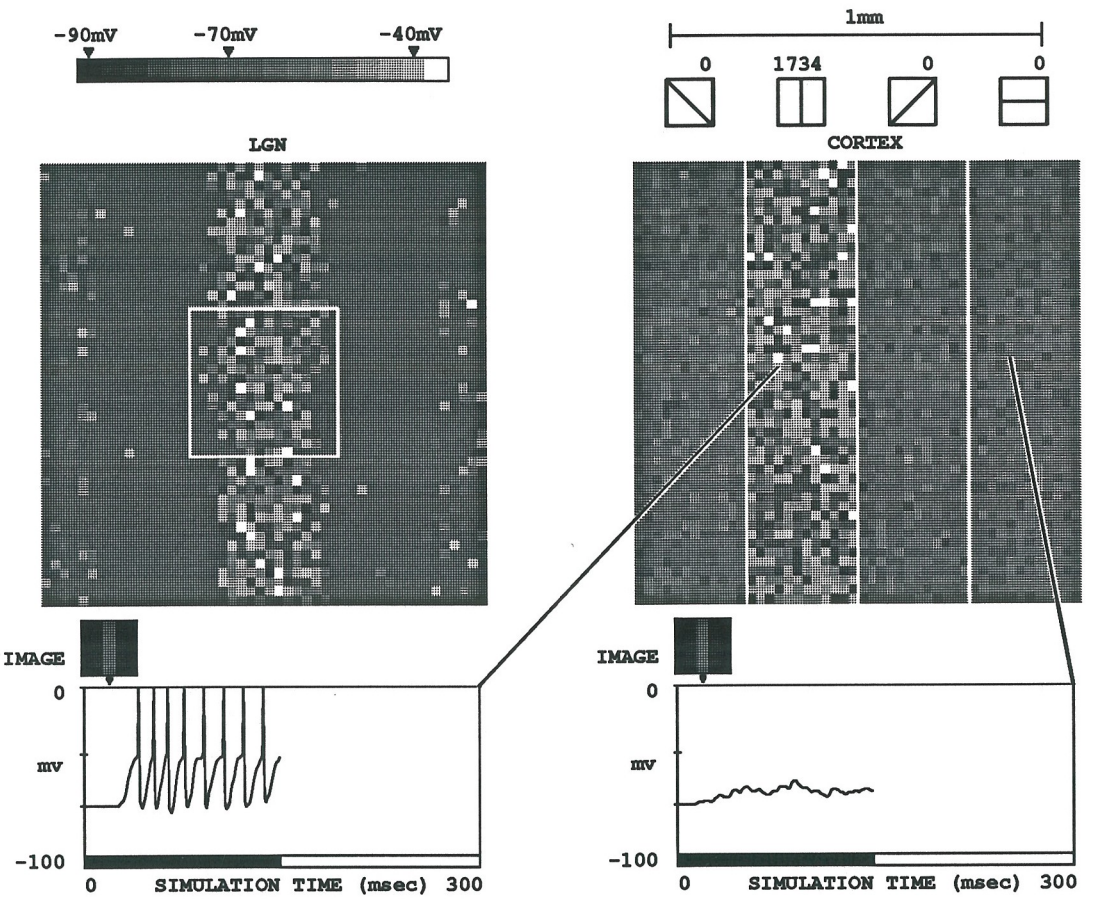

Figure 6.3a The response of the visual cortex model to different stimuli. Cortical inhibition has been inactivated during this run. Thus, cortical cells acquire orientation selectivity via a Hubel and Wiesel type of feedforward circuit. The color of each cell indicates its membrane potential (see the scale bar, action potentials are in white). Insets show the intracellular potential of two cortical neurins in the vertical and horizontal orientation columns. **(a) The response of the model to a vertical bar, which is projected onto the retina at** $20msec$**, is illustrated in the figure. Both the geniculate and the vertical orientation column in cortex respond vigorously.**

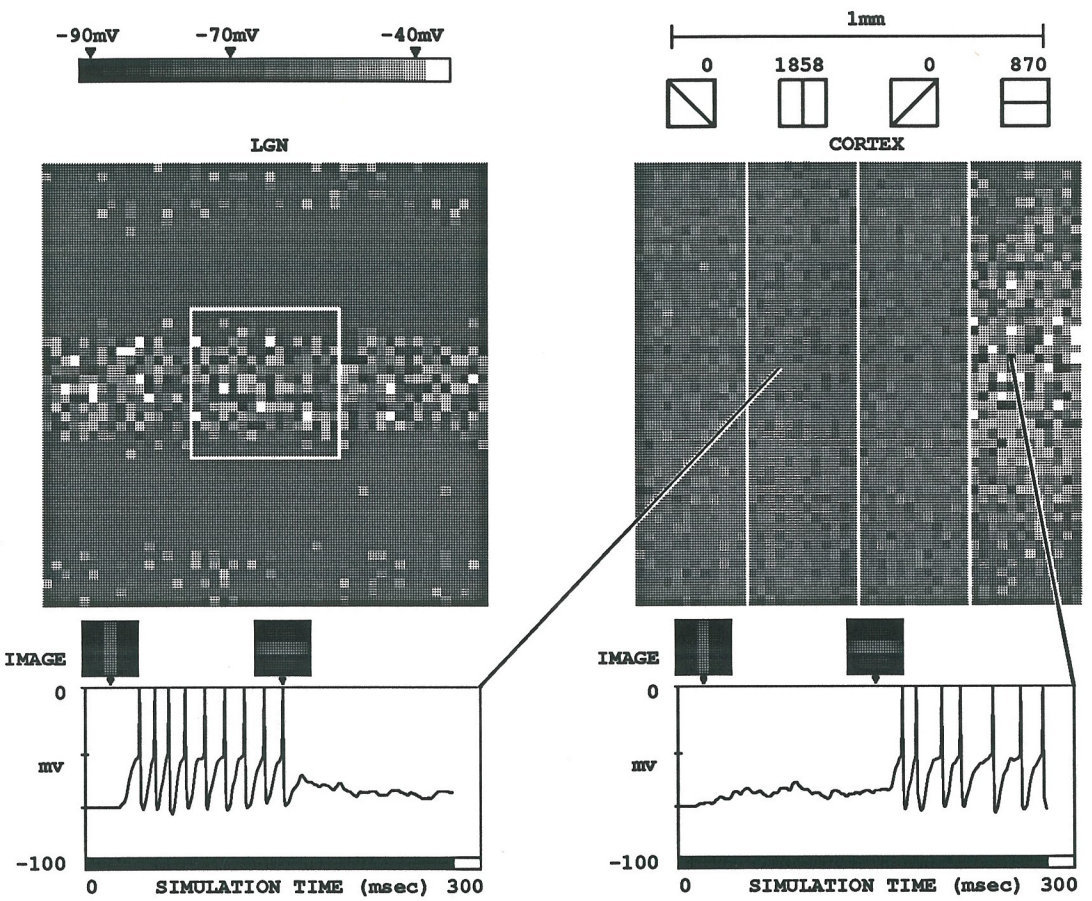

Figure 6.3b The response of the visual cortex model to different stimuli. Cortical inhibition has been inactivated during this run. Thus, cortical cells acquire orientation selectivity via a Hubel and Wiesel type of feedforward circuit. The color of each cell indicates its membrane potential (see the scale bar, action potentials are in white). Insets show the intracellular potential of two cortical neurins in the vertical and horizontal orientation columns. **(b) at** $150msec$ **the vertical bar, which is projected onto the retina at** $20msec$**, is switched to a horizontal bar. The horizontal orientation column in cortex responds vigorously.**

7.1

Modeling the Mammalian Visual System Development of the Interconnections

Introduction

Several developmental schemes have been proposed for the octal and orientation selectivity (Bienenstock, Cooper, and Munro, 1982; Linsker, 1986; Miller 1989). Linsker's work which outlined a frame work about development of feedforward pathways in an featureless environment actually stimulated our research on the development. His model has several layers. The development follows an inward path. In the first several layers, analog to cone and rod to ganglion and to LGN paths, the network developed center-surround feedforward connections. In the later layer, the random input pattern becomes kind of sinusoidal and consequently the forward projection becomes orientation selective. Interconnection within a single layer is included in his work at cortical level to develop the orientation columns. But these intralayer connections are unchanged during the development.

Our early work (Wehmeier, Dong, Koch, and Van Essen, 1989) in the functionality of the intralayer interconnections leads us to believe that the feedback pathway plays a very important role in shaping the orientation selectivity. Therefore, we further explore the role this pathway plays in the development while self organizing using the Hebbian rule. Our model distinguishes from others (like Linsker's) by its emphasis on the feedback pathway of the interconnection within the cortex. As we pointed out in Chapters 2 and 3, the dynamic is quite different, because it integrates the synaptic change and neuron activity change closely. Our network develops interconnection patterns which are important in shaping the orientation selectivity or in producing such selectivity, and important also in shaping the form of the feedforward pathway.

In the work of others (Bienenstock and et al., 1982; Linsker, 1987; Miller, 1989), the interaction between cortical neurons is assumed to play a weak role, i.e., 1) the

interconnections are not developing in their model, 2) to get a columnar organization, interconnections with a center-surround structure which itself lacks the columnar feature are used, and 3) they suggest the cortical interconnections structure may develop into columnized fashion after the development of the feedforward pathway. In our model, the network is developed in a time course just opposite to their model. The network first develops the columnar interconnections which guide the development of feedforward pathway. It is in accordance with an inside-out developmental rule of the visual pathway. We propose that the development of the interconnections is a complement to the development of feedforward pathway and in some sense an *a priori* requirement of that development.

The framework

The anatomical structure of the visual cortex area 17 has both inhibitory and excitatory interconnections. Excitatory cells send excitatory axons to other excitatory cells and to inhibitory cells. Inhibitory cells send inhibitory axons to other inhibitory cells and to excitatory cells. The range of the excitatory axons is about 20μ within which the excitatory is strong. There is about a region of range about 200μ within which both inhibitory and excitatory intralayer connection occur together. Outside that region is inhibitory interaction with range of about 500μ. The LGN inputs excitation to both the inhibitory and excitatory cells. The spread of LGN input from one LGN cell to cortex is about 400μ. (Lowel, S., Freeman, B., Singer, W., 1987; Gilbert, Wiesel, 1989; see Chapters 4 to 6 also.)

The next two sections show that for a more biological plausible system, one will get results similar to those in Chapter 3. The system has different neuron and synapse models from Chapter 3. The neuron model is more like a biological neuron with output dynamic range between zero and maximum frequency and a firing threshold for input. The synaptic change will follow the Hebbian rule but confined by biological

constrain so that excitatory connections will change between a positive value and zero and inhibitory connections will change between a negative value and zero. No sign change is allowed. Between two neurons, both positive and negative connections are allowed (through some supposed interneurons being excitatory and inhibitory respectively). The interconnections are not automatically symmetric. Initially, the synapse connections are grown out from one neuron with a probability of forming contact with other neurons.

The center-surround structure

We postulate that the initial projections of both excitatory and inhibitory connections are Gaussian distributed, i.e., the number of connections in unit area are proportional to $e^{-r^2/2\sigma^2}$ in which r is the distance between source and target cells and σ is the corresponding range of those kind of connections. The initial connection strengths for all the connections take a nonsaturated value. The LGN activity are treated as simple noise patterns to excite the network from one state to another using dynamic Equation 3.1 in Chapter 3.

During the development, the distribution functions $G_c(x, y)$ and $G_s(x, y)$ and the projections will not change while the strength of each synapse changes. Figure 7.1 shows a center-surround structure. Initially, the influence of interconnections are comparable to the influence of LGN inputs, such that the neuronal activities are able to change from one state to another and meanwhile the inputs from LGN cannot dominate. Since the approximate symmetry of the interconnections about different orientations, the neuronal activities go through states approximately symmetric about different orientations. Thus, the center-surround structure remains initially; only the strengths of each connection change.

When these connections grow big enough, the cortical state will be more and more influenced by intercortical connections. With a center-surround connection structure,

the neuronal activity tends to flow into periodic grating pattern. When symmetry breaking happens, the network will have periodic intercortical connections in some orientation.

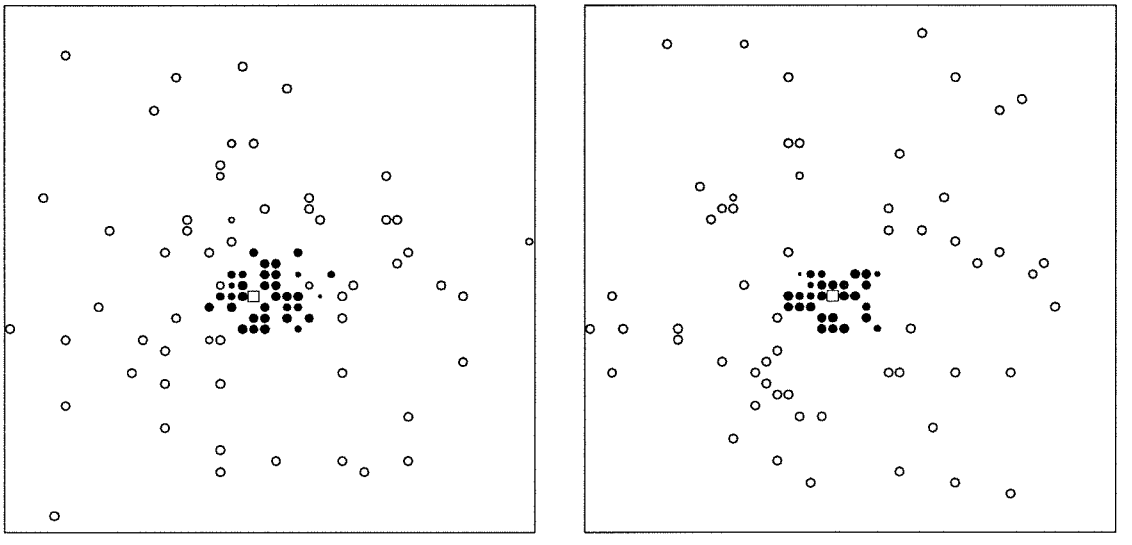

Figure 7.1 The simulated results of a sparsely interconnected network in which the projection follows a symmetric probability (Gaussian) distribution. On the left connections from cell 1270 to other cells are plotted. On the right connections from other cells to cell 1270 are plotted. The large rectangle in each plot outlines the area of cortex simulated. (See Chapters 4 to 6.) The small rectangle in each plot indicates the position of cell 1270. The initial learning keeps the center-surround structure. The correlation takes a form of a center region positive and surround region negative and only depends on the distance (i.e. isotropic). The excitatory connections (filled circles) in the center region tend to increase to its maximum, inhibitory ones tend to decrease to zero. In the surround region, the strength of excitatory connections tends to decrease to zero and inhibitory strength (blank circle) tends to increase to its maximum. The effective strength from a neuron to it surrounding ones is approximately a difference of Gaussian.

The symmetry breaking

The Figure 3.2 in Chapter 3 shows that for a symmetric kernel, the grating of any orientation will have equal Fourier transform components which are maximized at a single wavelength. Suppose the initial intercortical connections (as shown in the

last section) are a form of difference of Gaussian with center

$$G_c(x,y) = \frac{K_c}{2\pi\sigma_c^2} e^{-\frac{x^2+y^2}{2\sigma_c^2}} \quad [7.1]$$

and the surround

$$G_s(x,y) = \frac{K_s}{2\pi\sigma_s^2} e^{-\frac{x^2+y^2}{2\sigma_s^2}} \quad [7.2]$$

The Fourier transform of the center is

$$F_c(k_x,k_y) = K_c\, e^{-(k_x^2+k_y^2)2\sigma_c^2} \quad [7.3]$$

and of the surround is

$$F_s(k_x,k_y) = K_s\, e^{-(k_x^2+k_y^2)2\sigma_s^2} \quad [7.4]$$

It can be derived that

$$k_{max} = sqrt(\frac{ln(K_s\sigma_s^2) - ln(K_c\sigma_c^2)}{2(\sigma_s^2 - \sigma_c^2)}) \quad [7.5]$$

is the wavenumber corresponding to the maximum eigenvalue. The characteristic wavelength $\lambda_{max} = 2\pi/k_{max}$ and the wave could be in any direction (see Figure 3.2).

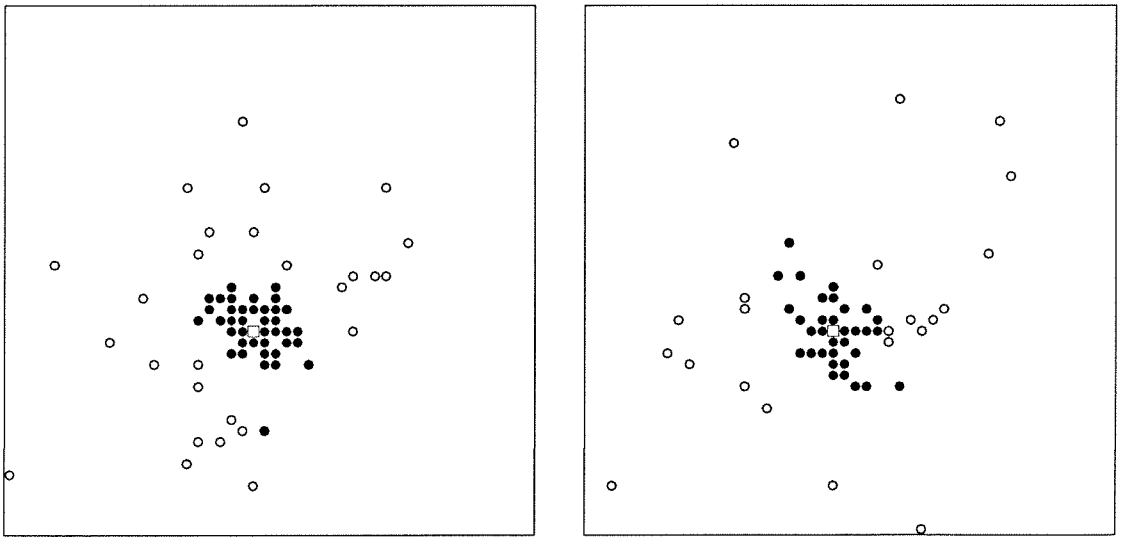

Figure 7.2 The initial stage of center-surround structure (see Figure 7.1). and final strip-like pattern are evident as same as symmetrically interconnected networks (see Chapter 3). The same as in Figure 7.1, on the left are the connections to the neuron and on the right are the connections from the neuron. Again the connections formed have an unsymmetric nature; most of neuron pairs which are connected have only a single connection, not bidirectional connections. But connections between groups of neurons, i.e., connections from neurons in one small region to neurons in another small region are roughly symmetric.

One important restriction is imposed on the extent that one cortical neuron can directly affect another part of the cortex. Both of the inhibitory and excitatory projection functions (that is, the number of possible connections in unit area) have limited effective regions. In our model, they are assumed to be Gaussian, and effectively zero outside several σ of the corresponding Gaussian. The arguments about symmetry breaking in Chpaters 2 and 3 apply here as well. The symmetry breaking global state is achieved by the locally effective intercortical connections (Figure 7.2).

The symmetry breaking of larger networks

The symmetry breaking demonstrated in Chapter 3 and in the last two sections deals only with a small section of the cortex. It exhibits the basic feature of the excitatory and inhibitory bands. To see the emerging of a strip-like intercortical connection structure, one needs to have a larger network. Hereafter, we will make use of the similarity in behavior of the network in Chapter 3 and the one in the last two sections, and use the simplified (symmetrically connected) network model of Chapter 3 for simulation of a larger size. The connections of one neuron to/from other neurons are shown in Figure 7.3a.

The symmetry breaking results in locally parallel strips and strips with different orientations are represented at different locations. It is columnar structure itself. Figure 7.3b shows the cortex neural activity state of one learning result. The cortex connections of the same learning results are shown in Figure 7.4. An excitatory connection between two neurons becomes +1 if the activities of the two neurons

are correlated (both +1 or both −1 in the learned strip-like state), an inhibitory connection between two neurons becomes −1 if the activities of the two neurons are anticorrelated (one +1 the other −1). Otherwise the connections becomes zero.

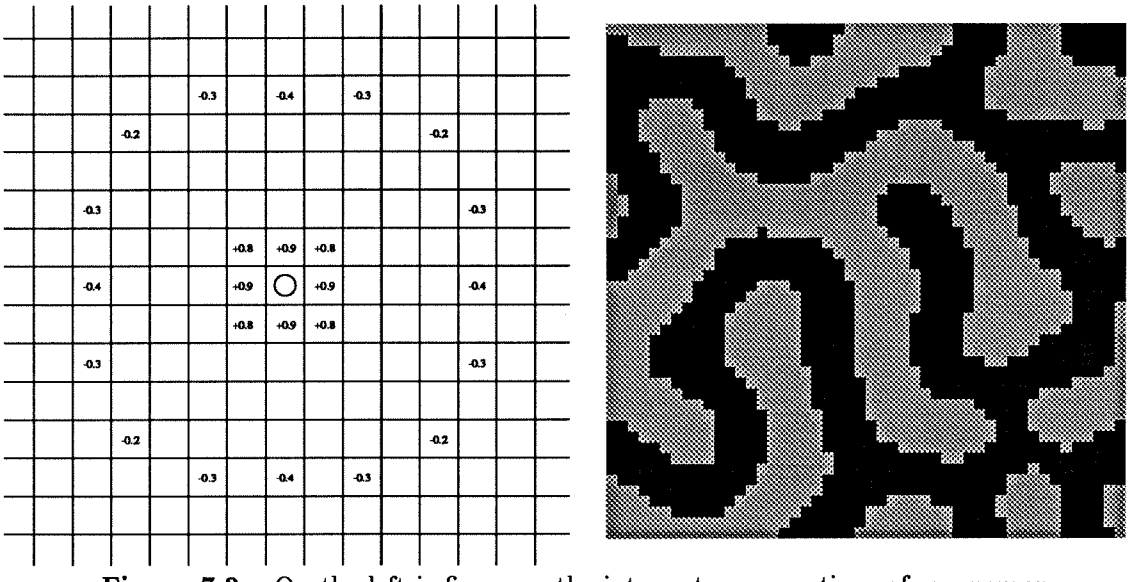

Figure 7.3 On the left is figure a: the intercortex connections of one neuron (blank circle) to/from other neurons. There are only 24 connections for each neuron. Excitatory connections are marked by "+" and inhibitory connections are marked by "−". The numbers represent the strengths of the initially learned center-surround connections. On the right is figure b: the symmetry breaking state of cortical neuronal activities (black represents −1). The strip-like pattern has a characteristic wave length of 10 but the directions are different at different position. See Figure 7.4 for the corresponding cortex connections pattern.

The feedforward pathways will be formed accordingly (Appendix C). The orientation of receptive field shifts with the same characteristic spatial frequency as the intercortical strips. As Linsker pointed out, similar orientation bands will tend to close to each other.

For our model, substitute $K_s = K_c$ and $\sigma_s = 10\sigma_c$ into Equation 7.5 the result is

$$\lambda_{max} = 2\pi/k_{max} = 4.0\sigma_s$$

For $\sigma_s = 300\mu$, the characteristic wavelength of the grating $\lambda_{max} = 1.2mm$. A comparison can be made with biological experiment. Lowel etc. studied the topographic

organization of the orientation column system in cat visual cortex by a 2-deoxyglucose experiment in which the characteristic periods of the band structure were $1.1mm$ (Lowel, Freeman and Singer, 1987; Gilbert, Wiesel, 1989). Our model predicts very well.

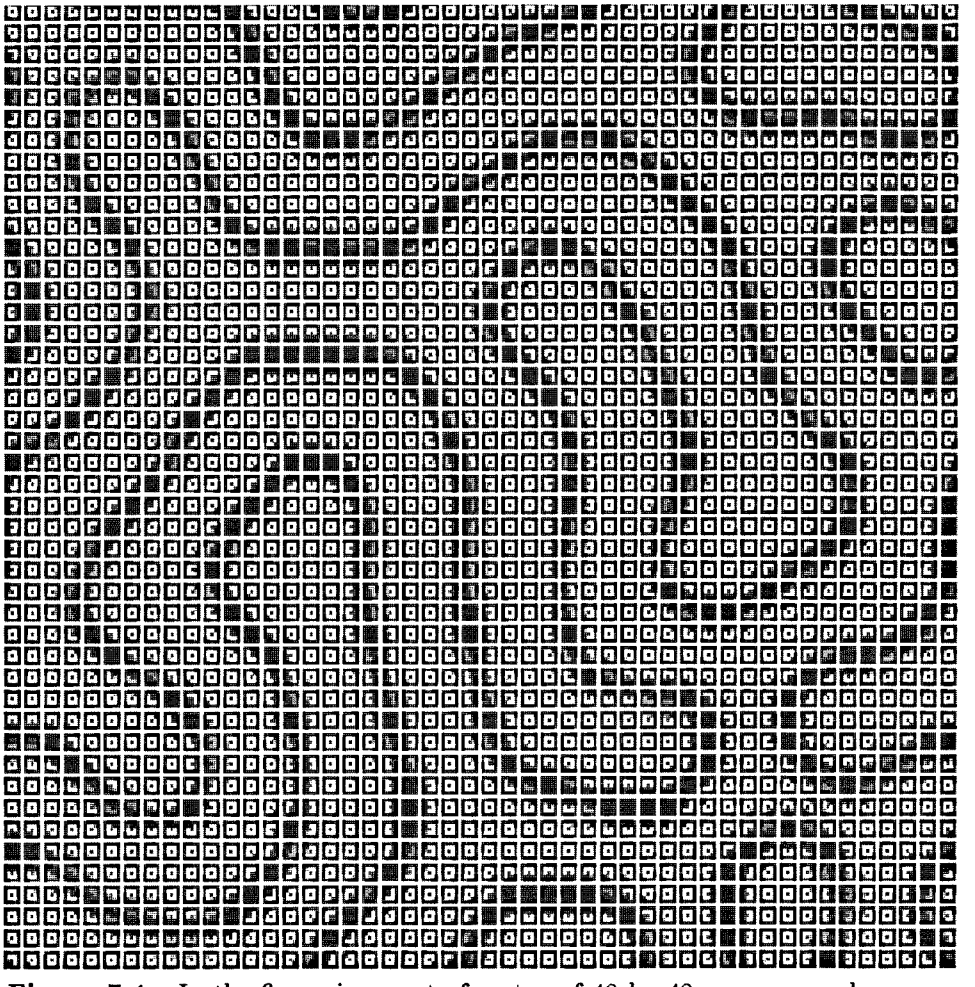

Figure 7.4 In the figure is a part of cortex of 48 by 48 neurons, each neuron connects to 5 by 5 other neurons (Figure 7.3a shows the connections of each neuron to/from other neurons, in which the values are the initially learned center-surround ones; after the symmetry breaking the values changed and different for each neurons as shown in here by gray scale: white represents +1, gray represents 0, and black represents −1). The symmetry breaking results in a stripelike pattern which has different orientation at different locations. The characteristic period of the locally parallel bands is 10 about the same size as the connections region, or twice the radii of anticorrelated region.

Discussion

Symmetric connections have been used for our theoretical analysis and for some of the simulations (Chapters 2 and 3). For the more biologically plausible network, the connections are not symmetric in a microscopic view, i.e., it is often happening that one neuron connects to the other but not *vice versa*. But macroscopic symmetric connections are sufficient to produce these general results, as was the case in previous sections where the projection function itself is symmetric. The interconnections we have been using in this modeling are a representation of the macroscopic interaction within cortex. In a microscopic view, the feedback loop is completed by going through several layers of visual cortex area 17 not just layer 4b. The several layers from 1 to 6, should be viewed as an integrated unit over depth, and units on the two-dimensional cortical surface interact with each other by the macroscopic interconnection we are using (Gilbert and Weisel, 1983, 1989).

Another difference between the modeling and neurobiology is the fact that a real neuron network works with action potentials which are discrete in nature. But action potentials, while they may be necessary for a truly quantitative comparison with experiments, are not necessary to generate or to understand the nature of the symmetry breaking. It is demonstrated in Chapters 4 to 6 that this accounts for more quantitative comparison of the simulation with biology experiments. It has been demonstrated that a simplified Hopfield kind of network without involving action potentials can achieve the same functionality qualitatively as orientation selectivity goes (Appendix B). As for the organization of the intercortical connections, it is sufficient to use the simplified model to get the results. A more biologically plausible, action potential driving network can be easily simulated to get more detailed prediction about the organization. But since there are not much data from biological experiment about this issue, it is not attempted in this research. The dynamic about symmetry

breaking about different orientations holds for inputs which are discrete pulses and whose strengths are described by time intervals between pulses (Figure 7.5).

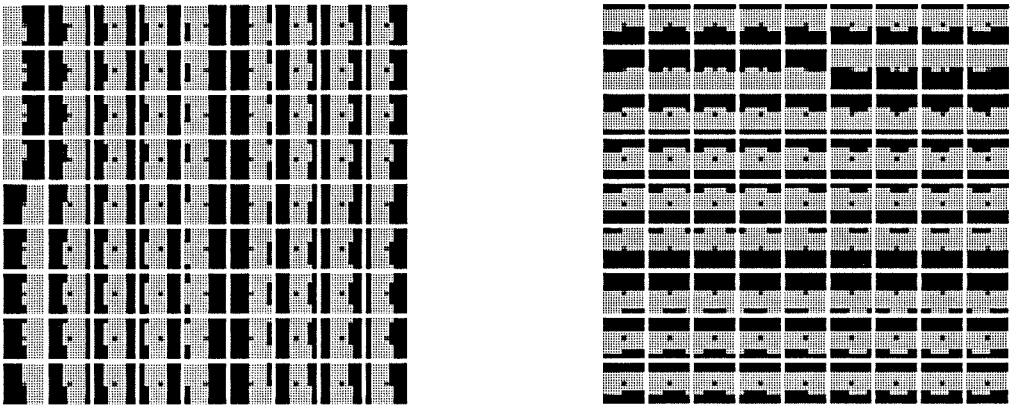

Figure 7.5 The simulated results of a interconnected network which is driven by pulsed inputs. The network will learn center-surround structure when the time interval between pulses is short corresponding to high frequency of action potentials, i.e., strong input. The symmetry breaking takes place when the inputs is weak corresponding to longer time intervals between input pulses.

There is evidence about Hebbian type synaptic developmental rule. NMDA is an often cited one (Cooper, Liberman, Oja, 1979; Miller, 1989). But that is basically an excitatory synaptic rule. There is little evidence about inhibitory Hebbian type developmental rules. Our model is not necessary to include the inhibitory Hebbian rule to get the symmetry breaking. The total effect from one cortex area to another is reflected by the summation of all inhibitory and excitatory connections. An increase of an inhibitory connection strength is equivalent to a decrease of an excitatory connection strength and *vice versa.* Suppose that the inhibitory connections are determined by genetic means and isotropic about different orientations and only the excitatory connections change according to Hebbian rules; similar results of symmetry breaking happens — but only the excitatory connections form the strip-like pattern.

Conclusion

Both intercortical connection structure and LGN to cortex connection structure break the symmetry about different orientations of the environmental inputs. The

functions of those structures have been compared in some detail with biological reality in Chapter 6. There are more biological details which can be incorporated into our model, but the main feature of orientation selective structure should be the same. What matters is the underling dynamics having the same properties, such as breaking up symmetry of input correlations and being stablized at those structures.

A.1

Example Program for Simulation Appendix A

```
/*
This is the program used to simulate the dynamics discussed in Chapter 2.
The draw_ routines are used to do interactive graphics, which are not
listed in here.
*/

#include <stdio.h>
#include <math.h>
#include "cdraw.h"

#ifndef TRUE
#define TRUE    1
#define FALSE   0
#endif
#ifndef max
#define max(x,y) ((x) > (y) ? (x) : (y))
#define min(x,y) ((x) < (y) ? (x) : (y))
#endif
#define MAXLONG   2147483647L
#define frandom(l,h) (((float)random()/MAXLONG)*((h)-(l))+(l))
#define sign(x)   ((x)<0?-1:1)
#define short_mode(x)((short)((x)*32767.0))
#define float_mode(x)((float)(x))/32767.0)
#define randsign() ((random()&01)*2-1)

int CORTEX_CONNNUM = 81;
int CORTEX_FIELD = 4;
int CELLNUM = 81;
int CELL_EDGE = 9;

float voltage[81];                      /* u in equation 24 */
float current[81];                      /* I in equation 24 */
float Connect[81][81];                  /* s in equation 24 */

/*
   curve array is used to save the developing connections of neuron 1
   to/from other neurons as a function of time.
*/

char curve[81][1000];

#define CURVE_AMP 63
#define CURVE_UNIT 1
#define CURVE_FREQ 200

int seed;
int step;
float gain=0.30;                        /* g in equation 24 */
```

```
float Hebb=1.00;                        /* H in equation 24 */
float ampl=30.0;                        /* A in equation 24 */
float Ampl=3.0;
float size=0.3;                         /* step size over a */
float Tize=0.001;                       /* step size over B */
int  freq=40;                           /* duration for each input */
char show_flag;
char flow_flag;

char menu[20][25] = {
   " initiate",
   " refresh",
   " Flow_flag",
   " Show_flag",
   " Read",
   " Write",
   " quit"};

float field[7][81];                      /* to store input patterns */

main(argc, argv)
int argc;
char *argv[];
   {
   long time0;
   FILE *fp;
      if (argc != 1) {
         seed =0;
         sscanf(argv[1], "%d", &seed);
      } else {
         time(&time0);
         seed = (int)(time0%65535);
      }
      fp = stdout;
      fprintf(fp, "(* seed = %d *)\n", seed);
      fprintf(fp, "(* gain = %.3f *)\n", gain);
      fprintf(fp, "(* Hebb = %.3f *)\n", Hebb);
      fprintf(fp, "(* size = %.3f *)\n", size);
      fprintf(fp, "(* Tize = %.3f *)\n", Tize);
      fprintf(fp, "(* ampl = %.3f *)\n", ampl);
      fprintf(fp, "(* Ampl = %.3f *)\n", Ampl);
      fprintf(fp, "(* freq = %5d *)\n", freq);
      fprintf(fp, "(* step = %5d *)\n", step);
      draw_init();
      initiate();
      refresh();
/*
   draw_loop() calls main_proc() when there is an input event
   (key stroke and mouse motion), otherwise calls main_step().
*/
      draw_loop();
   }

/*
   main_proc() interactively controls the flow of the programm
   by changing different flag and parameters.
*/
main_proc()
   {
      if ((t.up == 1 && t.x < 100) || (t.up == 0 && t.key == 'i') ) {
         initiate();
      } else if ((t.up == 1 && t.x < 200) || (t.up == 0 && t.key == 'r') ) {
         refresh();
      } else if ((t.up == 1 && t.x < 300) || (t.up == 0 && t.key == 'F') ) {
         flow_flag = (flow_flag+1)%3;
```

```
      if (flow_flag == 0 ) printf("flow : none\n");
      else if (flow_flag == 1 ) printf("flow : voltage\n");
      else if (flow_flag == 2 ) printf("flow : all\n");
    } else if ((t.up == 1 && t.x < 400) || (t.up == 0 && t.key == 'S') ) {
      show_flag = (show_flag+1)%3;
      if (show_flag == 0 ) printf("show : none\n");
      else if (show_flag == 1 ) printf("show : voltage\n");
      else if (show_flag == 2 ) printf("show : all\n");
    } else if ((t.up == 1 && t.x < 500) || (t.up == 0 && t.key == 'R') ) {
      read_connect();
    } else if ((t.up == 1 && t.x < 600) || (t.up == 0 && t.key == 'W') ) {
      write_connect();
    } else if ((t.up == 1 && t.x < 700) || (t.up == 0 && t.key == 'q') ) {
      quit();
    } else if ( (t.up == 1 && t.x > 800)
          || ((t.up == 0 && t.key >= '0' && t.key <= '6')) ) {
      rand_voltage((t.up == 0)?(t.key-'0'):((t.y-20)/100));
    } else if ((t.up == 1 && t.y < 200) || (t.up == 0 && t.key == 'g') ) {
      printf("gain = %f\n", gain);
      scanf("%f", &gain);
    } else if ((t.up == 1 && t.y < 250) || (t.up == 0 && t.key == 'H') ) {
      printf("Hebb = %f\n", Hebb);
      scanf("%f", &Hebb);
    } else if ((t.up == 1 && t.y < 300) || (t.up == 0 && t.key == 'a') ) {
      printf("ampl = %f\n", ampl);
      scanf("%f", &ampl);
    } else if ((t.up == 1 && t.y < 350) || (t.up == 0 && t.key == 'A') ) {
      printf("Ampl = %f\n", Ampl);
      scanf("%f", &Ampl);
    } else if ((t.up == 1 && t.y < 400) || (t.up == 0 && t.key == 's') ) {
      printf("size = %f\n", size);
      scanf("%f", &size);
    } else if ((t.up == 1 && t.y < 450) || (t.up == 0 && t.key == 'T') ) {
      printf("Tize = %f\n", Tize);
      scanf("%f", &Tize);
    } else if ((t.up == 1 && t.y < 500) || (t.up == 0 && t.key == 'f') ) {
      printf("freq = %d\n", freq);
      scanf("%d", &freq);
    } else if (t.up == 2) {
      plot_cell();
    }
  }

/*
  main_step() is where the simulation is done.
*/
main_step()
  {
  int i;
  char stmp[256];
  float outer();
    if (flow_flag >= 1) {
      draw_batch_on();
      draw_color(0);
      draw_area(0, 0, 350, 40);
      draw_color(1);
      sprintf(stmp, "%5d", step);
      for (i=1;i<7;i++)
        sprintf(stmp+(5*i), "%5d", (int)outer(voltage, field[i]));
      draw_text(20,20,stmp);
      if (show_flag >= 1) show_voltage_right();
/*
  if flow_flag >= 2, update connections according to Hebbian rule.
  Otherwise, only update voltage as a Hopfield network.
*/
```

```
        if (flow_flag >= 2) {
/*
  update input pattern after every freq number of steps
*/
          if (step%freq == 0) {
            rand_current();
            if (show_flag >= 2) show_current();
          }
          if (show_flag >= 2) show_Connect();
          step_Connect();
        }
        step_voltage();
        draw_batch_off();
/*
  save the current connections to/from neuron 1 after every
  CURVE_FREQ steps.
*/
        if (step%CURVE_FREQ == 0) save_curve();
        step += 1;
      }
    }

/*
  print out connections to/from cell pointed by mouse.
*/
plot_cell()
    {
    short x1, x2, x0;
    short y1, y2, y0;
    short cell, conn;
    FILE *fp;
    float func();
      fp = stdout;
      cell = (((t.y-50)/3 - CORTEX_FIELD)/(2*CORTEX_FIELD+2))*CELL_EDGE
           + (CELL_EDGE-1)/2;
      if (cell <0 || cell > CELLNUM-1 ) return;
      fprintf(fp,"cell = %d \n", cell);
      fprintf(fp,"ListPlot3D[{\n{");
      for( conn=0; conn<CORTEX_CONNNUM; conn++) {
        fprintf(fp,"%5.2f",
              func(Connect[cell][(conn+cell+(CORTEX_CONNNUM-1)/2+1)%81]));
        if (conn%9 == 8 && conn != 80) fprintf(fp,"},\n{");
        else if (conn != 80) fprintf(fp,",");
      }
      fprintf(fp,"}\n}]");
      fprintf(fp,"\n cell = %d \n", cell);
    }

show_Connect()
    {
    int cell, conn;
    short x0, y0;
    short x1, y1;
    short x2, y2;
    float mean[81];
    float allmean;
    float func();
      for( conn=0; conn<CORTEX_CONNNUM; conn++) {
        mean[conn] = 0.0;
      }
      for( cell=0; cell<CELLNUM; cell++) {
        x1 = cell%CELL_EDGE;
        y1 = cell/CELL_EDGE;
        for( conn=0; conn<CORTEX_CONNNUM; conn++) {
          x0 = 400 + 3*( (2*CORTEX_FIELD+2)*x1
```

```
            + CORTEX_FIELD );
        y0 = 50+3*( (2*CORTEX_FIELD+2)*y1
            + CORTEX_FIELD );
        if (conn != cell) {
          x2 = (conn)%CELL_EDGE;
          y2 = (conn)/CELL_EDGE;
          if (x2-x1 > CORTEX_FIELD) {
            x0 += 3*(x2-x1-CELL_EDGE);
          } else if (x2-x1 < -CORTEX_FIELD) {
            x0 += 3*(x2-x1+CELL_EDGE);
          } else {
            x0 += 3*(x2-x1);
          }
          if (y2-y1 > CORTEX_FIELD) {
            y0 += 3*(y2-y1-CELL_EDGE);
          } else if (y2-y1 < -CORTEX_FIELD) {
            y0 += 3*(y2-y1+CELL_EDGE);
          } else {
            y0 += 3*(y2-y1);
          }
          if (draw_depth == 1) {
            draw_color(Connect[cell][conn]>0?1:0);
          } else {
            draw_color((int)(8+7*func(Connect[cell][conn])));
          }
        } else {
          draw_color(0);
        }
        draw_area(x0, y0, x0+2, y0+2);
      }
    }
  }

show_voltage_left()
  {
  int cell;
  short x0, y0;
  short x1, y1;
  float func();
    for( cell=0; cell<CELLNUM; cell++) {
      x1 = cell%CELL_EDGE;
      y1 = cell/CELL_EDGE;
      x0 = 50+ 3*( (2*CORTEX_FIELD+2)*x1
          + CORTEX_FIELD );
      y0 = 350+3*( (2*CORTEX_FIELD+2)*y1
          + CORTEX_FIELD );
      if (draw_depth == 1) {
        draw_color(voltage[cell]>0?1:0);
      } else {
        draw_color((int)(8+7*func(voltage[cell])));
      }
      draw_area(x0-CORTEX_FIELD*3, y0-CORTEX_FIELD*3,
              x0+CORTEX_FIELD*3, y0+CORTEX_FIELD*3);
    }
  }

show_voltage_right()
  {
  int cell;
  short x0, y0;
  short x1, y1;
  float func();
    for( cell=0; cell<CELLNUM; cell++) {
      x1 = cell%CELL_EDGE;
      y1 = cell/CELL_EDGE;
```

```
        x0 = 400+ 3*( (2*CORTEX_FIELD+2)*x1
              + CORTEX_FIELD );
        y0 = 350+3*( (2*CORTEX_FIELD+2)*y1
              + CORTEX_FIELD );
        if (draw_depth == 1) {
           draw_color(voltage[cell]>0?1:0);
        } else {
           draw_color((int)(8+7*func(voltage[cell])));
        }
        draw_area(x0-CORTEX_FIELD*3, y0-CORTEX_FIELD*3,
                x0+CORTEX_FIELD*3, y0+CORTEX_FIELD*3);
     }
   }

show_current()
   {
   int cell;
   short x0, y0;
   short x1, y1;
   float func();
      for( cell=0; cell<CELLNUM; cell++) {
        x1 = cell%CELL_EDGE;
        y1 = cell/CELL_EDGE;
        x0 = 50+3*( (2*CORTEX_FIELD+2)*x1
              + CORTEX_FIELD );
        y0 = 50+3*( (2*CORTEX_FIELD+2)*y1
              + CORTEX_FIELD );
        if (draw_depth == 1)
           draw_color(current[cell]>0?1:0);
        } else {
           draw_color((int)(8+7*func(current[cell])));
        }
        draw_area(x0-CORTEX_FIELD*3, y0-CORTEX_FIELD*3,
                x0+CORTEX_FIELD*3, y0+CORTEX_FIELD*3);
     }
   }

show_vector_at(myvo, myxo, myyo)
   float myvo[];
   short myxo;
   short myyo;
   {
   int cell;
   short x0, y0;
   short x1, y1;
   float func();
      for( cell=0; cell<CELLNUM; cell++) {
        x1 = cell%CELL_EDGE;
        y1 = cell/CELL_EDGE;
        x0 = myxo+ ( (2*CORTEX_FIELD+2)*x1
              + CORTEX_FIELD );
        y0 = myyo+ ( (2*CORTEX_FIELD+2)*y1
              + CORTEX_FIELD );
        if (draw_depth == 1) {
           draw_color(myvo[cell]>0?1:0);
        } else {
           draw_color((int)(8+7*func(myvo[cell])));
        }
        draw_area(x0-CORTEX_FIELD, y0-CORTEX_FIELD,
                x0+CORTEX_FIELD, y0+CORTEX_FIELD);
     }
   }

/*
   change current to next input pattern
```

```
*/
rand_current()
   {
   int cell,conn;
   static short ff;
      ff = (ff+1)%6;
      for( cell=0; cell<CELLNUM; cell++) {
         current[cell] = ampl*(field[ff+1][cell]);
      }
   }

/*
   chage voltage to a test state
*/
rand_voltage(wp)
   int wp;
   {
   int cell;
   int ff;
      draw_batch_on();
      if (wp < 0) {
         ff = random()%7;
      } else {
         ff = wp;
      }
      if (ff == 0) {
         for( cell=0; cell<CELLNUM; cell++) {
            current[cell] = Ampl*(field[1][cell]+field[2][cell]);
            voltage[cell] = randsign();
         }
      } else {
         for( cell=0; cell<CELLNUM; cell++) {
            current[cell] = Ampl*(field[ff][cell]);
            voltage[cell] = randsign();
         }
      }
      show_current();
      show_voltage_left();
      draw_batch_off();
   }

/*
   generate six input patterns with inner products between them
   no larger than 3
*/
init_current()
   {
   int cell;
   float outer();
      for(cell=0;cell<CELLNUM;cell++) field[1][cell]=randsign();
      do {
         for(cell=0;cell<CELLNUM;cell++) field[2][cell]=randsign();
      } while (fabs(outer(field[1], field[2])) > 4
            );
      do {
         for(cell=0;cell<CELLNUM;cell++) field[3][cell]=randsign();
      } while (fabs(outer(field[2], field[3])) > 4
           || fabs(outer(field[1], field[3])) > 4
            );
      do {
         for(cell=0;cell<CELLNUM;cell++) field[4][cell]=randsign();
      } while (fabs(outer(field[3], field[4])) > 4
           || fabs(outer(field[2], field[4])) > 4
           || fabs(outer(field[1], field[4])) > 4
            );
```

```
      do {
         for(cell=0;cell<CELLNUM;cell++) field[5][cell]=randsign();
      } while (fabs(outer(field[4], field[5])) > 4
            || fabs(outer(field[3], field[5])) > 4
            || fabs(outer(field[2], field[5])) > 4
            || fabs(outer(field[1], field[5])) > 4
             );
      do {
         for(cell=0;cell<CELLNUM;cell++) field[6][cell]=randsign();
      } while (fabs(outer(field[5], field[6])) > 4
            || fabs(outer(field[4], field[6])) > 4
            || fabs(outer(field[3], field[6])) > 4
            || fabs(outer(field[2], field[6])) > 4
            || fabs(outer(field[1], field[6])) > 4
             );
   }

init_voltage()
   {
   int cell;
      for( cell=0; cell<CELLNUM; cell++) {
         voltage[cell] = 0.0;
      }
   }

init_Connect()
   {
   int cell;
   int conn;
   int memo;
      for( cell=0; cell<CELLNUM; cell++) {
         Connect[cell][cell] = 0.0;
         for( conn=cell+1; conn<CORTEX_CONNNUM; conn++) {
            Connect[cell][conn] = 0.0;
            Connect[conn][cell] = Connect[cell][conn];
         }
      }
   }

step_voltage()
   {
   register float tmp;
   int cell;
   int conn;
   float y[81];
   float func();
      for( cell=0; cell<CELLNUM; cell++) {
         tmp = 0.0;
         for( conn=0; conn<CORTEX_CONNNUM; conn++) {
            tmp += func(Connect[cell][conn])*func(voltage[conn]);
         }
         y[cell]=voltage[cell]+size*(gain*tmp+current[cell]-voltage[cell]);
      }
      for( cell=0; cell<CELLNUM; cell++) {
         voltage[cell] = y[cell];
      }
   }

step_Connect()
   {
   int cell;
   int conn;
   float func();
      for( cell=0; cell<CELLNUM; cell++) {
         for( conn=cell+1; conn<CORTEX_CONNNUM; conn++) {
```

```
            Connect[cell][conn] +=
                Tize*(Hebb*func(voltage[cell])*func(voltage[conn])
                      -Connect[cell][conn]);
            Connect[conn][cell] = Connect[cell][conn];
          }
        }
    }

initiate()
    {
      show_flag = 0;
      flow_flag = 2;
      step = 0 ;
      srandom((int)(seed));
      init_current();
      init_voltage();
      init_Connect();
      putchar((char)7);
      printf("Done. initiate.\n");
    }

refresh()
    {
    int i;
    char stmp[80];
    int cell;
    int conn;
    float tmp;
    int memo;
    float func();
    float outer();
      printf("Energy: ");
      for (memo=0;memo<7;memo++) {
        tmp = 0.0;
        for( cell=0; cell<CELLNUM; cell++) {
          for( conn=cell+1; conn<CORTEX_CONNNUM; conn++) {
            tmp +=
                  func(field[memo][cell])
                 *func(Connect[cell][conn])
                 *func(field[memo][conn]);
          }
        }
        printf("%7.1f", 2.0*tmp);
      }
      printf("\n");
      draw_batch_on();
      draw_color(3);
      draw_clear();
      show_current();
      show_voltage_left();
      show_Connect();
      show_voltage_right();
      draw_color(1);
      for (i=0; i<7; i++) {
        draw_rect(i*100,670,(1+i)*100,700);
        draw_text(i*100,690,menu[i]);
      }
      sprintf(menu[10], "seed = %5d", seed);
      sprintf(menu[11], "gain = %.3f", gain);
      sprintf(menu[12], "Hebb = %.3f", Hebb);
      sprintf(menu[13], "size = %.3f", size);
      sprintf(menu[14], "Tize = %.3f", Tize);
      sprintf(menu[15], "ampl = %.3f", ampl);
      sprintf(menu[16], "Ampl = %.3f", Ampl);
      sprintf(menu[17], "freq = %5d", freq);
```

```
    sprintf(menu[18], "step = %5d", step);
    for (i=0; i<9; i++) {
      draw_text(700,100+i*50,menu[i+10]);
    }
    for (i=0; i<16; i++){
      draw_color(i);
      draw_area(i*30, 640, i*30+27, 670);
    }
    draw_color(1);
    draw_rect(0, 640, 480, 670);
    printf("Outer : ");
    for (i=0; i<7; i++){
      show_vector_at(field[i], 850, 20+i*100);
      printf("%7.1f", outer(current, field[i]));
    }
    printf("\n");
    draw_batch_off();
    putchar((char)7);
    printf("Done. refresh.\n");
  }

read_connect()
  {
  int cell;
  int conn;
  int tt=0;
  FILE *fp;
    if ( (fp=fopen("develop.conn","r")) == NULL ) {
      printf("can not open file develop.conn!\n");
      return;
    }
    fscanf(fp, "(* seed = %d *)\n", &seed);
    fscanf(fp, "(* gain = %f *)\n", &gain);
    fscanf(fp, "(* Hebb = %f *)\n", &Hebb);
    fscanf(fp, "(* size = %f *)\n", &size);
    fscanf(fp, "(* Tize = %f *)\n", &Tize);
    fscanf(fp, "(* ampl = %f *)\n", &ampl);
    fscanf(fp, "(* Ampl = %f *)\n", &Ampl);
    fscanf(fp, "(* freq = %d *)\n", &freq);
    fscanf(fp, "(* step = %d *)\n", &step);
    fscanf(fp, "ListPlot3D[{\n");
    for( cell=0; cell<CELLNUM-1; cell++) {
      fscanf(fp, "{");
      for( conn=0; conn<CORTEX_CONNNUM-1; conn++) {
        if (conn%12 == 0) fscanf(fp,"\n");
        fscanf(fp,"%f,", &Connect[cell][conn]);
      }
      for( conn=CORTEX_CONNNUM-1; conn<CORTEX_CONNNUM; conn++) {
        if (conn%12 == 0) fscanf(fp,"\n");
        fscanf(fp,"%f", &Connect[cell][conn]);
      }
      fscanf(fp, "},\n");
    }
    for( cell=CELLNUM-1; cell<CELLNUM; cell++) {
      fscanf(fp, "{");
      for( conn=0; conn<CORTEX_CONNNUM-1; conn++) {
        if (conn%12 == 0) fscanf(fp,"\n");
        fscanf(fp,"%f,", &Connect[cell][conn]);
      }
      for( conn=CORTEX_CONNNUM-1; conn<CORTEX_CONNNUM; conn++) {
        if (conn%12 == 0) fscanf(fp,"\n");
        fscanf(fp,"%f", &Connect[cell][conn]);
      }
      fscanf(fp, "}\n");
    }
```

```
      fscanf(fp, "}]\n");
      fclose(fp);
      putchar((char)7);
      printf("Done. read.\n");
   }

write_connect()
   {
   int cell;
   int conn;
   int tt=0;
   FILE *fp;
      if ( (fp=fopen("develop.conn","w")) == NULL ) {
         printf("can not open file develop.conn!\n");
         return;
      }
      fprintf(fp, "(* seed = %5d *)\n", seed);
      fprintf(fp, "(* gain = %.3f *)\n", gain);
      fprintf(fp, "(* Hebb = %.3f *)\n", Hebb);
      fprintf(fp, "(* size = %.3f *)\n", size);
      fprintf(fp, "(* Tize = %.3f *)\n", Tize);
      fprintf(fp, "(* ampl = %.3f *)\n", ampl);
      fprintf(fp, "(* Ampl = %.3f *)\n", Ampl);
      fprintf(fp, "(* freq = %5d *)\n", freq);
      fprintf(fp, "(* step = %5d *)\n", step);
      fprintf(fp, "ListPlot3D[{\n");
      for( cell=0; cell<CELLNUM-1; cell++) {
         fprintf(fp, "{");
         for( conn=0; conn<CORTEX_CONNNUM-1; conn++) {
            if (conn%12 == 0) fprintf(fp,"\n");
            fprintf(fp,"%5.2f,", Connect[cell][conn]);
         }
         for( conn=CORTEX_CONNNUM-1; conn<CORTEX_CONNNUM; conn++) {
            if (conn%12 == 0) fprintf(fp,"\n");
            fprintf(fp,"%5.2f", Connect[cell][conn]);
         }
         fprintf(fp, "},\n");
      }
      for( cell=CELLNUM-1; cell<CELLNUM; cell++) {
         fprintf(fp, "{");
         for( conn=0; conn<CORTEX_CONNNUM-1; conn++) {
            if (conn%12 == 0) fprintf(fp,"\n");
            fprintf(fp,"%5.2f,", Connect[cell][conn]);
         }
         for( conn=CORTEX_CONNNUM-1; conn<CORTEX_CONNNUM; conn++) {
            if (conn%12 == 0) fprintf(fp,"\n");
            fprintf(fp,"%5.2f", Connect[cell][conn]);
         }
         fprintf(fp, "}\n");
      }
      fprintf(fp, "}]\n");
      fclose(fp);
      putchar((char)7);
      write_curve();
      printf("Done. write.\n");
   }

save_curve()
   {
   short i;
   short posi;
      posi = step/CURVE_FREQ;
      for (i=0;i<CORTEX_CONNNUM;i++) {
         curve[i][posi] = (char)(Connect[CURVE_UNIT][i]*CURVE_AMPL);
      }
```

```
   }

write_curve()
   {
   short i,j;
   short num;
   FILE *fp;
      if ( (fp = fopen("develop.curv","w")) == NULL ) {
         printf("can not open develop.curv!\n");
         return;
      }
      fprintf(fp, "(* seed = %d *)\n", seed);
      fprintf(fp, "(* gain = %.3f *)\n", gain);
      fprintf(fp, "(* Hebb = %.3f *)\n", Hebb);
      fprintf(fp, "(* size = %.3f *)\n", size);
      fprintf(fp, "(* Tize = %.3f *)\n", Tize);
      fprintf(fp, "(* ampl = %.3f *)\n", ampl);
      fprintf(fp, "(* Ampl = %.3f *)\n", Ampl);
      fprintf(fp, "(* freq = %5d *)\n", freq);
      fprintf(fp, "(* step = %5d *)\n", step);
      fprintf(fp, "(* CURVE_FREQ %5d *)\n", CURVE_FREQ);
      fprintf(fp, "(* CURVE_UNIT %5d *)\n", CURVE_UNIT);
      fprintf(fp, "ListPlot[{\n");
      num = (short)(step/CURVE_FREQ);
      for (i=0;i<CORTEX_CONNNUM;i++) {
         fprintf(fp, "{0.0, 0.0},\n");
         for (j=0;j<num;j++) {
            fprintf(fp, "{%.1f, %.2f},",
                  (float)(j), (float)(curve[i][j])/CURVE_AMPL);
            if (j%5 == 4) fprintf(fp, "\n");
         }
         fprintf(fp, "{%.1f,0.0},\n", (float)(num-1));
      }
      fprintf(fp, "{0.0, 0.0}\n");
      fprintf(fp, "}, PlotJoined -> True, PlotStyle -> {Thickness[.001]}]\n");
      fclose(fp);
   }

quit()
   {
      write_connect();
      exit();
   }

/* The function F in equation 24 */
float func(y)
   float y;
   {
      y = y>1?1:y<-1?-1:y;
      return (y);
   }

/* The outer product */
float outer(x,y)
   float x[];
   float y[];
   {
   int i;
   float tmp;
      tmp = 0.0;
      for (i=0;i<81;i++) {
         tmp += func(x[i])*func(y[i]);
      }
      return (tmp);
   }
```

B.1

Simple Model of Orientation Selectivity Appendix B

Introduction

There is great controversy as to the wiring underlying orientation selectivity in mammalian visual cortex. Various experiments show the crucial nature of inhibition in shaping orientation selectivity. We propose a network model to explain how orientation selectivity arises from inhibition between cells of visual cortex. We implement this model as a Hopfield network (Hopfield, 1984). The results show that all the cortical cells can have proper orientation selectivity.

In this research, we emphasize the important role the interconnections play to the emerging property of a layered network. Various research has been concentrated on the projection of axons from one layer of neurons to another layer in which the interconnections within the same layer of neurons are either ignored or play a side role. But it is observed in the cortex that the majority of synaptic connections in most cortex areas are the interconnections originated and running though the same layer. This kind of connection plays an important role in shaping up the functionality of the neurons in that layer.

Orientation selectivity in cat visual cortex was first observed in the post synaptic targets of afferent fibers to the striate cortex (V1) originating in the lateral geniculate nucleus (LGN). These cells respond optimally to a bar at their preferred orientation and similar oriented cells form columns. Hubel and Wiesel proposed the first detailed model to explain this (Figure 1).

B.2

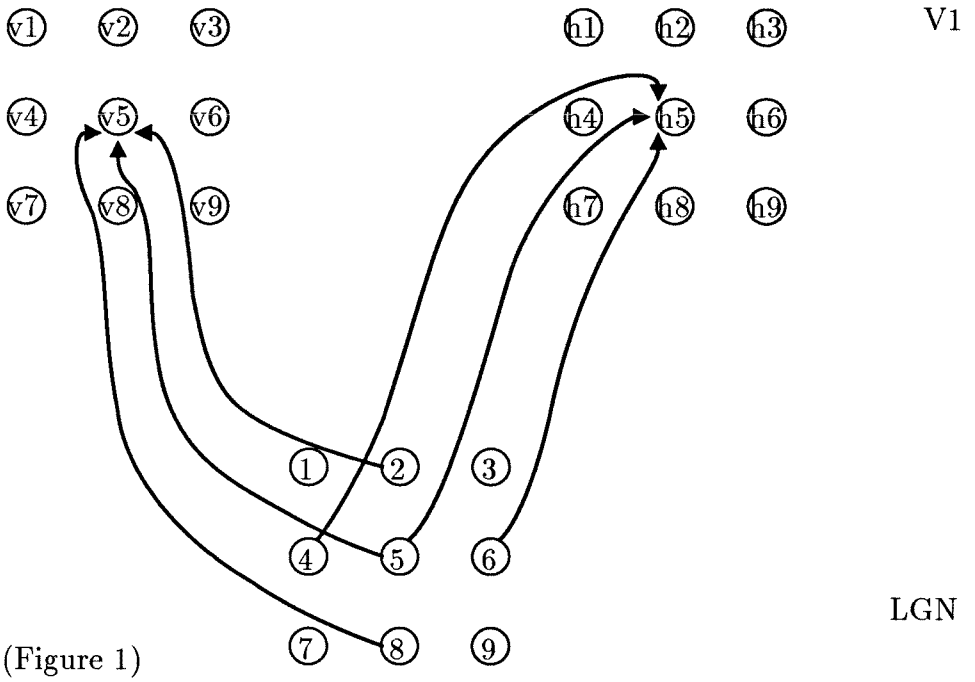

(Figure 1)

In their model cortical cells in V1 are excited by a number of cells in LGN which are arranged in a row. (In vertical oriented column, v5 excited by 2, 5 and 8 in LGN. In horizontal oriented column h5 excited by 4, 5 and 6 in LGN.) By setting proper threshold the cortical cell will fire when and only when the summation of LGN cells in the row exceed a fixed value. This is an "excitatory" model in which the orientation selectivity arises from the anisotropic excitatory connections from LGN to cortical cells (Malsburg, Cowan 1982; Ferster, 1986).

But a strong evidence in favor of inhibition comes from experiments in which the presumed GABAergic cortical inhibition is blocked by GABA antagonists (Sillito, 1975; 1980). When these drugs are applied to the cortex, cells lose orientation selectivity and their receptive field become circularly symmetrical and equal to that expected from one or few overlapping LGN cells.

Many people believe that inhibition is important and proposed various models of orientation selectivity depending on cortical inhibitory interneurons (Bishop, 1971;

Benevento, 1972; Heggelund, 1981, 1983; Nielsen, 1983; Gilbert, 1977). However, these models always assume the existence of non-oriented inhibitory interneurons which receive input from the LGN and inhibit the orientation selective cell at non-optimal orientations. But as Gilbert pointed out, no significant population of non-oriented cells has been reported in cat striate cortex.

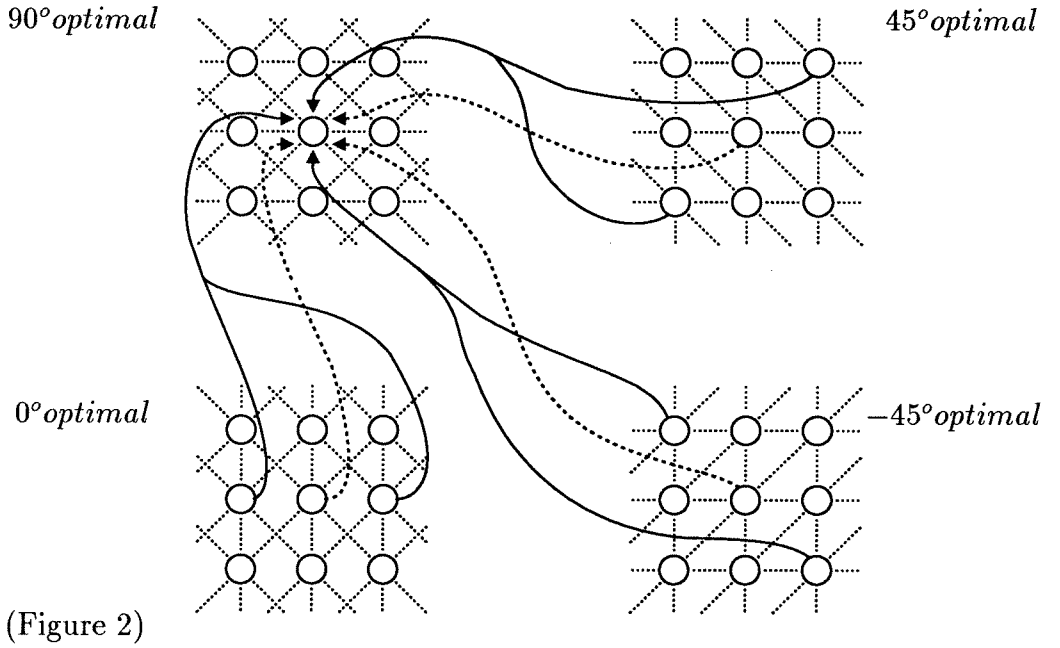

(Figure 2)

We believe that inhibition between cortical cells plays an important role in orientation selectivity in cat visual cortex and have postulated inhibition model of orientation selectivity as illustrated in Figure 2 and Figure 4. In this model the input connection from excitatory LGN cells to each cortical cell is isotropic. The orientation selectivity arises from the interaction between cortical cells and all of the cortical cells have orientation selectivity.

The inhibitory network model

In our model the excitatory LGN input connections to cortex are isotropic. To simplify our simulation, the cortical cells which corresponding to the same spacial

location but in different orientation columns receive the same excitatory input from one LGN cell. (v5 and h5 only receive input from LGN cell 5 , v4 and h4 only receive input from LGN cell 4 , etc.) We simulate four columns.

Within same column, cortical cells are inhibited by all their neighbors except the cells in the preferring orientation. (h5 is inhibited by h1, h2, h3, h7, h8 and h9). Between different columns, each cell (v5) receives inhibition from the cell at the same spacial location of other column (h5) and its neighbors in the optimal orientation (h4 and h6). Figure 2 shows the inhibition version of our model, which consists entirely of inhibitory cortical cells. (All the inhibitory connections to the cell in the center of 90° column are shown).

We can drive the dynamic equation:

$$\frac{du_{ij}^n}{dt} = -\frac{1}{\tau_s}\sum_{k,l}\sigma_{ijkl}^n V_{kl}^n - \frac{1}{\tau_d}\sum_{m\neq n} V_{ij}^m - \frac{1}{\tau_e}\sum_{k,l,m\neq n}(1-\sigma_{ijkl}^m)V_{kl}^m \qquad [B.1]$$

$$-\frac{1}{\tau_t}u_{ij}^n + \frac{1}{\tau_g}I_{ij} \qquad [B.2]$$

in which

$$V_{ij}^n = \frac{1}{1+e^{(-\alpha\times(u_{ij}^n-\theta))}} \qquad [B.3]$$

α — amplification

θ — threshold

I_{ij} — output of the LGN cell at location (i,j)

u_{ij}^n — input of the cell at location (i,j) in orientation column n

V_{ij}^n — output of the cell at location (i,j) in orientation column n

$$\sigma_{ijkl}^n = \delta_{i,k+1}\delta_{j,l}\eta_{1,0}^n + \delta_{i,k-1}\delta_{j,l}\eta_{-1,0}^n + \delta_{i,k}\delta_{j,l+1}\eta_{0,1}^n + \delta_{i,k}\delta_{j,l-1}\eta_{0,-1}^n \qquad [B.4]$$

$$+\delta_{i,k+1}\delta_{j,l-1}\eta_{1,-1}^n + \delta_{i,k-1}\delta_{j,l+1}\eta_{-1,1}^n + \delta_{i,k+1}\delta_{j,l+1}\eta_{1,1}^n + \delta_{i,k-1}\delta_{j,l-1}\eta_{-1,-1}^n \qquad [B.5]$$

The matrix η^n is shown in Figure 3,

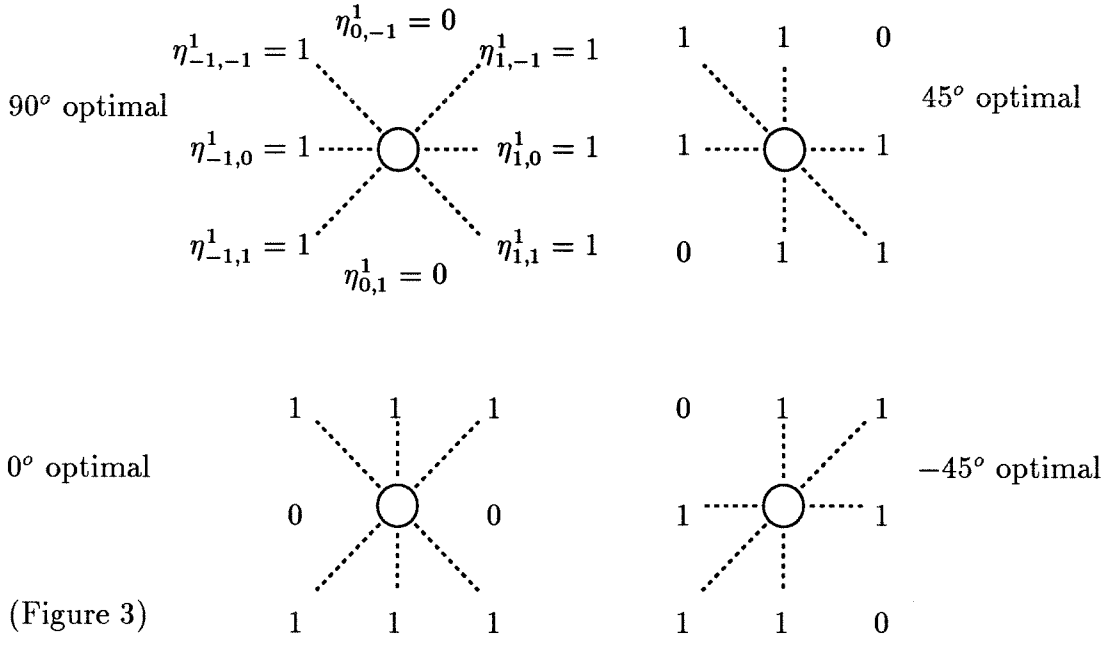

(Figure 3)

On the right side of the dynamic equation, the first term represents the inhibition within the same column, the second and the third terms represent the inhibition between different columns, the fourth term is the decay term and the fifth term is the input from the LGN layer. For each term there is a corresponding time constant. Those time constants are parameters in our simulation.

One should choose:

$$\frac{1}{\tau_d} < \frac{1}{\tau_g} \quad , \quad \frac{1}{\tau_e} < \frac{1}{\tau_g} \qquad [B.6]$$

and

$$\frac{1}{\tau_d} + \frac{1}{\tau_e} > \frac{1}{\tau_g} - \frac{\theta}{\tau_t} \qquad [B.7]$$

Since $\tau_d > \tau_g$ and $\tau_e > \tau_g$, one cell alone in one column cannot strongly inhibit a cell in another column which is excited by the input from LGN. Since $\frac{1}{\tau_d} + \frac{1}{\tau_e}$ is large enough, the two cells excited in the preferred column can strongly inhibit cells at corresponding locations in other columns.

We use the set of parameter

$$\tau_g = 1.000 \quad \tau_d = 2.500 \quad \tau_s = 6.000 \quad \tau_e = 3.000 \qquad [B.8]$$

$$\alpha = 64 \quad \theta = 0.100 \quad \tau_t = 0.187 \qquad [B.9]$$

It works very well. The simulation results are shown in Figures 5 through 8. The network always goes to the stable states within the order of ten total time constant (τ_t).

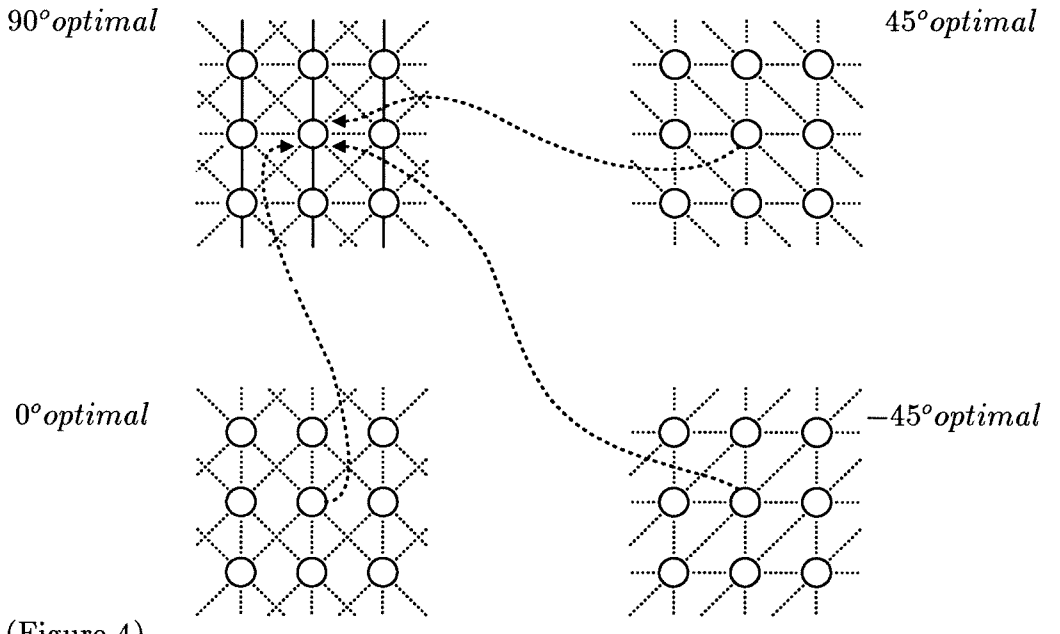

(Figure 4)

The inhibitory and excitatory model

Figure 4 shows another possible structure. Cortical cells are excited by neighbor cells in preferred direction and inhibited by other neighbor cells. Optionally, one can add in inhibition between different orientation columns. (excitatory connections, solid lines, are only drawn in for 90° cells).

It is easy to derive the dynamic equation

$$\frac{du_{ij}^n}{dt} = -\frac{1}{\tau_s}\sum_{k,l}\sigma_{ijkl}^n V_{kl}^n - \frac{1}{\tau_d}\sum_{m\neq n} V_{ij}^m + \frac{1}{\tau_e}\sum_{k,l}(1-\sigma_{ijkl}^n)V_{kl}^n \qquad [B.10]$$

$$-\frac{1}{\tau_t}u_{ij}^n + \frac{1}{\tau_g}I_{ij} \qquad [B.11]$$

in which the third term represents the excitation within the same column.

One should choose:

$$\frac{1}{\tau_e} < \frac{\theta}{\tau_t} \quad , \quad \frac{1}{\tau_g} < \frac{\theta}{\tau_t} \qquad [B.12]$$

and

$$\frac{1}{\tau_e} + \frac{1}{\tau_g} > \frac{\theta}{\tau_t} \qquad [B.13]$$

One should choose $\frac{1}{\tau_g}$ not too large in order that the LGN excitation alone will only excite cortical cells near to threshold. One should choose $\frac{1}{\tau_e}$ not too large, otherwise the excitation between two neighbor cells will be too strong and it will excite the neighbor cell above threshold. One should choose $\frac{1}{\tau_e} + \frac{1}{\tau_g}$ large enough, so that if the stimulus line is in the preferred direction of the column, the neighbor cells on the line will excite each other and then jump above the threshold. If the stimulus line is not in the preferred direction, the neighbor cells on the line will inhibit each other and will stay below the threshold.

We use the set of parameter

$$\tau_g = 1.000 \quad \tau_d = 12.00 \quad \tau_s = 2.300 \quad \tau_e = 2.700$$

$$\alpha = 64 \quad \theta = 0.200 \quad \tau_t = 0.166$$

The results are very similar to what we have showed for section 2.

Conclusion

The simulation shows our model works. As mentioned before the orientation selectivity arises from the interaction between cortical cells and each cortical cell has orientation selectivity. Thus this kind of orientation selectivity is a population property. At cross-point of two presenting lines, which one of the corresponding cells

in the two orientation columns will fire may depend on their previous state. All other cells, no matter what their previous state is, fire for the correct spacial locations and within the correct orientation columns. Like other inhibitory models, when inhibition is blocked (set corresponding time constants to infinite), the orientation selectivity disappears (as in GABA experiment), cells in all columns will fire if stimulus fall on their spacial locations. (See Figure 10 and Figure 12.)

Discussion

The inhibitory model presented in this paper works qualitatively. In order to compare the model quantitatively with neuronal data (for example, different responses to different contrasts), we have implemented the model in a more biological plausible way which confirmed the qualitative result. The detail is beyond the scope of this chapter.

From the analysis of section 2, one can find out that the inhibition within the same column is not necessary at all for the model shown in Figure 2, i.e., cross inhibition between different columns alone is enough. See Figure 9, in which we used the following parameters:

$$\tau_g = 1.000 \quad \tau_d = 2.500 \quad \tau_s = 1e^{+10} \quad \tau_e = 3.000$$

$$\alpha = 64 \quad \theta = 0.100 \quad \tau_t = 0.230$$

On the other hand the model shown in Figure 4 can work without cross inhibition between different columns. See Figure 11, in which we used the following parameters:

$$\tau_g = 1.000 \quad \tau_d = 1e^{+10} \quad \tau_s = 2.300 \quad \tau_e = 2.700$$

$$\alpha = 64 \quad \theta = 0.200 \quad \tau_t = 0.173$$

It is also possible that the network assumes a combinative form of the two models. But two points are clear: all cortical cells can have orientation selectivity which arises

from the interaction between cortical cells, and inhibition plays an important role in the orientation selectivity.

The biological structure of orientation selectivity could be a combinatione of both feedforward structure from LGN to cortex and feedback structures within cortex. In Chapters 4 to 6, we study the neuronal network in a more plausible way by constructing the network in parallel with the real visual pathway and by using anatomic parameters. The result is qualitatively agreed with results here. Some quantitative results is derived and can be compared with experimental results.

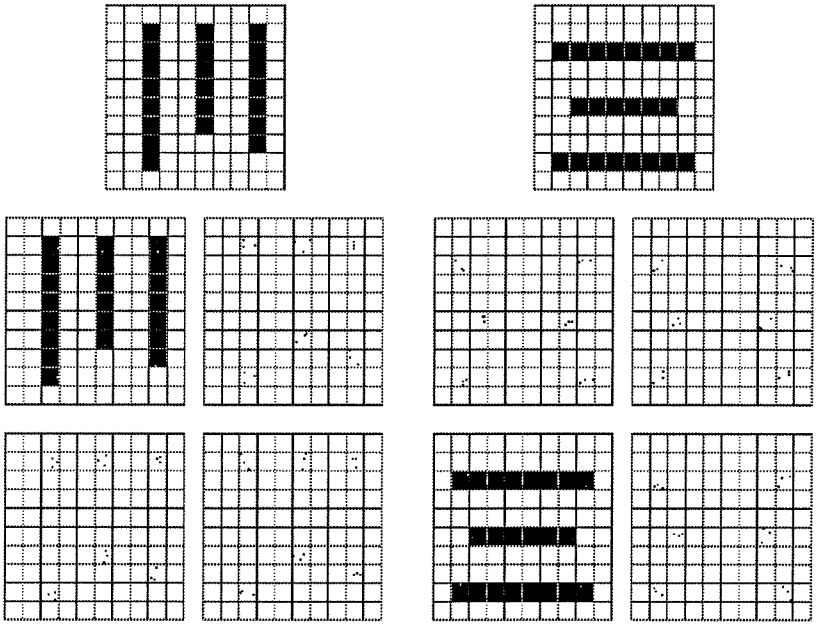

Figures 5, 6, 7, and 8: The figures above and below show a sequence of simulation results. There are five checkerboards in each figure. The top one represents the state of LGN , the other four represent the states of four cortical columns with different orientation selectivity. 10x10 squares represent 10x10 cells and the number of dots in each square is proportional to the activity, i.e., I_{ij} for LGN and V_{ij}^n for cortex.

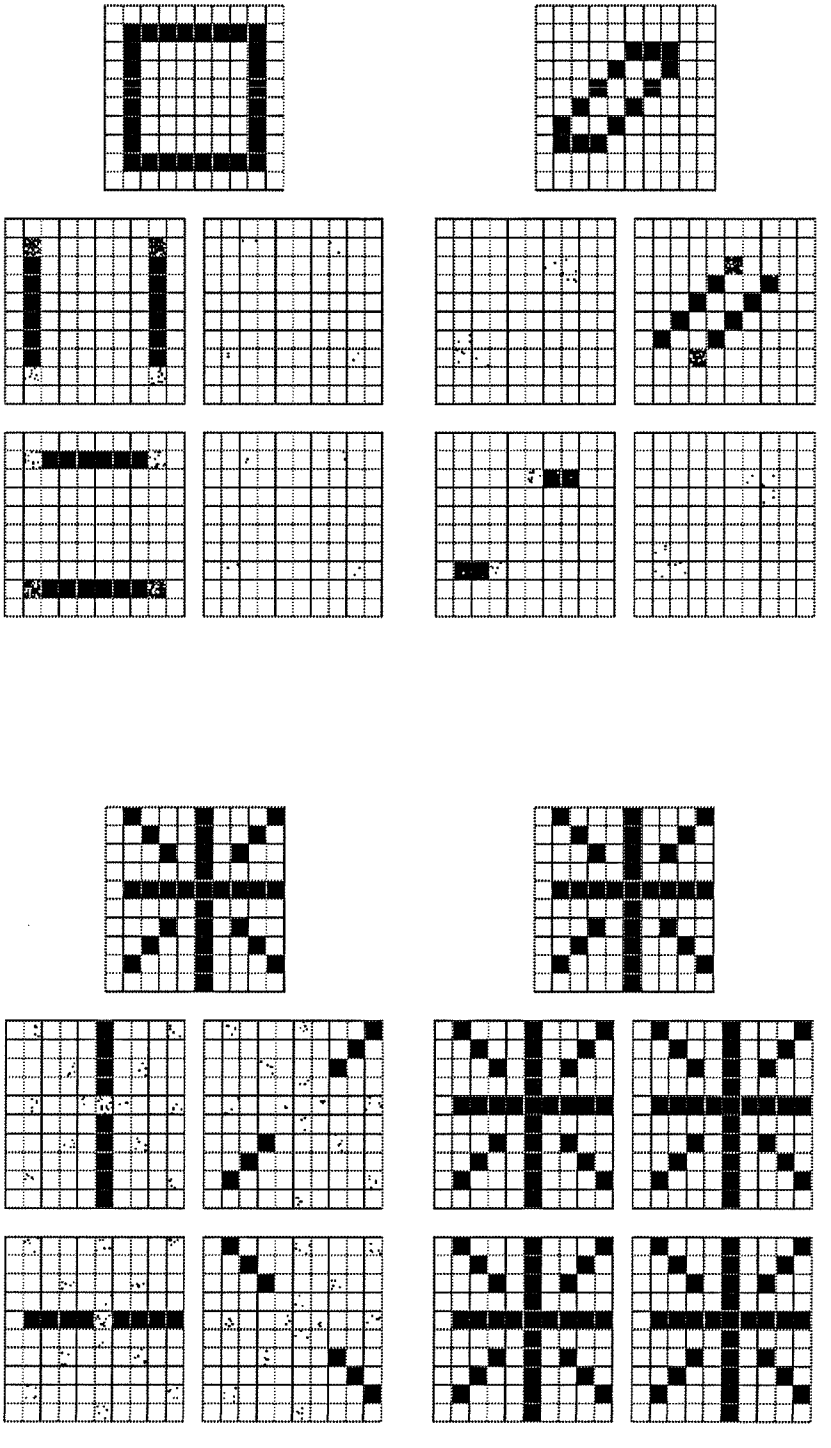

Figures 9 and 10: 9 — with inhibition and 10 — without inhibition. The figures above show the role of inhibition in the model illustrated in Figure 2.

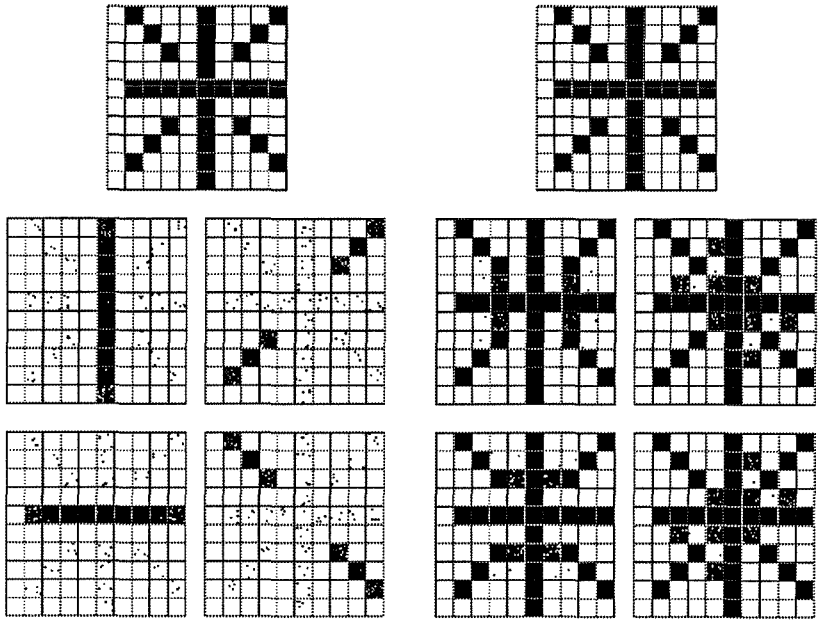

Figures 11 and 12: 11 — with inhibition and 12 — without inhibition. The figures above show the role of inhibition in the model illustrated in Figure 4.

C.1

Development of Feedforward Connections Appendix C

Dynamics of feed forward connections

Consider a network of neurons which are assigned onto a 2-dimensional plane. All the neurons feed forward to a neuron in another layer (output neuron). The neuron activities are center-surround correlated, i.e., the activities of nearby neurons are correlated and the activities of further away neurons are anti-correlated (see Table C.1). A Hebbian type of developmental rule can be applied to the development of the feed forward connections (Linsker, 1986; Miller, 1989). By using the dynamic equation derived from the Hebbian rule, the network can learn an oriented stripe structure of the feed forward connections. Again, a symmetry breaking happens in the development. A brief derivation of the dynamic equation is as follow.

$$\begin{pmatrix} -6 & -6 & -6 & -6 & -6 & -6 & -6 \\ -6 & -7 & -7 & -7 & -7 & -7 & -6 \\ -6 & -7 & 34 & 34 & 34 & -7 & -6 \\ -6 & -7 & 34 & 40 & 34 & -7 & -6 \\ -6 & -7 & 34 & 34 & 34 & -7 & -6 \\ -6 & -7 & -7 & -7 & -7 & -7 & -6 \\ -6 & -6 & -6 & -6 & -6 & -6 & -6 \end{pmatrix}$$

Table C.1 The correlation of the neuron activities. On the center, the correlation of the same neuron to itself is scaled to 40. It is center-surround structure with positive correlation of center and negative correlation of surround.

The set of variables $\{V_i(t), P_i(t)\}$ are used to describe the state of the network, in which $\{V_i(t)\}$ are neuron activities and $\{P_i(t)\}$ are forward connections. The output neuron activity is $V^{\alpha}(t)$.

The the dynamic equations is as follow :

$$\begin{aligned} a\frac{dV^\alpha}{dt} &= -V^\alpha + \sum_i P_i V_i \\ B_i\frac{ds_i}{dt} &= -s_i + V^\alpha V_i \\ P_i &= H_i(s_i) \end{aligned} \qquad [C.1]$$

In the following study, the gain functions are

$$H_i(x) = L(Hx) \qquad [C.2]$$

in which H is constants (gain) and

$$L(x) = \begin{cases} +1, & \text{if } x > +1; \\ x, & \text{if } -1 < x < +1; \\ -1, & \text{if } -1 > x. \end{cases} \qquad [C.3]$$

The learning time constants B_i are much longer than the neuron dynamic time constant a. One can approximate that:

$$V^\alpha(t) = \sum_i P_i V_i \qquad [C.4]$$

So that

$$B_i\frac{ds_i}{dt} = -s_i + V_i \sum_j P_j V_j \qquad [C.5]$$

Suppose that $V_i(t)$ changes in a fast time scale comparing to B_i and one can substitute $V_i(t)V_j(t)$ by its average value

$$B_i\frac{ds_i}{dt} = -s_i + \sum_j C_{ij} P_j \qquad [C.6]$$

in which C_{ij} is the center-surround correlation matrix.

$$\begin{pmatrix} -1 & -1 & 1 & 1 & 1 & -1 & -1 \\ -1 & -1 & 1 & 1 & 1 & -1 & -1 \\ -1 & -1 & 1 & 1 & 1 & -1 & -1 \\ -1 & -1 & 1 & 1 & 1 & -1 & -1 \\ -1 & -1 & 1 & 1 & 1 & -1 & -1 \\ -1 & -1 & 1 & 1 & 1 & -1 & -1 \\ -1 & -1 & 1 & 1 & 1 & -1 & -1 \end{pmatrix}$$

Table C.2 A vertical strip like feed forward connection P_i pattern is developed. This pattern is corresponding to a state of energy minimum. Similar horizontal, 45^o and -45^o strips are also energy minimum.

It is obvious that C_{ij} is a symmetric matrix and one can derive a similar energy function for the differential equation. The P_i states corresponding to the energy minima are strip patterns as shown in Table C.2. Here we skip the discussion about the symmetry breaking which has been discussed in detail in others work (Linsker, 1986; Kamman, 1989; Mackay, Miller, 1990).

Formation of columns

The development of LGN projections (receptive field) will follow the similar rule as Linsker proposed which is discussed briefly in the last section. Without intracortical connections, the development of LGN cell i to cortex cell α connection P_i^α:

$$\begin{aligned} B\frac{ds_i^\alpha}{dt} &= -s_i^\alpha + \sum_j C_{ij} P_j^\alpha \\ P_i^\alpha &= L(Hs_i^\alpha) \end{aligned} \qquad [C.7]$$

Since the correlation matrix C_{ij} is independent of cortex cell, the projections to different cortex cells are developed independently. All the learned structures are orientation selective as shown on the left of Figure C.2, but their orientations are not correlated.

To get the equation including the intracortical effect, we approximate the activity V^α of cortical neuron α as follow,

$$V^\alpha(t) = \sum_\beta T^{\alpha\beta} V^\beta + \sum_i P_i^\alpha V_i \qquad [C.8]$$

in which $T^{\alpha\beta}$ is the interconnection between cortex cells. This approximation is valid in the case when the LGN inputs to cortex are strong, i.e., effect of $\sum_i P_i^\alpha V_i$ are stronger than intracortical effect $\sum_\beta T^{\alpha\beta} V^\beta$. Thus

$$V^\alpha(t) = \sum_\beta D^{\alpha\beta} \sum_i P_i^\beta V_i \qquad [C.9]$$

in which $D = (I - T)^{-1}$. So

$$B\frac{ds_i^\alpha}{dt} = -s_i^\alpha + \sum_{j\beta} D^{\alpha\beta} C_{ij} P_j^\beta \qquad [C.10]$$

Each cortex cell receives inputs from LGN cells, the spatial arrangement of those input connections are shown in Figure C.1a. The correlations between different LGN cells are calculated by a DOG functions (only a function of the distance between cells) as shown in Figure C.1b. Now the interconnections developed in Chapter 3 and Chapter 7 can be used in the development of feedforward connections.

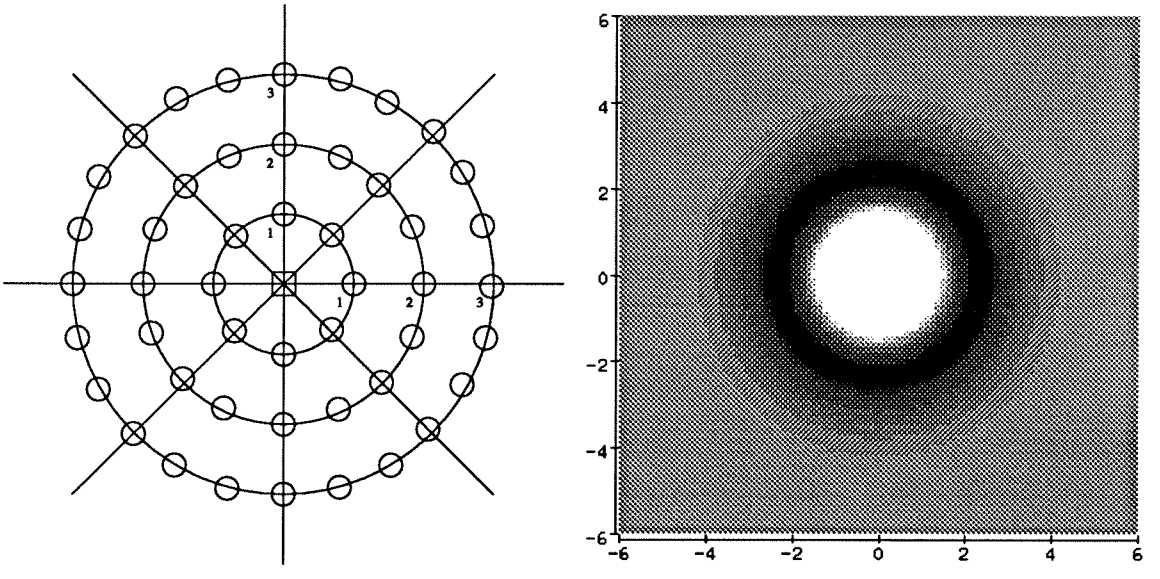

Figure C.1 On the left is figure a: the spatial arrangement of feedforward connections from LGN to one cortex neuron. The activity correlation between those LGN cells has been shown in Table C.1. The reason to use this kind of spatial arrangement is to make it symmetric about different orientations (at least about 0, 45, 90, and 135 degrees). On the right is figure b: a plot of the correlation function been used, i.e., $2 * exp(-r^2/2.0) - exp(-r^2/4.0)$. Table C.1 is calculated from this function and all the correlation terms needed in the simulation are calculated from this function as well. Note: in these two figures, the spatial scale is in LGN unit (In our simulation, 6 LGN units equal to 10 cortex units).

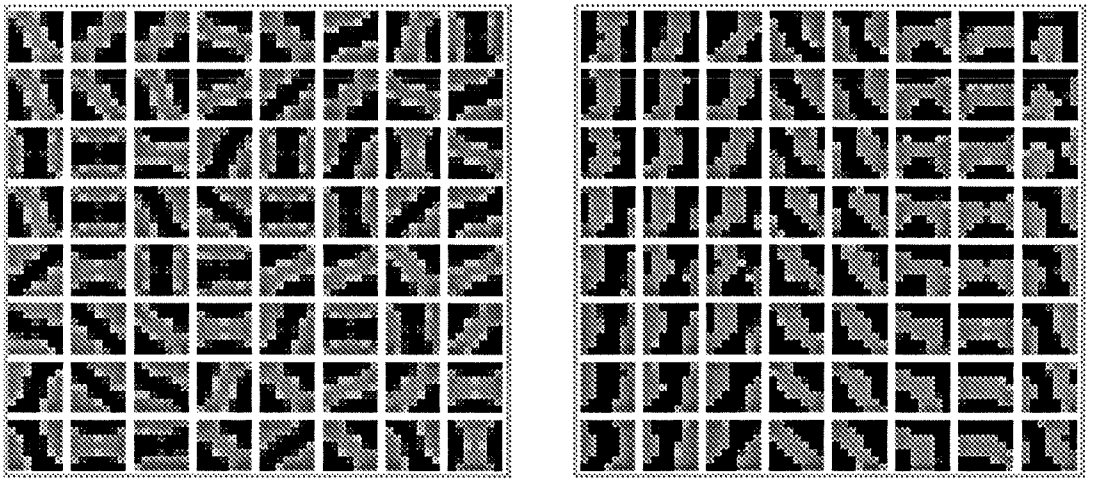

Figure C.2 The formation of LGN to cortex connections. On the left, the receptive fields of each cortical cells are randomly oriented strips when developing without intracortical connections. On the right with the intracortical connection structure as in Figure 3.3, the orientations are organized into columns.

The orientation of the symmetry breaking of the LGN to cortex projection should be coordinated by the learned intercortical connections which is itself symmetry breaking strip. As pointed out before, we suppose that the intracortical connections developed first and did not change during the development of LGN to cortex connections. A development result under the influence of a vertical strip of intracortical connection structure is shown on the right of Figure C.2. The positive connections along the vertical direction tend to keep the receptive fields along a vertical line to have the same orientation. Along the horizontal direction the intracortical connections are partial positive and partial negative, thus the cells' receptive fields change orientation gradually. Cooper and etc., 1982, have shown the same result in a one dimensional case with a postulated intracortical connection structure as the horizontal one in our model. Figure C.3 shows the result of feedforward development for the larger network discussed in Chapter 7.

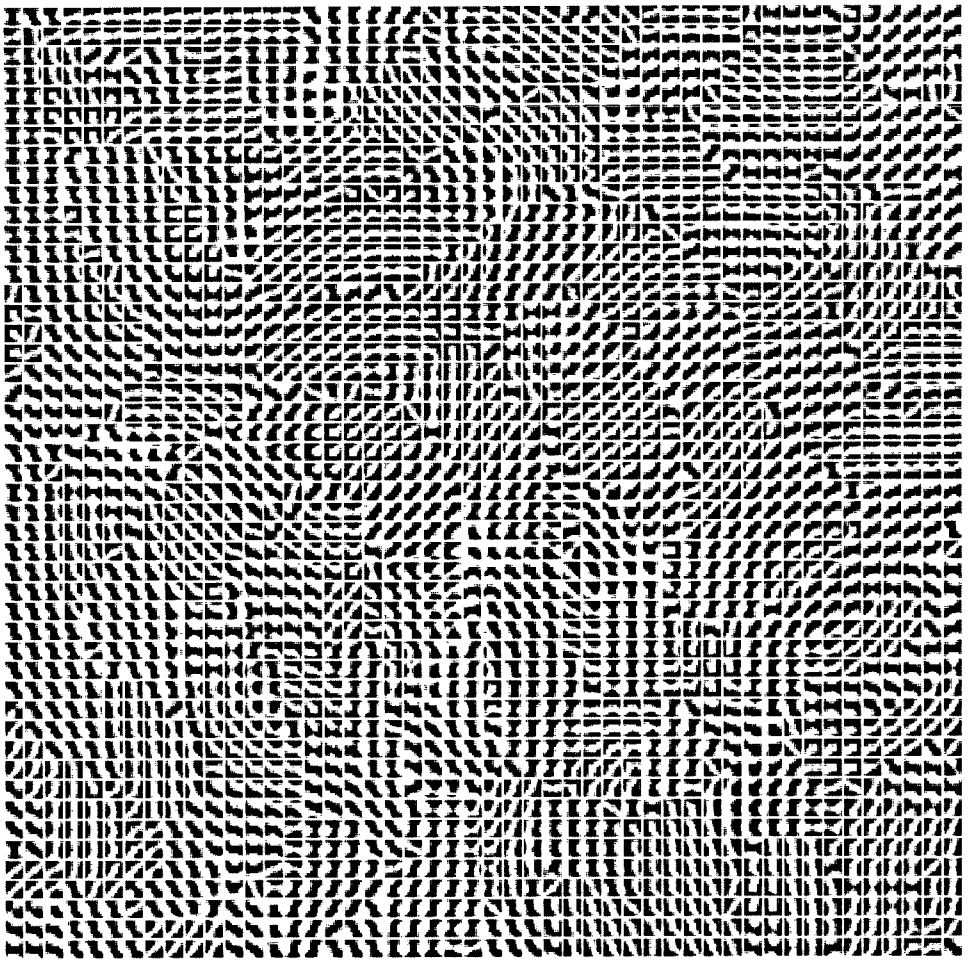

Figure C.3 In the figure is a 48 by 48 cortex, each neuron receives inputs from LGN cells (the spatial arrangement is shown in Figure C.1a). The intracortex connections are the symmetry breaking results as in Figure 7.3. The feedforward connections develop after the formation of intracortex connections. The feedforward connections for each cell form specific orientation selective structure (white for $+1$, black for -1, and gray scale in between). Cells with similar orientation selectivities are close to each other. The period of orientation change from 0 to 180 is about the same as the period of the strip-like pattern of intracortical connections.

Discussion

There are only excitatory projections from LGN to cortex. It is mathematically equal to have on-center and off-center connections as Linsker (1986) and Miller (1989) proposed. The mathematics about the development of the feedforward pathway has

been worked out by various authors (Bienenstock, et al., 1982; Linsker, 1986; Kamman, Yuille, 1989; Miller, 1989), it is not the main concern of our current model.

Reference
Appendix D

Albus, A. (1975) Quantitative study of the projection area of the central and the paracentral visual field in Area 17 of the cat. I. The Precision of the Topography. *Exp. Brain Res.* **24:** 159–179.

Beaulieu, C. and Colonnier, M. (1983) The number of neurons in the different laminae of the binocular and monocular regions of Area 17 in the Cat. *J. Comp. Neurol.* **217:** 337–344.

Benevento, L.A., Creutzfeldt, O.D. and Kuhnt, U. (1972) Significance of intracortical inhibition in the visual cortex. *Nature New Biol.* **238:** 124–126.

Bienenstock, E. L., Cooper, L. N., Munro, P. W. (1982) A Theory for the development of neuron selectivity: Orientation Specificity and binocular interaction in visual cortex. *Journal of neuroscience* **V. 2:** pp. 32-48

Bishop, P.O., Kozak, W. and Vakkur, G.J. (1962) Some quantitative aspects of the cat's eye: axis and plane of reference, visual field coordinates and optics. *J. Physiol. (London)* **163:** 466–502.

Bishop, P.O., Coombs J.S., and Henry, G.H. (1971) Interaction effects of visual contours on the discharge frequency of simple striate neurons. *J. Physiol. (London)* **219:** 659–687.

Bloomfield, S.A., Hamos, J.E., and Sherman, S.M. (1987) Passive cable properties and morphological correlates of neurons in the lateral geniculate nucleus of the cat. *J. Physiol. (London)* **383:** 653–692.

Boycott, B.B. and Wässle, H.(1974) The morphological types of ganglion cells of the domestic cat's retina. *J. Physiol. (London)* **240:** 307–410.

Braitenberg, V. and Braitenberg, C. (1979) Geometry of orientation columns in the visual cortex. *Biol. Cybern.* **33:** 179–186.

Bullier, J. and Norton, T.T. (1979) X and Y relay cells in cat lateral geniculate nucleus: quantitative analysis of receptive—field properties and classification. *J. Neurophysiol.* **42:** 244–291.

Chomsky, N. (1965) *Aspects of the Theory of Syntax*, MIT Press, Cambridge.

Cleland, B.G., Dubin, M.W., and Levick, W.R. (1971) Sustained and transient neurons in the cat's retina and lateral geniculate nucleus. *J. Physiol. (London)* **217:** 473–496.

Cleland, B.G. and Levick, W.R. (1974) Properties of rarely encountered types of ganglion cells in the cat's retina and an overall classification. *J. Physiol. (London)* **240:** 457–492.

Cohen, M., Grossberg, S. (1983) Absolute stability of global pattern formation and parallel memory storage by competitive neural networks. *IEEE Trans Systems Man and Cybernetics* **v. SMC-12, n. 5:** p. 815.

Cooper, L., Liberman, F., Oja, E. (1979) A theory for the acquisition and loss of neuron specificity in visual cortex. *Biological Cybernetics* **v. 33:** 9-28.

Crick, F. (1984) The function of the thalamic reticular complex: the searchlight hypothesis. *Proc. Natl. Acad. Sci. USA* **81:** 4586–4590.

Dawis, S., Shapley, R., Kaplan, E., and Tranchina, D. (1984) The receptive field organization of X-cells in the cat: spatiotemporal coupling and asymmetry. *Vision Res.* **24:** 549–564.

Daugman, J.G. (1985) Uncertainty relation for resolution in space, spatial frequency, and orientation optimized by two-dimensional visual cortical filters. *J. Opt. Soc. Am.* **2:** 1160–1169.

Dong, D.W. (1991) Dynamic properties of neural network *IEEE (IJCNN-91), Seattle, Proceedings.*

Enroth-Cugell, C. and Robson, J.G. (1966) The contrast sensitivity of retinal ganglion

cells of the cat. *J. Physiol. (London)* **187:** 517–552.

Enroth-Cugell, C., Robson, J.G., Schweizer-Tong, D.E., and Watson, A.B. (1983) Spatio-temporal interactions in cat retinal ganglion cells showing linear spatial summation. *J. Physiol. (London)* **341:** 279–307.

Ferster, D. (1986) Orientation selectivity of the synaptic potentials in neurons of cat primary visual cortex. *J. Neurosci.* **6:** 1284–1301.

Ferster, D. (1988) Spatially opponent excitation and inhibition in simple cells of the cat visual cortex. *J. Neurosci.* **8:** 1172–1180.

Ferster, D. and Koch, C. (1987) Neuronal connections underlying orientation selectivity in cat visual cortex. *Trends Neurosci.* **10:** 487–492.

Fischer, B. (1973) Overlap of receptive field centers and representation of the visual field in the opic tract, *Vision Res.* **13:** 2113–2120.

Fitzpatrick, D., Penny, G.R., and Schmechel, D.E. (1984) Glutamic acid decarboxylase immunoreactive neurons and terminals in the lateral geniculate nucleus of the cat. *J. Neurosci.* **4:** 1809–1829.

Freund, T.F., Martin, K.A.C., and Whitteridge, D. (1985a) Innervation of cat visual areas 17 and 18 by physiologically identified X- and Y-type thalamic afferents. I. Arborization patterns and quantitative distribution of postsynaptic elements. *J. Comp. Neurol.* **242:** 263–274.

Gilbert, C. (1977) Laminar differences in receptive field properties of cells in cat primary visual cortex. *J. Physiol. (London)* **268:** 391–421.

Gilbert, C. and Wiesel, T. (1983) Clustered intrinsic connections in cat visual cortex. *J. Neurosci.* **3:** 1116-1133.

Gilbert, C. and Wiesel, T. (1989) Columnar Specificity of intrinsic horizontal and corticocortical connections in cat visual cortex. *J. Neurosci.* **9(7):** 2432-2442.

Gremillion, M., Mandell, A., and Travis, B. (1987) Neural nets with complex struc-

ture: a model of the visual system. In *IEEE 1st Intl. Conf. Neural Networks*, Vol. 4, Institute of Electrical and Electronics Engineers, San Diego, pp. 235–246.

Hebb, D.O. (1948) *The Organization of Behavior: A Neuropsychological Theory*, John Wiley, New York.

Heggelund, P. (1981) Receptive field organization of simple cells in cat striate cortex. *Exp. Brain Res.* **42:** 89–98.

Heggelund, P. (1986) Quantitative studies of the discharge fields of single cells in cat striate cortex. *J. Physiol. (London)* **373:** 272–292.

Hendry, S.H.C., Schwark, H.D., Jones, E.G., and Yan. J. (1987) Numbers and proportions of GABA- immunoreactive neurons in different areas of monkey cerebral cortex. *J. Neurosci.* **7:** 1503-1519.

Herrnstein, R.J., Loveland, D.H., Cable, C. (1976) Natural Concepts in Pigeons. *J. Exp. Psy.* **2(4):** 285-302.

Hodgkin, A.L. and Huxley, A.F. (1952) A quantitative description of membrane current and its application to conduction and excitation in nerve. *J. Physiol. (London)* **117:** 500–544.

Hoffman, K.P., Stone, J., and Sherman, S.M. (1972) Relay of receptive-field properties in dorsal lateral geniculate nucleus of cat. *J. Neurophys.* **35:** 518–531.

Hopfield, J.J. (1982) Neural networks and physical systems withe emergent collective computational abilities. *Proc. Natl. Acad. Sci. USA* **v. 79:** p. 2554

Hopfield, J.J. (1984) Neurons with graded response have collective computational properties like those of two-state neurons. *Proc. Nat. Acad. Sci. USA* **81:** 3088–3092.

Hopfield, J.J. (1990) The effectiveness of analogue "neural network" hardware. *Network*, v. 1, p. 27.

Hubel, D.H. and Wiesel, T.N. (1961) Integrative action in the cat's lateral geniculate

body. *J. Physiol.(London)* **155:** 385–398.

Hubel, D.H. and Wiesel, T.N. (1962) Receptive fields, binocular interactions, and functional architecture in the cat's visual cortex. *J. Physiol. (London)* **160:** 106–154.

Hubel, D.H. and Wiesel, T.N. (1963) Shape and arrangement of columns in cat's striate cortex. *J. Physiol. (London)* **165:** 559–568.

Hubel, D.H. (1988) Chapter 9. *Eye, brain, and vision.*

Humphrey, A.L., Sur, M., Uhlrich D.J., and Sherman, S.M. (1985) Projection patterns of individual X- and Y-cell axons from the lateral geniculate nucleus to cortical area 17 in the cat. *J. Comp. Neurol.* **233:** 159–189.

Jones, E.G., Hendry, S.H.C., and DeFelipe, J. (1987) GABA-peptide neurons of the primate cerebral cortex: a limited cell class. In: *Cerebral Cortex*, Jones, E.G. and Peters, A. (eds.), Plenum Press, New York, pp. 237–266.

Jones, J.P. and Palmer, L.A. (1987) An evaluation of the two-dimensional gabor filter model of simple receptive fields in cat striate cortex. *J. Neurophysiol.* **58:** 1233–1258.

Jones, J.P., Stepnoski, A., and Palmer, L.A. (1987) The two-dimensional spectral structure of simple receptive fields in cat striate cortex, *J. Neurophys.* **58:** 1212–1232.

Kammen, D.M., Yuille, A.L. (1989) Spontaneous symmetry-breaking energy functions and the emergence of orientation selective cortical-cells. *Biological Cybernetics* **V59 (1):** 23—31.

Kisvarday, Z.F., Martin, K.A.C., Whitteridge, D., and Somogyi, P. (1985) Synaptic connections of intracellularly filled clutch cells: a type of small basket cell in the visual cortex of the cat. *J. Comp. Neurol.* **241:** 111–137.

Koch, C. (1987) A network model for cortical orientation selectivity in cat striate

cortex. *Invest. Ophthalmol. Vis. Sci.* **28:** 126.

Kohonen, T. (1984) *Self-organization and associative memory*, Springer-Verlag.

Lee, B.B., Cleland, B.G., and Creutzfeldt, O.D. (1977) The retinal input to cells in area 17 of the cat's cortex. *Exp. Brain Res.* **30:** 527–538.

Lowel, S., Freeman, B., Singer, W. (1987) Topographic organization of the orientation column system in large flat-mounts of the cat visual-cortex - a 2-deoxyglucose study. *J. Comp. Neurol.* **v 255(3) :** 401—415.

Linsenmeier, R.A., Frishman, L.J., Jakiela, H.G., and Enroth-Cugell, C. (1982) Receptive field properties of X and Y cells in the cat retina derived from contrast sensitivity measurements. *Vision Res.* **22:** 1173–1183.

Linsker, R. (1986) From basic network principles to neural architecture ... *Proc. Natl. Acad. Sci. USA* **v. 83:** p. 7508, p. 8390, p. 8779.

Mackay, D.J., Miller, K.D. (1990) Analysis of Linsker's application of Hebbian rules to linear networks. *Network* **v.1(3):** 257-297

Marr, D. and Hildreth, E. (1980) Theory of edge detection. *Proc. R. Soc. Lond. B* **207:** 187–127.

Martin, K.A., Somogyi, P., and Whitteridge, D. (1983) Physiological and morphological properties of identified basket cells in the cat's visual cortex. *Exp. Brain Res.* **50:** 193–200.

Miller, K. D., Keller, J. B., Stryker, M. P. (1989) Ocular dominance column development - analysis and simulation. *Science* **v. 245:** p. 605-615.

Minsky, M. (1969) *Perceptrons*, MIT Press.

Morrone, M.C., Burr, D.C., and Maffei, L. (1982) Functional implications of cross-orientation inhibition of cortical visual cells. I. Neurophysiological evidence. *Proc. R. Soc. Lond. B* **216:** 335–354.

Orban, G.A. (1984) *Neuronal Operations in the Visual Cortex*, Springer, Berlin.

Orban, G.A., Gulyas, B., and Vogels, R. (1987) Influence of moving textured background on direction selectivity of cat striate cortex. *J. Neurophysiol.* **57:** 1792–1812.

Peichl, L. and Wässle, H. (1979) Size, scatter and coverage of ganglion cell receptive field centres in the cat retina. *J. Physiol. (London)* **291:** 117–141.

Peters, A. and Jones, E.G. (1984) *Cerebral Cortex*, Vols. 1 and 6, Plenum Press, New York.

Ramoa, A.S., Shadlen, M., Skottun, B.C., and Freeman, R.D. (1986) A comparison of inhibition in orientation and spatial frequency selectivity of cat visual cortex. *Nature* **321:** 237–239.

Richter, J. and Ullman, S. (1982) A model for the temporal organization of X- and Y-type receptive fields in the primate retina. *Biol. Cybern.* **43:** 127–145.

Rodieck, R. (1965) Quantitative analysis of cat retinal ganglion cell response to visual stimuli. *Vision Res.* **5:** 583–601.

Rodieck, R. (1979) Visual pathways. *Ann. Rev. Neurosci.* **2:** 193–225.

Rumelhart, D., ed. (1986) *Parallel distributed processing*, MIT Press.

Sanderson, K.J. (1971) Visual field projection columns and magnification factors in the lateral geniculate nucleus of the cat. *Exp. Brain Res.* **13:** 159-177.

Schwartz, E.L. (1980) Computational anatomy and functional architecture of striate cortex: a spatial mapping approach to perceptual coding. *Vision Res.* **20:** 645–669.

Sejnowski, T., Koch, C., and Churchland, P. (1988) Computational neuroscience. *Science*, **241:** 1299-1306.

Shapley, R. and Enroth-Cugell, C. (1984) Visual adaptation and retinal gain control. *Prog. Retinal Res.* **3:** 263–346.

Shapley, R.M. and Lennie, P. (1985) Spatial frequency analysis in the visual system.

Ann. Rev. Neurosci. **8:** 547–583.

Sherman, M. (1985) Functional organization of the W-, X- and Y-cell pathways: a review and hypothesis. In: *Progress in Psychobiology and Physiological Psychology*, Vol. 11, Sprague. J.M. and Epstein, A.N. (eds.), Academic Press, New York, pp. 233-314.

Sherman, S.M. and Koch, C. (1986) The control of retinogeniculate transmission in the mammalian lateral geniculate nucleus. *Exp. Brain Res.* **63:** 1–20.

Sillito, A.M. (1975) The contribution of inhibitory mechanisms to the receptive field properties of neurons in the striate cortex of the cat. *J. Physiol. (London)* **250:** 305–322.

Sillito, A.M., Kemp, J.A., Milson, J.A., and Berardi, N. (1980) A re-evaluation of the mechanisms underlying simple cell orientation selectivity. *Brain Res.* **194:** 517–520.

Singer, W. and Creutzfeldt, O.D. (1970) Reciprocal lateral inhibition of on- and off-center neurons in the lateral geniculate body of the cat. *Exp. Brain Res.* **10:** 311–330.

Skottun, B., Bradley, A., Sclar, G., Ohzawa, I., and Freeman, R. (1987) The effects on contrast on visual orientation and spatial frequency discrimination: a comparison of single cells and behaviour. *J. Neurophys.* **57:** 773–786.

Stone, J. and Dreher, B. (1973) Projection of X- and Y-cells of the cat's lateral geniculate nucleus to areas 17 and 18 of visual cortex. *J. Neurophysiol.* **36:** 551–567.

Stone, J. (1983) *Parallel Processing in the Visual System*, Plenum Press, New York.

Tanaka, K. (1983) Cross-correlation analysis of geniculostriate neuronal relationships in cats. *J. Neurophysiol.* **49:** 1303–1318.

Tömböl, T. (1974) An electron microscopic study of the neurons of the visual cortex.

J. Neurocytol. **3:** 525-531.

Tusa, R.J., Palmer, L.A., and Rosenquist, A.C. (1978) The retinotopic organization of area 17 (striate cortex) in the cat. *J. Comp. Neur.* **177:** 213-236.

Victor, J.D. (1987) The dynamics of the cat retinal X cell centre. *J. Physiol. (London)* **386:** 219–246.

Vidyasagar, T.R. and Heide, W. (1984) Geniculate orientation biases seen with moving sine wave gratings: implications for a model of simple cell afferent connectivity. *Exp. Brain Res.* **57:** 196–200.

von der Malsburg, C., Cowan, J.D. (1982) Outline of a theory for the ontogenesis of iso-orientation domain in visual cortex. *Biol. Cybern.* **45:** p49-56

Wässle, H., Boycott, B.B., and Illing, R.-B. (1981) Morphology and mosaic of on- and off-beta cells in the cat retina and some functional considerations. *Proc. R. Soc. Lond. B* **212:** 177–195.

Wässle, H., Peichl, L., and Boycott, B.B. (1983) A spatial analysis of on- and off-ganglion cells in the cat retina. *Vision Res.* **10:** 1151–1160.

Watkins, D.W. and Berkley, M.A. (1974) The orientation selectivity of single neurons in cat striate cortex. *Exp. Brain Res.* **19:** 433–446.

Wehmeier, U., Dong, D., Koch, C. and D. Van Essen, D. (1989) Modeling the mammalian visul system. In: *Methods in Neuronal Modeling: From Synapses to Networks*, Koch, C. and Segev, I. (Eds.), MIT Press, Cambridge, MA, pp. 335-360.

Wiggins, S. (1988) *Global Bifurcations and Chaos: Analytical Methods*, Springer-Verlag, New York.

Winfield, D.A., Gatter, K.C., and Powell, T.P.S. (1980) An electron microscopic study of the types and proportions of neurons in the cortex of the motor and visual areas of the cat and rat. *Brain* **103:** 245–258.

Wilson, M., and Bower, J. (1989) The Simulation of Large-Scale Neural Network In:

D.10

Methods in Neuronal Modeling: From Synapses to Networks, Koch, C. and Segev, I. (Eds.), MIT Press, Cambridge, MA, pp. 291-335.